MARS: PAST, PRESENT, AND FUTURE—RESULTS FROM THE MSATT PROGRAM

LPI Technical Report Number 93-06, Part 1

Lunar and Planetary Institute 3600 Bay Area Boulevard Houston TX 77058-1113

LPI/TR--93-06, Part 1

MARS: PAST, PRESENT, AND FUTURE—
RESULTS FROM THE MSATT PROGRAM

Edited by

R. M. Haberle

Convened by

The MSATT Steering Committee

Held at
Houston, Texas

November 15–17, 1993

Sponsored by
Mars Surface and Atmosphere Through Time (MSATT) Study Group
Lunar and Planetary Institute

Lunar and Planetary Institute 3600 Bay Area Boulevard Houston TX 77058-1113

LPI Technical Report Number 93-06, Part 1
LPI/TR--93-06, Part 1

Compiled in 1993 by
LUNAR AND PLANETARY INSTITUTE

The Institute is operated by the University Space Research Association under Contract No. NASW-4574 with the National Aeronautics and Space Administration.

This report may be cited as

Haberle R. M., ed. (1993) *Mars: Past Present, and Future—Results from the MSATT Program*. LPI Tech. Rpt. 93-06, Part 1, Lunar and Planetary Institute, Houston. 58 pp.

This report is distributed by

ORDER DEPARTMENT
Lunar and Planetary Institute
3600 Bay Area Boulevard
Houston TX 77058-1113

Mail order requestors will be invoiced for the cost of shipping and handling.

Preface

This volume contains papers that have been accepted for presentation at the workshop on Mars: Past, Present, and Future—Results from the MSATT Program, November 15–17, 1993, in Houston, Texas. The Program Committee consisted of J. Bell (*NASA Ames Research Center*), R. Haberle (*NASA Ames Research Center*), S. Lee (*University of Colorado*), B. Schuraytz (*Lunar and Planetary Institute*), and K. Tanaka (*U.S. Geological Survey, Flagstaff*).

Logistics and administrative and publications support were provided by the Publications and Program Services Department staff at the Lunar and Planetary Institute.

Contents

N94-33191

Abstracts

S1-91 ABS. ONLY 8631

DEPTH-DIAMETER RATIOS FOR MARTIAN IMPACT CRATERS: IMPLICATIONS FOR TARGET PROPERTIES AND EPISODES OF DEGRADATION. N. G. Barlow, Lunar and Planetary Institute, 3600 Bay Area Boulevard, Houston TX 77058, USA.

Mariner 9 and Viking imagery reveal that martian impact craters exhibit a wide variety of crater depths that have been attributed to varying stages of crater degradation. In 1984, Pike and Davis derived an empirical relationship between fresh crater depth and diameter based on a photoclinometric analysis of 47 simple and 84 complex craters across Mars [1]. A new study combining photoclinometric and shadow estimation techniques for the derivation of crater depths reveals that a single depth-diameter (d/D) relationship does not adequately describe the observations across all of Mars. When a statistically reliable d/D relationship for fresh craters within a specific region can be derived, d/D ratios for nonpristine craters in the same area can be compared to the ratio for fresh craters for an estimate of the degree of degradation that has affected the region. Preliminary analysis indicates that most of the studied regions display well-defined localized variations in crater degradation, suggesting episodes of enhanced regional obliteration.

This study determines crater depth through use of photoclinometric profiles [2]. Random checks of the photoclinometric results are performed using shadow estimation techniques. The images are Viking Orbiter digital format frames; in cases where the digital image is unusable for photoclinometric analysis, shadow estimation is used to determine crater depths. The two techniques provide depth results within 2% of each other. Crater diameters are obtained from the photoclinometric profiles and checked against the diameters measured from the hard-copy images using a digitizer. All images used in this analysis are of approximately 40 m/pixel resolution. The sites that have been analyzed to date include areas within Arabia, Maja Valles, Memnonia, Acidalia, and Elysium. The d/D analysis of fresh craters within the five regions is listed in Table 1. Only results for simple craters (craters <5 km in diameter) are discussed here because of the low numbers of complex craters presently measured in the analysis. General results indicate that impact craters are deeper than average within the Medusae Fossae Formation of the Amazonis-Memnonia region. This is likely the result of impact into fine-grained, friable deposits [3]. A wide range in d/D values exists within the heavily cratered terrain of Arabia, Maja Valles, and Memnonia; this may reflect either differences in the particle size of the target material or in the composition of the target. Craters within the martian northern plains show a tendency to become shallower with increasing latitude, as exemplified by the different d/D ratios in Elysium vs. Acidalia. This result has been proposed by previous investigators [4] as an indication of increasing amounts of subsurface ice as the polar regions are approached. This explanation is supported by evidence of lobate ejecta morphologies surrounding fresh impact craters down to 1 km in diameter in Acidalia, based on the theory that lobate ejecta morphologies result from impact into subsurface ice reservoirs [5]. Sufficient numbers of fresh impact craters have been included in the d/D analysis within the Maja Valles, Elysium, and Acidalia regions of Mars to provide a statistically viable relationship. Within these regions we can therefore compare the d/D ratios of nonpristine impact craters to the average d/D ratio for fresh craters and obtain an estimate of the amount of degradation that the nonpristine impact craters have experienced. Dividing the measured crater depth by the depth expected for fresh craters of identical size gives a percentage change in depth. Restricting the comparison to simple craters provides a quantitative measure of the degree of degradation suffered by craters <5 km in diameter within the region of study. The results indicate that localized areas within the general regions have experienced varying amounts of degradation. No correlation between the region of degradation and geologic unit or thermal inertia is observed. Crater size-frequency distribution analyses can provide some general information about the timing of these obliteration episodes, but the error bars are large and therefore little about the relative timing of these episodes can be deduced at the present time. Continuing analysis with larger numbers of impact craters will help to reduce these error limits and perhaps allow comparisons of the timing of these obliteration episodes between different regions.

In conclusion, a single d/D relationship for fresh impact craters on Mars does not exist due to changes in target properties across the planet's surface. Within regions where target properties are approximately constant, however, d/D ratios for fresh craters can be determined. In these regions, the d/D ratios of nonpristine craters can be compared with the fresh crater d/D relationship to obtain information on relative degrees of crater degradation. This technique reveals that regional episodes of enhanced degradation have occurred. However, the lack of statistically reliable size-frequency distribution data prevents comparison of the relative ages of these events between different regions, and thus determination of a large-scale episode (or perhaps several episodes) cannot be made at this time.

TABLE 1.

	Simple Craters		Complex Craters	
Region	N	d/D	N	d/D
Arabia	8	0.07 (±0.05)	1	0.09 (± ∞)
Maja Valles	41	0.06 (±0.06)	7	0.04 (±0.02)
Memnonia				
Noachian Terrain	14	0.21 (±0.05)	11	0.17 (±0.05)
Medusae Fossae	6	0.35 (±0.04)	6	0.23 (±0.05)
Elysium	32	0.12 (±0.02)	5	0.05 (±0.05)
Acidalia	57	0.06 (±0.03)	8	0.06 (±0.05)

Error limits reflect the range of d/D values for the data used.

References: [1] Pike R. J. and Davis P. A. (1984) *LPSC XV*, 645–646. [2] Davis P. A. and Soderblom L. A. (1984) *JGR, 89*, 9449–9457. [3] Barlow N. G. (1993) *LPS XXIV*, 61–62. [4] Cintala M. J. and Mouginis-Mark P. J. (1980) *GRL, 7*, 329–332. [5] Barlow N. G. and Bradley T. L. (1990) *Icarus, 87*, 156–179.

N94-33192

52-91 ABS. ONLY

STATIONARY EDDIES IN THE MARS GENERAL CIRCULATION AS SIMULATED BY THE NASA-AMES GCM.

J. R. Barnes[1], J. B. Pollack[2], and R. M. Haberle[2], [1]Oregon State University, Corvallis OR 97331, USA, [2]NASA Ames Research Center, Moffett Field CA 94035, USA.

Quasistationary eddies are prominent in a large set of simulations of the Mars general circulation performed with the NASA-Ames GCM. Various spacecraft observations have at least hinted at the existence of such eddies in the Mars atmosphere. The GCM stationary eddies appear to be forced primarily by the large Mars topography, and (to a much lesser degree) by spatial variations in the surface albedo and thermal inertia. The stationary eddy circulations exhibit largest amplitudes at high altitudes (above 30–40 km) in the winter extratropical regions. In these regions they are of planetary scale, characterized largely by zonal wavenumbers 1 and 2. Southern hemisphere winter appears to be dominated by a very strong wave 1 pattern, with both waves 1 and 2 being prominent in the northern hemisphere winter regime. This difference seems to be basically understandable in terms of differences in the topography in the two hemispheres.

The stationary eddies in the northern winter extratropics are found to increase in amplitude with dust loading. This behavior appears to be at least partly associated with changes in the structure of the zonal-mean flow that favor a greater response to wave 1 topographic forcing. There are also strong stationary eddy circulations in the tropics and in the summer hemisphere. The eddies in the summer subtropics and extratropics are substantially stronger in southern summer than in northern summer. The summer hemisphere stationary circulations are relatively shallow and are characterized by smaller zonal scales than those in the winter extratropics.

N94-33193

53-91 ABS. ONLY

THERMAL EMISSION MEASUREMENTS (5–25 μm) OF HAWAIIAN PALAGONITIC SOILS WITH IMPLICATIONS FOR MARS.

J. F. Bell III[1] and T. L. Roush[2], [1]Mail Stop 245-3, NRC/NASA Ames Research Center, Moffett Field CA 94035-1000, USA, [2]San Francisco State University and NASA Ames Research Center, Mail Stop 245-3, Moffett Field CA 94035-1000, USA.

Background: There is ample evidence that abundant Fe-bearing minerals are present on Mars. This evidence takes the form of *in situ* analyses [1–4], previous and continuing Earth-based telescopic spectroscopic observations (reviewed in [5,6]), Viking Lander and Orbiter multispectral imaging [7–10], and Phobos 2 multispectral imaging [11,12]. Information regarding the crystalline or amorphous nature of the Fe-bearing (and other) surface materials on Mars can provide insight into the availability of liquid water at the surface and the duration, mode, and extent of weathering.

Data from Viking X-ray fluorescence analyses, magnetic experiments, and aerosol imaging were interpreted as indicating the presence of a variety of Fe-rich materials, including iron oxides [1–4,13]. However, since the Viking Landers did not carry any instruments capable of determining mineralogy, the exact mineralogical form of the Fe-bearing material remains uncertain.

Interpretations of continuing visual, near-, mid-, and far-infrared (IR) spectroscopic observations of Mars from the Earth and spacecraft over the past 20 years have revealed that the ferric mineralogy occurs in two distinct forms: (1) nanophase or truly amorphous Fe^{3+}-bearing materials [14,15] that spectrally resemble certain terrestrial palagonites [e.g., 16–20]; and (2) well-crystalline ferric oxides like hematite (α-Fe_2O_3), maghemite (γ-Fe_2O_3), or magnetite (Fe_3O_4) [1,13,15,21–24]. The available data indicate that the poorly crystalline "palagonite-like" phases are spectrally dominant [e.g., 5,6, and references within] and that the highly crystalline ferric oxides cannot constitute an abundance of more than about 4–8 wt% [24].

The research presented here represents the initial phase of a broader project that is intended to provide data in the mid- and far-IR spectral region for both well-characterized iron oxides/oxyhydroxides and poorly crystalline or amorphous materials (e.g., palagonites). Such information can be used in the interpretation of data to be returned by the Mars Observer Thermal Emission Spectrometer (TES). Additionally, this same information will prove useful for assessing the information content of existing Kuiper Airborne Observatory, Mariner 7, and Mariner 9 spectra, which also cover the thermal IR wavelength region.

Spectral Studies: In the mid IR (5–25 μm), spectral features arise from vibrational motions of atoms and molecules that compose the materials. These fundamental modes are 1–2 orders of magnitude more intense than any associated combination and/or overtones of these modes that occur at wavelengths less than 5 μm, and hence remote sensing observations in the IR are extremely sensitive to minor concentrations of these absorbing species.

From a planetary perspective, in the mid to far IR these diagnostic features occur where thermal emission rather than reflected sunlight supplies the observed photons. They occur under two sets of conditions. First, suspended particles in a nonisothermal atmosphere produce features near their vibrational fundamentals since these bands modulate the wavelength behavior of both the extinction coefficient and the single scattering albedo of the atmospheric layers within

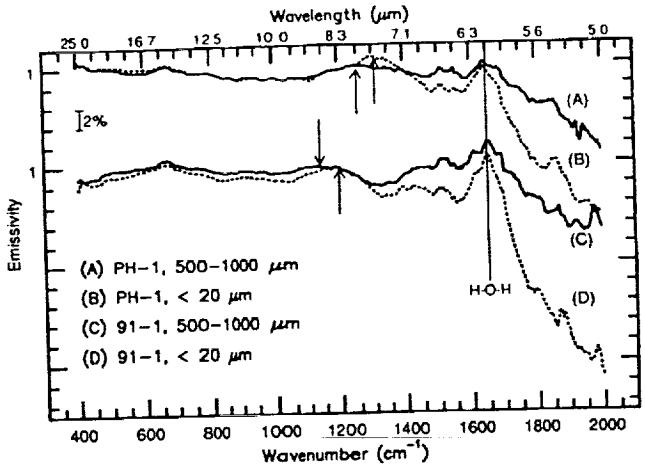

Fig. 1. Emissivity spectra of Hawaiian palagonitic samples PH-1 (thermally altered palagonitic tephra from Mauna Kea) and 91-1 (palagonitic tephra from South Point, island of Hawaii). Both coarse and fine size fraction spectra are shown. Arrows indicate subtle shifts in emissivity peak position between the two particle size regimes shown. The vertical line shows the frequency of the strong H-O-H bending fundamental caused by molecular water associated with these samples.

which they reside [25]. Second, solid and particulate surfaces exhibit spectral features in the thermal IR domain due to a spectral dependence of the surfaces' emissivity [e.g., 26,27].

Careful laboratory studies have shown that the coloring agent in certain Mars analog Hawaiian palagonitic soils is nanophase iron oxide [18,19,28]. We have measured the emissivity of two Mauna Kea palagonitic soils whose transmission spectra exhibit different spectral features [29] and of a thermally altered volcanic tephra sample that exhibits a wide range of crystallinity and degree of alteration (from black cinders to fully hematitic) [19]. Both of these samples may represent analogs for formation mechanisms involving the production of highly altered secondary weathering products on Mars. The emission spectra of all samples were measured at the TES spectroscopy laboratory [30] at Arizona State University with the cooperation of Dr. P. Christensen. The data were converted to emissivity using blackbody measurements combined with measurements of each sample at different temperatures [31].

Results: Emissivity spectra for coarse and fine particle size separates of each sample are shown in Fig. 1. Several trends are immediately obvious. First, the finer particle size fractions exhibit increasingly lower emissivity than the coarser sizes at wavenumbers above 1400 cm^{-1}. This effect may be a manifestation of the increased importance of multiple scattering at these frequencies rather than Fresnel-like reflections at lower frequencies. Second, emissivity peaks in the 1000–1400 cm^{-1} region in the fine fraction samples are shifted to higher frequencies relative to the same feature in the coarse fraction samples. This may be a particle size effect or it may be due to variations in the silicate and/or Fe-bearing mineralogy between the coarse and fine samples [e.g., 19]. While we do not make specific mineralogic assignments for the various spectral features seen in these data, we note that a broad emissivity peak possibly due to silicates is present near 1200–1300 cm^{-1} and that narrower features near 1400–1600 cm^{-1} and near 400 cm^{-1} are possibly consistent with crystalline iron oxide minerals like hematite and/or goethite [32].

This preliminary study has demonstrated that naturally occurring palagonites, thought to be good visible to near-IR spectral analogs for Mars, exhibit complex emissivity spectra at thermal wavelengths. Disentangling the various spectral signatures that make up the emissivity spectra of these complex assemblages may prove quite important in the interpretation of the Mars Observer TES data and of other mid-IR Mars datasets.

References: [1] Hargraves R. B. et al. (1977) *JGR, 82,* 4547. [2] Toulmin P. et al. (1977) *JGR, 82,* 4625. [3] Clark B. C. et al. (1977) *JGR, 82,* 4577. [4] Clark B. C. et al. (1982) *JGR, 87,* 10059. [5] Soderblom L. A. (1992) in *Mars* (H. H. Kieffer et al., eds.), 557. [6] Roush T. L. et al. (1993) in *Remote Geochemical Analysis* (C. Pieters and P. Englert, eds.), 367. [7] Soderblom L. A. et al. (1978) *Icarus, 34,* 446. [8] McCord T. B. et al. (1982) *JGR, 87,* 10129. [9] Adams J. B. et al. (1986) *JGR, 91,* 8098. [10] Arvidson R. E. et al. (1989) *JGR, 94,* 1573. [11] Murchie S. et al. (1993) *Icarus,* in press. [12] Mustard J. F. et al. (1993) *JGR, 98,* 3387. [13] Pollack J. B. et al. (1977) *JGR, 82,* 4479. [14] Morris R. V. and Lauer H. V. Jr. (1990) *JGR, 95,* 5101. [15] Morris R. V. et al. (1989) *JGR, 94,* 2760. [16] Singer R. B. et al. (1979) *JGR, 87,* 10159. [17] Evans D. L. and Adams J. B. (1980) *LPS XI,* 757. [18] Morris R. V. et al. (1990) *JGR, 95,* 14427. [19] Bell J. F. III et al. (1993) *JGR, 98,* 3373. [20] Banin A. (1992) *LPI Tech. Rept. 92-04,* 1. [21] Morris R. V. et al. (1985) *JGR, 90,* 3126. [22] Bell J. F. III et al. (1990) *JGR, 95,* 14447. [23] Hargraves R. B. et al. (1979) *JGR, 84,* 8379. [24] Bell J. F. III (1992) *Icarus, 100,* 575. [25] Toon O. B. et al. (1977) *Icarus, 30,* 663. [26] Salisbury J. W. and Eastes J. W. (1985) *Icarus, 64,* 586. [27] Salisbury J. W. et al. (1987) *JGR, 92,* 702. [28] Golden D. C. et al. (1993) *JGR, 98,* 3401. [29] Roush T. L. (1992) *LPI Tech. Rpt. 92-04,* 32. [30] Anderson D. L. et al. (1991) *LPS XXII,* 21. [31] Christensen P. R. and Harrison S. T. (1993) *JGR,* submitted. [32] Salisbury J. W. et al. (1991) *Infrared (2.1–25 μm) Spectra of Minerals,* 267, Johns Hopkins Univ.

54-91 ABS. ONLY

THERMAL STUDIES OF MARTIAN CHANNELS AND VALLEYS USING TERMOSKAN DATA: NEW RESULTS.

B. H. Betts[1,2] and B. C. Murray[1], [1]Mail Code 170-25, California Institute of Technology, Pasadena CA 91125, USA, [2]Now at San Juan Capistrano Research Institute, 31872 Camino Capistrano, San Juan Capistrano CA 92675, USA.

The Termoskan instrument onboard the Phobos '88 spacecraft acquired the highest-spatial-resolution thermal data ever obtained for Mars [1–3]. Included in the thermal images are 2 km/pixel midday observations of several major channel and valley systems (see Fig. 1), including significant portions of Shalbatana Vallis, Ravi Vallis, Al-Qahira Vallis, Ma'adim Vallis, the channel connecting Valles Marineris with Hydraotes Chaos, and channel material in Eos Chasma. Termoskan also observed small portions of the southern beginnings of Simud, Tiu, and Ares Valles and some channel material in Gangis Chasma. Simultaneous broad band visible data were obtained for all but Ma'adim Vallis. Here we present new results that go beyond the analysis presented in [4].

We find that most of the channels and valleys have higher inertias than their surroundings, consistent with Viking IRTM-based thermal studies of martian channels [e.g., 5–8]. We see for the first time that thermal inertia boundaries closely match all flat channel floor boundaries. Combining Termoskan thermal data, relative observations from Termoskan visible channel data, Viking absolute bolometric albedos from [9], and a thermal model of the Mars surface based upon [10], we have derived lower bounds on channel thermal inertias. Lower bounds on typical channel thermal inertias range from 8.4 to 12.5 (10^{-3} cal cm^{-2} $s^{-1/2}$ K^{-1}) (352 to 523 in SI units). Lower bounds on inertia differences with the surrounding heavily cratered plains range from 1.1 to 3.5 (46 to 147 in SI units).

Atmospheric and geometric effects are not sufficient to cause the inertia enhancements. We agree with previous researchers [5,6,8] that localized, dark, high inertia areas within channels are likely eolian in nature. However, the Termoskan data show that eolian deposits do not fill the channels, nor are they responsible for the overall thermal inertia enhancement, contrary to the IRTM-based conclusions of [6] and [8]. Thermal homogeneity and strong correlation of thermal boundaries with the channel floor boundaries lead us to favor noneolian overall explanations.

Higher inertia channel floors do not appear to be associated with catastrophic flood channels, although very few of these were observed. Eastern Ravi and southern Ares Vallis are the only two major channel segments observed that are not thermally distinct. They do not have flat floors. In contrast, channel floor inertia enhancements are strongly associated with channels showing fret-

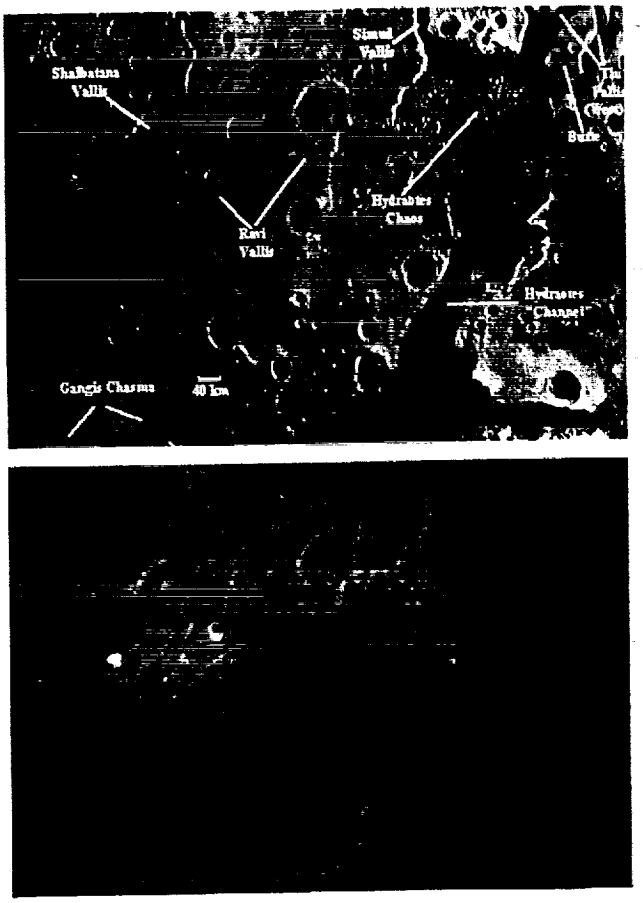

Fig. 1. Termoskan thermal (top) and visible (bottom) images centered approximately upon 1°S, 39°W. North is top. In the thermal image, darker is cooler. Shalbatana, Simud, and Tiu Valles all continue for several hundred kilometers north of this image. Note the cool and generally uniform floors of all channels except the eastern (and rough floored) end of Ravi Vallis. The thermal boundaries closely match the boundaries of the channel floors and depart significantly from albedo boundaries seen in the visible image. Note also the dark, presumably eolian deposits localized within the southern portions of Shalbatana Vallis and the southwestern portion of Hydraotes Chaos and spreading onto the surrounding plains in both cases. Buttes within the channels appear similar in temperature and appearance to the surrounding plains, not the channels. See, for example, the butte in the northeast corner of the image.

ting morphologies such as wide, flat floors and steep, scalloped walls. Therefore, we favor fretting processes over catastrophic flooding for explaining the inertia enhancements. Fretting may have emplaced more blocks on channel floors or caused increased bonding of fines due to increased availability of water. Alternatively, postchannel formation water that was preferentially present due to the low, flat fretted floors may have enhanced bonding of original fines or dust fallout.

Extended areal coverage from future missions will determine whether fretting is globally associated with enhanced channel floor inertias. In addition, future missions will be able to distinguish between our hypotheses for the small-scale causes of the inertia enhancements. Finally, we note that thermally distinctive channel floors represent interesting locations for future landers due to their unique history and the probable surface presence of material from various stratigraphic layers and locations.

References: [1] Murray B. C. et al. (1991) *Planetary and Space Science, 39, 1/2,* 237–265. [2] Selivanov A. S. et al. (1989) *Nature, 341,* 593–595. [3] Betts B. H. (1993) Ph.D. thesis, Caltech. [4] Betts B. H. and Murray B. C. (1993) *LPS XXIV,* 103–104. [5] Christensen P. R. and Kieffer H. H. (1979) *JGR, 84,* 8233–8238. [6] Zimbelman J. R. (1986) in *Symposium on MECA,* 112–114, LPI. [7] Zimbelman J. R. and Leshin L. A. (1987) *Proc. LPSC 17th,* in *JGR, 92,* E588–E596. [8] Craddock R. A. et al. (1988) *LPSC XIX,* 215–216. [9] Pleskot L. K. and Miner E. D. (1981) *Icarus, 45,* 179–201. [10] Clifford S. M. et al. (1987) Lunar and Planetary Institute.

55-91 ABS. ONLY **N94-33195**

THE IMPORTANCE OF ENVIRONMENTAL CONDITIONS IN REFLECTANCE SPECTROSCOPY OF LABORATORY ANALOGS FOR MARS SURFACE MATERIALS.

J. Bishop[1], S. Murchie[2], S. Pratt[1], J. Mustard[1], and C. Pieters[1], [1]Brown University, Providence RI 02912, USA, [2]LPI, Houston TX 77058, USA.

Reflectance spectra are presented here for a variety of particulate, ferric-containing analogs to martian soil (Fe^{3+}-doped smectites and palagonites) to facilitate interpretation of remotely acquired spectra. The analog spectra were measured under differing environmental conditions to evaluate the influence of exposure history on water content and absorption features due to H_2O in these samples. Each of these materials contains structural OH bonded to metal cations, adsorbed H_2O, and bound H_2O (either in a glass, structural site, or bound to a cation). Previous experiments involving a variety of Mars analogs have shown that the 3-μm H_2O band in spectra of palagonites is more resistant to drying than the 3-μm H_2O band in spectra of montmorillonites [1]. Other experiments have shown that spectra of ferrihydrite and montmorillonites doped with ferric sulfate also contain sufficient bound H_2O to retain a strong 3-μm band under dry conditions [2,3]. Once the effects of the environment on bound water in clays, oxides, and salts are better understood, the hydration bands measured via reflectance spectroscopy can be used to gain information about the chemical composition and moisture content of real soil systems. Such information would be especially useful in interpreting observations of Mars where subtle spatial variations in the strengths of metal-OH and H_2O absorptions have been observed in telescopic [4] and ISM [5,6] spectra.

Experimental Procedures: We measured bidirectional reflectance spectra of several Mars soil analogs under controlled environmental conditions to assess the effects of moisture content on the metal-OH and H_2O absorptions. The samples analyzed include chemically altered montmorillonites, ferrihydrite, and palagonites from Hawaii and Iceland. Procedures for preparation of the cation-exchanged montmorillonites, ferric-salt doped montmorillonites, and ferric oxyhydroxides are described in detail elsewhere [2,3].

One set of experiments involved desiccating the samples by heating. Reflectance spectra were measured initially for these samples under humidified conditions and under N_2 purged of H_2O and CO_2. The samples were then heated in an oven to 175°C at a rate of 1°C/min, cooled in a desiccator and measured again. This procedure was repeated for heating the samples to 275°C. Water contents for these samples were measured independently using thermal gravimetric analysis.

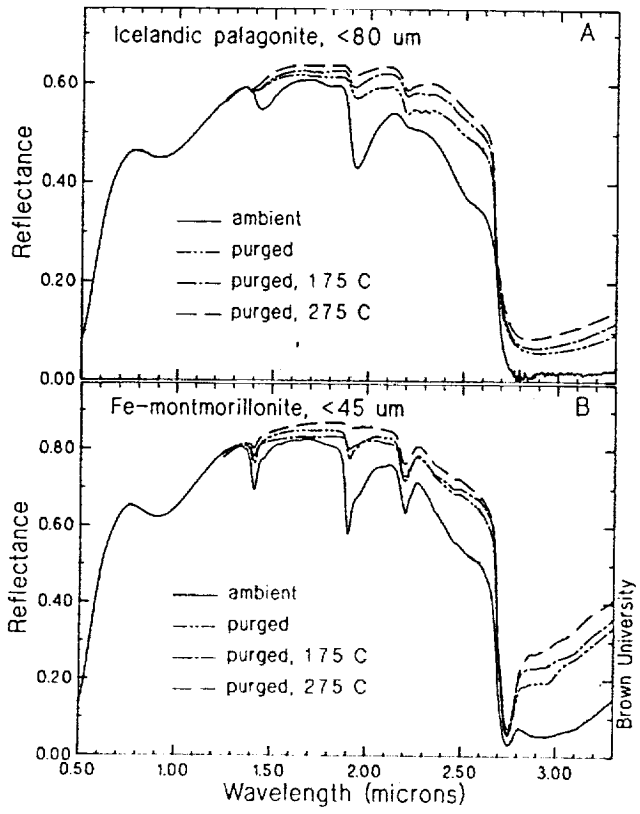

Fig. 1. Reflectance spectra 0.5–3.3 μm. (a) Icelandic palagonite; (b) Fe^{3+}-doped montmorillonite.

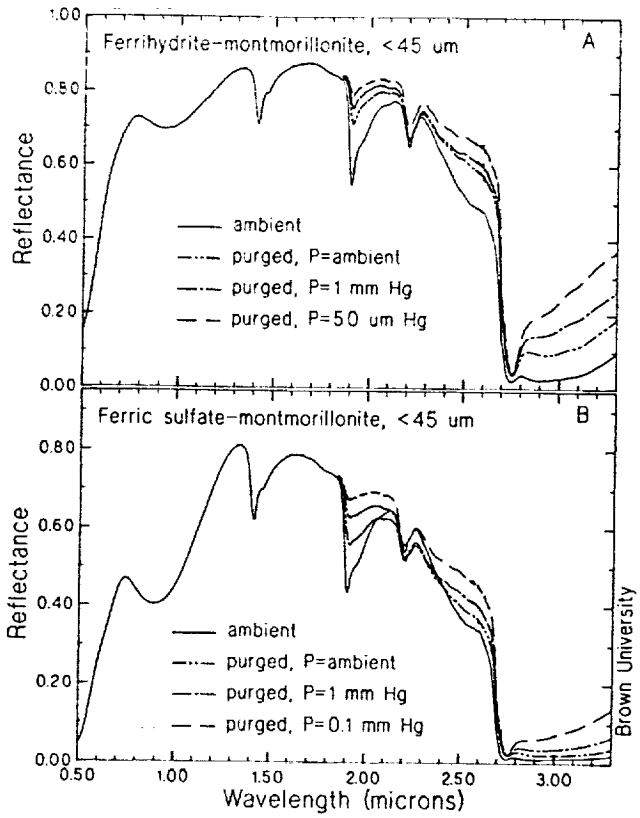

Fig. 2. Reflectance spectra 0.5–3.3 μm. (a) Ferrihydrite-doped montmorillonite; (b) ferric-sulfate-doped montmorillonite.

A second set of experiments involved drying the samples by reducing the atmospheric pressure in an environment chamber. Reflectance spectra were measured first for each sample under ambient pressure, and then under successively reduced atmospheric pressures to as low as ~10 μm Hg (10^{-5} bar).

Results: Reflectance spectra from 0.5 to 3.3 μm are shown in Fig. 1 for Icelandic palagonite and Fe^{3+}-doped montmorillonite. These spectra were measured under humidified conditions, after exposure to dry N_2, and after heating to 175°C and 275°C. The H_2O and structural OH absorptions in palagonites and montmorillonites are affected differently by drying in this manner. The broad 3-μm band observed in the montmorillonite spectra measured under humid conditions changes upon desiccation to a sharp feature at 2.75 μm, due to structural OH, and weaker features in the 2.8–3.3-μm region due to bound interlayer water. Most of the adsorbed water in montmorillonites is removed by flowing dry N_2 over the samples or by heating to less than 175°C. The overall band shape in the palagonite spectra does not change significantly with drying, although the strength of the 3-μm band continued to decrease with heating up to 275°C.

The montmorillonite spectra show absorptions at 1.41 μm and 1.91 μm under humid and arid conditions; however, the shoulders at 1.45 μm and 1.96 μm due to adsorbed water are only observed in the ambient spectrum. The intensity of these H_2O features near 1.4 μm and 1.9 μm are greatly subdued after desiccation in the spectra of smectites and palagonites. The water combination band occurs at 1.93 μm in the ambient palagonite spectrum and at 1.91 μm in the spectrum after heating to 275°C. A shift toward shorter wavelength upon drying is also observed for the absorption near 1.4 μm in the palagonite spectra.

Reflectance spectra are shown in Fig. 2 from 0.5 to 3.3 μm for ferrihydrite-doped montmorillonite and ferric-sulfate-doped montmorillonite. The spectra shown were measured under ambient conditions, and purged of H_2O and CO_2 under dry N_2 at 1-bar pressure and finally under successively reduced atmospheric pressures. The broad 3-μm H_2O feature in the reflectance spectra of the ferric-sulfate-doped montmorillonite and ferrihydrite (not shown) remains strong after exposure to extremely drying conditions, while this band is suppressed under the same drying conditions in the spectra of the ferrihydrite-doped montmorillonite and other montmorillonites (not shown). Suppression of the 1.9-μm feature is observed for each of these samples upon desiccation.

Discussion and Conclusions: As seen in Figs. 1 and 2, reflectance spectra of each of these analog materials measured under humid conditions exhibit prominent infrared absorptions due to molecular H_2O. However, analog materials studied under more Mars-like environmental conditions tend to fall into two groups: those that retain a strong 3-μm band, and those that do not. This depends on the type of bonding of the H_2O in these materials. Those that lose a large proportion of the 3-μm band intensity upon mild heating or drying

contain H_2O physisorbed on grain surfaces or interlayer surfaces in smectites (see Figs. 1b and 2a). Other materials that retain a large amount of water, as seen by a strong 3-μm band under dry conditions (e.g., at temperatures above ~150°C, or pressures below ~1 mm Hg) contain H_2O that is bound in the structure (see Figs. 1a, 2b, and ferrihydrite spectrum [3]). In the ferric-sulfate-doped montmorillonites water forms strong bonds to the sulfate ions because of its highly polarizing nature [7].

The hydration feature near 1.9 μm is a combination of the H_2O vibrations at ~3 μm and ~6 μm, and is also affected by the environmental conditions and the type of H_2O bonding. The band strength and energy of this feature in spectra of smectites is dependent as well on the interlayer chemistry [3]. An important application to Mars is that a ferric montmorillonite in a dry environment would have a relatively weak 1.9-μm feature that is difficult to observe in Mars spectra.

In conclusion, we would like to stress the importance of considering environmental conditions when measuring infrared spectra of laboratory samples as analogs for Mars surface materials. The strength and character of features due to molecular water (~1.4, ~1.9, ~3, and ~6 μm) in the spectra of clays, palagonites, and hydrated minerals are especially sensitive to the moisture environment of the samples. These features are influenced by the exposure history (atmospheric temperature, pressure, and composition) of the samples, as well as the environmental conditions at the time of measurement.

Acknowledgments: The authors would like to thank Dr. A. Basilevksy for contributing the palagonites used in this study. Support through the NASA Graduate Student Researchers Program and NASA grant NAGW-28 is much appreciated. RELAB is a multi-user facility supported by NASA under grant NAGW-748, and the Nicolet was acquired by a grant from the Keck Foundation.

References: [1] Bruckenthal (1987) M.S. thesis, Univ. of Hawaii. [2] Bishop et al. (1993) *LPS XXIV*, 115–116. [3] Bishop et al. (1993) *GCA*, in press. [4] Bell and Crisp (1993) *Icarus*, in press. [5] Murchie et al. (1993) *Icarus*, in press. [6] Bibring et al. (1989) *Nature, 341*, 591–592. [7] Bishop et al., this volume.

56-91 ABS. ONLY **N94-33196**

FERRIC SULFATE MONTMORILLONITES AS MARS SOIL ANALOGS.

J. L. Bishop[1], C. M. Pieters[1], and R. G. Burns[2], [1]Brown University, Providence RI 02912, USA, [2]Massachusetts Institute of Technology, Cambridge MA 02139, USA.

Spectroscopic analyses have shown that Fe^{3+}-doped smectites prepared in the laboratory exhibit important similarities to the soils on Mars [1,2]. Ferrihydrite in these smectites has features in the visible to near-infrared region that resemble the energies and band-strengths of features in reflectance spectra observed for several bright regions on Mars [3]. Ferric-sulfate-montmorillonite samples have been prepared more recently because they are a good compositional match with the surface material on Mars as measured by Viking [4]. Reflectance spectra of montmorillonite doped with ferric sulfate in the interlayer regions include a strong 3-μm band that persists under dry conditions [5,6]. This is in contrast to spectra of similarly prepared ferric-doped montmorillonites, which exhibit a relatively weaker 3-μm band under comparable dry environmental conditions. Presented here are reflectance spectra of a suite of ferric-sulfate-exchanged montmorillonites prepared with variable ferric sulfate concentrations and variable pH conditions.

Experimental Procedures: The Na and Ca interlayer cations in SWy-1 montmorillonite (Clay Mineral Society, Source Clays Repository) were exchanged with 0.5 N ferric sulfate solution in the clay suspension at pH 1.6–1.8 after titration with dilute HCl. The pH was raised dropwise with dilute NaOH to at least 3.0 in order to retain the ferric sulfate in the montmorillonite interlayer regions. The suspensions were then centrifuged and lyophilized to form a fine powder, which was dry sieved to <45 μm.

Biconical reflectance spectra were measured relative to a rough gold surface using a Nicolet 740 FTIR in a H_2O- and CO_2-purged environment. A PbSe detector was used from 0.9 to 3.2 μm and a DTGS detector from 1.8 to 25 μm. Bulk powdered samples are measured horizontally in this system. Spectra are averaged from two locations on each of two replicates for each kind of sample.

Additional bidirectional spectra were measured relative to Halon from 0.3 to 3.6 μm using an InSb detector under ambient conditions with the RELAB (reflectance experiment laboratory) spectrometer at Brown University. A detailed description of this instrument is provided elsewhere [7].

Results: Reflectance spectra (0.3 μm–3.5 μm) of natural and chemically altered SWy montmorillonite and ferrihydrite measured under dry (H_2O- and CO_2-purged) conditions are shown in Fig. 1.

The spectra of each of these ferric-bearing materials exhibits absorptions in the visible region near 0.5 μm and 0.9 μm, an inflection near 0.6 μm, and a reflectance maxima near 0.74 μm, although physical and chemical constraints on the Fe^{3+} sites in each mineral structure influence the exact energy of the crystal field transitions. The strengths of these electronic transitions are stronger in the ferric-sulfate-exchanged montmorillonites than in the other ferric-bearing materials shown in Fig. 1.

The spectra of each of these samples contain an absorption near 2.75 μm due to OH bound to cations in the structure, and an absorption near 3.0 μm due to H_2O bound to Fe^{3+} in the interlayer regions, H_2O bound to sulfate anions, or H_2O adsorbed on the grain surfaces. The ferric-sulfate-containing samples exhibit a much stronger absorption near 3 μm and a much stronger 1.96-μm shoulder than both the ferrihydrite and the ferrihydrite-montmorillonite.

Reflectance spectra are shown in Fig. 2 (0.3 μm–1.1 μm) for telescopic spectra of Mars [8], ferrihydrite-montmorillonite, and ferric sulfate-montmorillonite. This ferric sulfate-montmorillonite spectrum is that with the weakest 0.9-μm and 3-μm absorptions from Fig. 1. The spectra are scaled at 0.75 μm to facilitate comparison of the spectral features.

Room-temperature Mössbauer spectra of the ferrihydrite-montmorillonite and ferric sulfate-montmorillonite are very similar; a doublet is observed with quadrupole splitting less than 1 mm/s. However, the Mössbauer spectra measured at 4.2 K exhibit a field strength of ~46 T for the ferric sulfate-montmorillonite and a field strength of ~48 T for the ferrihydrite-montmorillonite. The differences in field strengths of these two samples are sufficient to distinguish among them. The ferric sulfate species in the ferric sulfate-montmorillonite is also distinct from jarosite, which has a field strength of ~49 T. Asymmetry in the peaks of the sextet in the low-temperature Mössbauer spectra of the ferric sulfate-montmorillonite may indicate that multiple ferric phases are present.

Discussion: The intensity of the 0.9-μm absorption increased with ferric sulfate concentration as expected, but tends to be stronger in general than the 0.9-μm absorption in the ferrihydrite-montmorillonite. The band center for the ferric sulfate-montmorillonite occurs

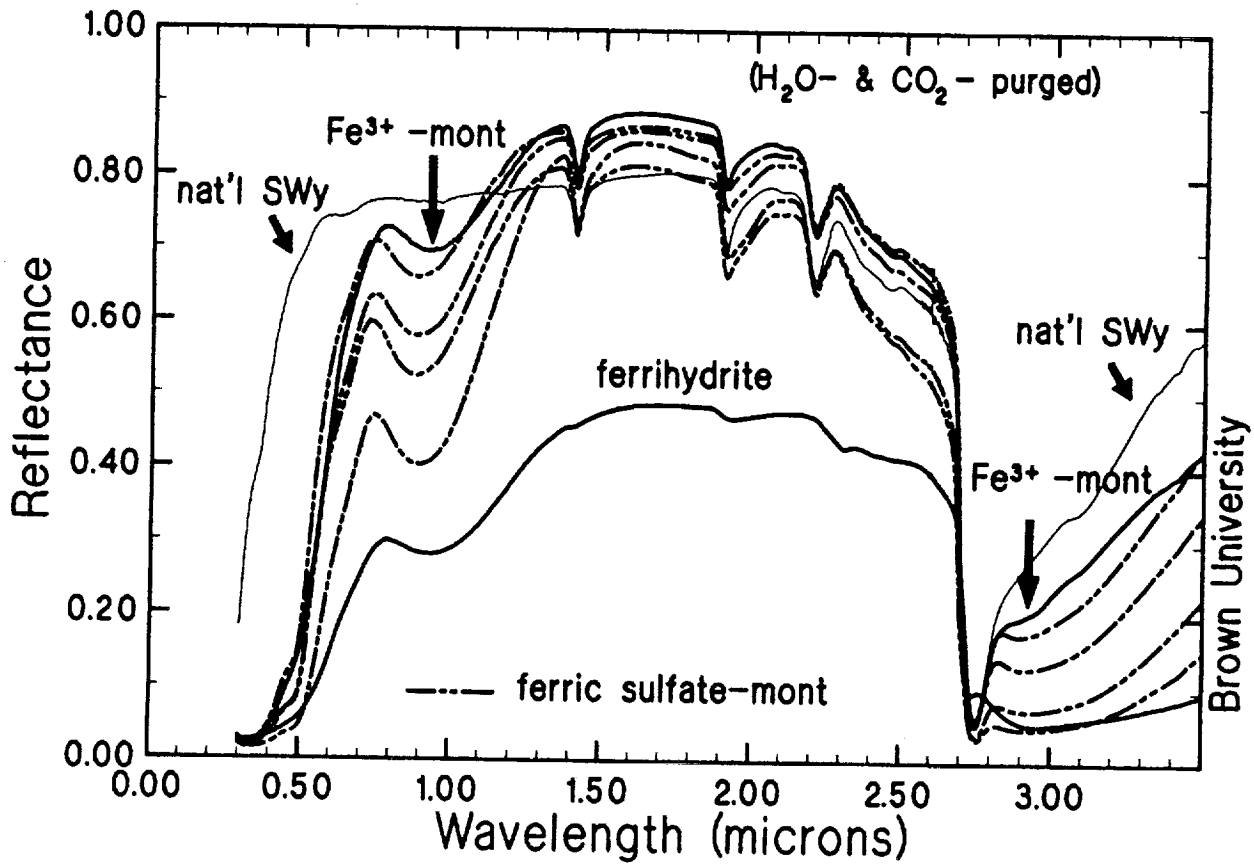

Fig. 1. Reflectance spectra (0.3–3.5 μm) are shown in solid lines for natural SWy montmorillonite, ferric-doped montmorillonite and ferrihydrite. Preparation of these samples is described in [2]. Spectra of four ferric-sulfate-doped montmorillonites are shown in broken lines. Increasing intensity of the spectral absorptions at 0.9 μm and 3 μm is observed with increasing concentration of ferric sulfate in the montmorillonite interlayer regions.

at 0.88–0.89 μm, regardless of concentration or pH, which is a slightly shorter wavelength than that observed for the ferrihydrite-montmorillonite. The reflectance maxima varied from 0.725 μm for the ferric sulfate-montmorillonites prepared under pH ~3.0 to 0.745 μm for the ferric sulfate-montmorillonites prepared under pH ~4.0. Telescopic spectra of many regions on Mars exhibit similar visible spectral characteristics: a shoulder near 0.6 μm, a reflectance maxima near 0.74 μm, and an absorption band near 0.9 μm [3,8].

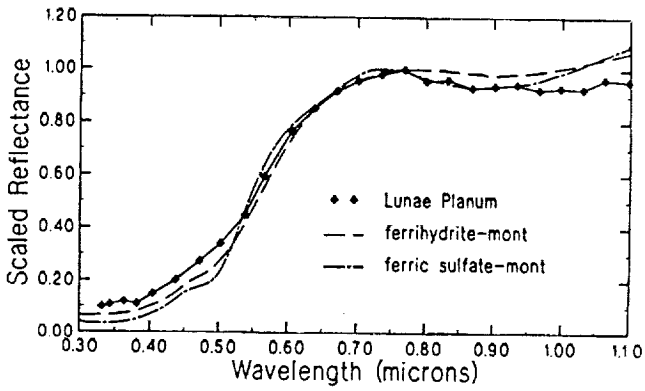

Fig. 2. Reflectance spectra of Mars and Mars analogs.

The intensity of the 1.96-μm and ~3-μm features in the ferric sulfate-montmorillonite spectra increased with increasing ferric sulfate concentration and increasing pH. The ferric sulfate-montmorillonite spectrum with the strongest 3-μm absorption in Fig. 1 was also examined under extremely dry conditions; these spectra retain a strong 3-μm band [6]. The SO_4^{2-} is highly polarizing and binds rather tightly to the interlayer water molecules in the montmorillonite. The magnitude of the H_2O absorptions may also be enhanced due to strong polarization of the H_2O molecules by the sulfate anions.

Conclusions: Montmorillonites doped with ferric sulfate compare well with the surface material on Mars with respect to the chemical composition and reflectance spectra in the visible to infrared. These analogs are especially promising because of the shape of the visible features and the strength of the 3-μm band.

Acknowledgments: Support through the NASA Graduate Student Researchers Program and NASA grants NAGW-28 and NAGW-2220 is much appreciated. RELAB is a multi-user facility supported by NASA under grant NAGW-748, and the Nicolet was acquired by a grant from the Keck Foundation.

References: [1] Banin and Rishpon (1979) *J. Molec. Evol., 14*, 133–152. [2] Bishop et al. (1993) *GCA*, in press. [3] Bell et al. (1990) *JGR, 95*, 14447–14461. [4] Clark et al. (1982) *JGR, 87*,

10059–10067. [5] Bishop et al. (1993) *LPS XXIV*, 115–116. [6] Bishop et al., this volume. [7] Mustard and Pieters (1989) *JGR*, 92, 10376–10390. [8] McCord et al. (1977) *Icarus*, *31*, 25–39.

57-91 ABS. ONLY

N94-33197

CONSTRAINTS ON THE MARTIAN CRATERING RATE IMPOSED BY THE SNC METEORITES AND VALLIS MARINERIS LAYERED DEPOSITS. J. E. Brandenburg, Research Support Instruments, Alexandria VA, USA.

P. 3

Introduction: Martian Cratering Rate and Mars Past: The rate at which craters form on the martian surface is a crucial parameter for understanding the geologic history of that planet. However, until samples can be returned from known locations on Mars, the rate of cratering cannot be correlated accurately with geologic ages but must be estimated. In this paper an attempt is made to use two separate bodies of data that seem incongruous with currently accepted models for correlating cumulative crater densities with geologic ages: the measured depths of the interior layered deposits in the Candor Chasma region [1] and nearby areas of the Vallis Marineris system and the measured cosmic ray exposure times and crystallization ages of the SNC meteorites [2], to constrain estimates of the martian cratering rates. That is, rather than considering these two bodies of data to represent special or peculiar circumstances in conventional cratering age schemes, we instead assume they represent conventional circumstances and attempt to find what adjustments to present cratering-age correlation models are required for the models to be reconciled. The preliminary results of this study indicate that the interior layered deposits,which may be lake sediments dating from the "liquid water era" on Mars (the period when large amounts of liquid water apparently helped shape the planets surface), and the SNC meteorites, which are believed to represent samples of the martian surface carried to Earth by one or several impacts on the martian surface, independently constrain the past martian cratering rate to be many times the past lunar cratering rate.

Several models for correlating geologic ages with cumulative crater densities have been proposed [3,4]. These models assume that the rate of crater formation has varied in time beginning with an intense period of bombardment shortly after the formation of the planet followed by a period of lower cratering rate in the later periods of planetary history. The models differ principally in their assumed rate of cratering in this later period. These rates are usually represented as being a multiple of the lunar rate of cratering, the Moon being the one planetary surface where cratering history has been preserved and from which samples have been returned. The models of Neukum and Hiller [5] are most illustrative of this type of model and demonstrate that if the rates of martian cratering are assumed to be 1, 2, and 3× the lunar rate (Neukum and Hiller models I, II, and III respectively, hereafter referred to as NHI, NHII, and NHIII) then the picture of Mars varies dramatically. The difference between the history of Mars under NHI and NHIII is the difference between a planet whose climate was Moon-like and one that was Earth-like for much of its history (see Fig. 1).

Under NHI the cratering rate is assumed to be lunar, and the erosive rate must be low to give the observed cumulative crater densities. What results is a very lunar set of ages for many martian surface formations, and an age for most water channels that is very old, indicating that Mars must have had a dense Earth-like atmosphere and temperatures for only a geologically brief period of 1 b.y. This means that most liquid-water-produced features must have ages of 3.5 b.y. and mean surface ages of approximately 3.0 b.y. However, under NHII Mars was a dynamic changing planet for most of its history, with the liquid water era and vigorous channel formation lasting until late in the planet's history. The effect of the 2× lunar cratering rate assumed under NHII is not only to make the mean age of large areas of the martian surface younger but also to increase the variation of ages. This occurs because (1) the ages of many surface formations that were formerly confined to a narrow range of ages between 3 b.y. and 4.5 b.y. are now expanded across the span of martian history, and (2) the model is consistent with an Earth-like climate for Mars for much of its history, allowing free movement of liquid water across its surface. The model NHII is thus consistent with water-formed features late in the planet's history and a mean surface age of approximately 2 b.y. The consistency of NHII and the even more extended model NHIII with late water-formed features allows features such as the Candor Chasma layered sediments to be accommodated easily without recourse to special models.

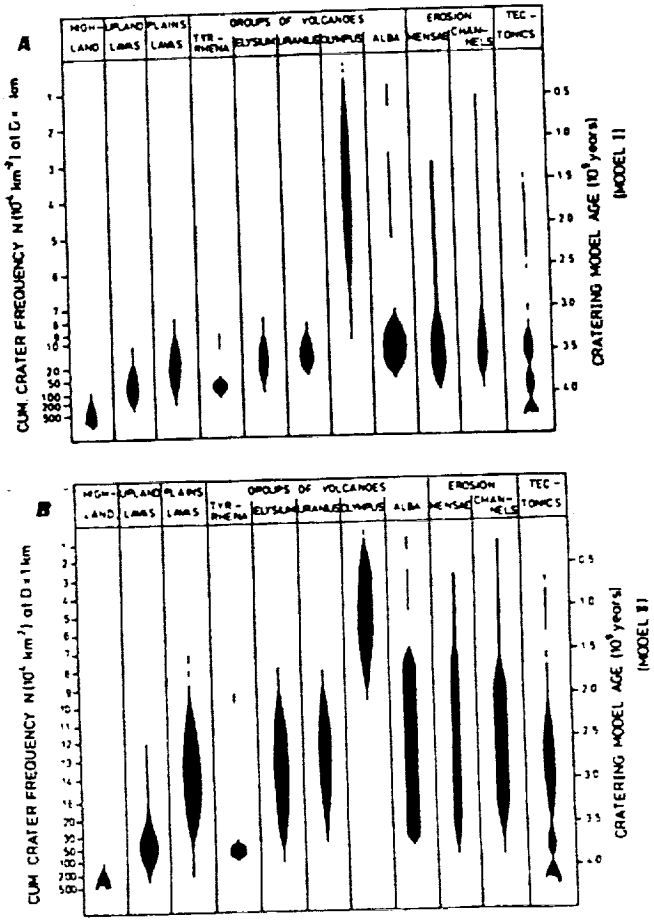

Fig. 1. (a) Neukum-Hiller model I: Mars cratering rate same as for the Moon. (b) Neukum-Hiller model II: Impact fluxes factor of 2 higher than on the Moon.

Layered Deposits of Candor and Associated Chasmas of Vallis Marineris: The interior layered deposits seen extensively

in the Candor, Ophir, and Hebe Chasmas of the Vallis Marineris postdate the canyon system and appear roughly contemporary with the formation of the Tiu and Simud outflow channels [3], which are proposed to result from catastrophic floods. Thus the period of formation appears to coincide with a period where large quantities of water could move freely across the martian surface. The interior deposits themselves appear to be lacustrine, and because of their extensive lateral continuity, suggest deposition over a long period in a quiescent, low-energy aqueous environment, despite the fact that lava intrusions may have occurred periodically into the lake bottoms, since evidence of lava intrusion is seen in nearby Chasmas [5]. Because of these considerations it seems likely the interior layered deposits were formed during a time when liquid water was a thermodynamically stable state on the martian surface rather than being a peculiar circumstance of a nonequlibrium resection preserved under a thick ice sheet from an atmosphere in which it would boil away explosively once exposed. Thus the conditions of formation of the interior layered deposits seem most easily accommodated by conditions of atmospheric pressure approaching 1 bar.

The interior deposits are estimated to be approximately 5 km thick over large areas, implying they were emplaced over a long geologic period. These sedimentary depths are quite thick by terrestrial standards, where sedimentary depths average approximately 2 km and usually represent roughly 0.5 b.y. A terrestrial analog to the lacustrine origin for layered deposits is the Green River Formation [6] in the Wyoming-Utah area, where sediment depths reach 1 km and were believed to have formed over 4 m.y. for a deposition rate of 0.25 km/m.y. A Green River Formation analog gives an estimated deposition period of 20 m.y. for the layered deposits. This is a rapid buildup of sediments but is consistent with rates in terrestrial basins. An upper bound on this period of deposition, using an analog perhaps more in keeping with a low-energy environment, would be found in deep-ocean red clay sediment deposition [7]. The rate of this deep-ocean deposition is much slower, 3 km/b.y. The period of interior layered deposit deposition can thus be estimated between 20 m.y. to 1.5 b.y. based on Earth analogs. Accordingly, the interior layered deposits appear to suggest a geologically significant period of time when large bodies of liquid water could be stable on the martian surface. Since this coincides with the periods of catastrophic flooding into Chryse Planitia, this does not seem unreasonable; however, the floods were apparently geologically short-lived events, whereas the layered deposits were apparently formed over a long geologic period of apparently stable conditions.

The problem the interior layered deposits create in cratering chronologies based on 1× lunar cratering rates is that the layered deposits postdate the formation of the Vallis Marineris canyon system or at least major portions of it, and the Marineris system apparently dates from the middle to late period of martian history. This means that for a period of the order of 0.02–1.5 b.y. during the middle to late period of martian history, ages 2.5–1.0 b.y., large lakes could apparently exist and quiescently collect sediment. Unless recourse is made to special geologic and thermodynamic circumstances, interior layered deposits thus indicate that the period of dense warm atmosphere favorable to liquid water, believed to have existed in the Noachian Era, persisted until at least the early Amazonian and possibly the middle Amazonian. Such conditions are only consistent with cratering chronologies assuming ≤2× lunar crater rates on Mars. Thus the existence and properties of the interior layered deposits in the Candor and nearby Chasmas appear to constrain the assumed cratering rates to be much higher than lunar and thus much more consistent with NHII or perhaps even NHIII. Other independent constraints exist that suggest a similar requirement.

SNC Meteorites and Martian Cratering Flux: The discovery of the martian origin for the SNC meteorites at this point in our exploration of Mars has been extremely fortunate and may strongly effect the course of future Mars studies. Enough is known about Mars at this time from remote sensing to define major questions (for example, what was the volatile inventory, what is the average age of the martian surface, and how widespread was martian volcanism) so that the sudden availability of probable samples of the martian surface can make a major contribution to our understanding. Most major contributions to knowledge in a particular subject come as a surprise, and the data from the SNC meteorites are certainly surprising; the SNC data seem to indicate that the mean surface age of Mars appears to be much younger than previously supposed.

It is now believed that the SNC meteorites represent the result of at least three separate events on Mars [8], and may thus be a representative sampling of the martian surface. They differ in composition but are essentially basaltic and most show little shock damage. They were all ejected recently in geologic time, having cosmic ray exposure times from 0.5 m.y. to 11 m.y. Thus, they were apparently ejected from Mars by meteor impacts of large energy on that planet and became part of a general population of small bodies on chaotic orbits in Mars-Earth space before finally being swept up by the Earth. The brevity and variety of the cosmic ray exposure ages tells us that energetic impacts are probably much more frequent on Mars than previously supposed. However, a more direct method by which the SNCs argue for a higher cratering rate on Mars is that the crystallization ages are so much lower than expected.

If the SNC meteorites are truly martian and represent multiple events, as seems most likely, then their crystallization ages, which vary from 1.3 b.y. to 160 m.y., suggest that the mean surface age for Mars is on the order of 1 b.y. This is an enormous difference from the ~3.0 b.y. that is presently estimated using 1× lunar cratering flux, and suggests that the Mars cratering rate is several times this number, possibly 2 or even higher. Thus, NHII and NHIII are the only recent models that come close to providing the mean surface age required by the SNCs.

The fact that the SNC data forces an upward revision of the martian cratering flux is a robust result that is fairly insensitive to assumptions about the number of impacts ejecting SNC material. The model of ejection of the SNC material by one large impact [9] on a region of young lava suffers from the lack of a large recent crater on the Tharsis formations [10], thought to be the youngest lavas on Mars. Large craters have been found, and a large one is required to account for such a considerable amount of varied samples and breadth of exposure ages; however, the crater must itself be crater dated using an assumed rate of cratering. This means the only way to reconcile the recent ejection of the SNC material, in single event, with the large number of craters found in the ejection candidate impact basins is to dramatically revise the cratering rate upward. If one instead assumes that one of the smaller impact basins may have been the point of origin for the SNCs, then the number of candidate impact basins multiplies, the variation in SNC compositions becomes troublesome, and the single-impact theory becomes hard to justify.

Therefore, if the SNCs come from multiple impacts, they force the mean surface age downward, because if they are multiple they form

representative samples of the crust and crystallized recently; if they are from a single impact in young lavas, they force the large crater ages downward, because they were ejected recently. In either case the cratering rate must move upward to produce the required downward shift in ages of the surface areas of interest. Finally, the very fact that recent impacts on Mars have transported comparable or even larger masses of martian material to Earth than has been transported from the Moon (the ratio of SNC to lunar meteorite recovered masses is quite large) reinforces the suggestion that the martian cratering rate must be many times lunar, though it is difficult to quantify this latter argument at this time. In any case, the simplest SNC scenario, that the SNCs were ejected by multiple events, appears only reconcilable with the NHII model or even higher cratering rate models.

Summary: Therefore, following two independent lines of evidence—estimates of the age and formation time of a portion of the martian geologic colunn exposed in the layered deposits and the crystallization and ejection ages of the of the SNC meteorites—it appears that the martian cratering rate must be double the lunar rate or even higher. This means models such as NHII or NHIII, which estimate the martian cratering rate as being several times lunar, are probably far closer to reality on Mars than lunar rates. The effect of such a shift is profound: Mars is transformed from a rather Moon-like place into a planet with vigorous dynamics, multiple large impacts, erosion, floods, and volcanism throughout its history.

A strong shift upward in cratering rates on Mars apparently solves some glaring problems; however, it creates others. The period of time during which Earth-like atmospheric conditions existed, the liquid water era on Mars, persists in NHIII up to only 0.5 b.y. ago. Scenarios of extended Earth-like conditions on Mars have been discounted in the past because they would have removed many of the craters from the early bombardment era found in the south. It does appear that some process of crater removal was quite vigorous in the north during Mars' past. Evidence exists that the northern plains may have been the home of long-lived seas [11] or perhaps even a paleo-ocean [12], so models exist for highly localized destruction of craters in the north. However, the question of how the ancient crater population could be preserved in the south under a long liquid-water era found in any high-cratering-rate models is a serious question that must be addressed. It does appear to be a higher-order problem because it involves low-energy dynamics acting in localized areas, i.e., erosion of craters in the south of Mars, whereas the two problems with the low-cratering-rate models involve high-energy events acting over large areas: the formation of the Vallis Marineris, the SNC ejecting impacts, and the global atmospheric pressure and temperature conditions that allow liquid water to exist as a robust entity anywhere on the martian surface.

In any case, it appears Mars is a more complex and dynamic planet than previously supposed. It has canyons dating from the middle to late period of its history that contain apparent lake sediments bedded deeper than most sediments on Earth. Recent multiple, violent impacts on Mars have apparently provided us with multiple random samples of its surface that all crystallized less than 1.5 b.y. ago. These things cannot be accommodated in our present cratering chronologies of Mars, based on 1× lunar cratering rates, without great difficulties. These difficulties suggest that a new chronology, probably based on NHII or even NHIII, should be adopted; this new chronology will provide us with a new view of Mars as a dynamic planet of rich history.

References: [1] Nedell S. S. and Squyres S W. (1986) *LPI Tech. Rpt. 87-01*, 20–23. [2] McGetchin T. R et al. (1981) *BVSP*, 1246–1254, Pergamon. [3] Masursky H. et al. (1977) *JGR, 82*, 4016–4038. [4] Neukum G. and Greely R. (1988) *LPS XIX*, 852–853. [5] Lucchitta B. K. (1987) *Science, 235*, 565–567. [6] Blatt H. et al. (1980) *Origin of Sedimentary Rocks*, 645, Prentice Hall. [7] *Origin of Sedimentary Rocks*, 32. [8] Bannin A. et al. (1992) *in Mars* (H. Hugh et al., eds.), 610–611, Tucson. [9] Vickery A. M. and Melosh H. J. (1987) *Science, 237*, 738–743. [10] Klause K. et al. (1992) *JGR*, 97, 10213–10225. [11] Parker T. J. et al. (1986) *LPI Tech. Rpt. 87-01*, 96–97. [12] Brandenburg J. E. (1986) *LPI Tech. Rpt. 87-01*, 20–23.

N94-33198

DEPOSITION RATES OF OXIDIZED IRON ON MARS. R. G. Burns, Department of Earth, Atmospheric and Planetary Sciences, Massachusetts Institute of Technology, Cambridge MA 02139, USA.

Introduction: The reddened oxidized surface of Mars is indicative of temporal interactions between the martian atmosphere and its surface. During the evolution of the martian regolith, primary ferromagnesian silicate and sulfide minerals in basaltic rocks apparently have been oxidized to secondary ferric-bearing assemblages. To evaluate how and when such oxidized deposits were formed on Mars, information about the mechanisms and rates of chemical weathering of Fe^{2+}-bearing minerals has been determined [1,2]. In this paper, mechanisms and rates of deposition of ferric oxide phases on the martian surface are discussed.

Mechanisms of Oxidation of Ferrous Iron: Oxidation of Fe^{2+} ions derived from basaltic olivine, pyroxene, and sulfide minerals may have proceeded via several mechanisms. They include:

1. *Solid-state processes involving atmosphere-surface interactions that occur without the intervention of water.* However, the kinetics of such processes involving dry mineral surfaces are extremely slow, as testified by the negligible oxidation products observable in the Magellan radar images of the surface of Venus. Nevertheless, photochemical processes may have produced coatings of oxidants on outermost arid surfaces of Mars [3], which subsequently could influence redox reactions of Fe.

2. *Reactions that occur in an aqueous medium.* Such processes involving dissolved Fe include (a) oxidation of aqueous Fe^{2+} in groundwater by dissolved atmospheric O

$$Fe^{2+}_{(aq)} + 1/4\ O_{2(aq)} + 3/2\ H_2O \rightarrow FeOOH_{(s)}\downarrow + 2H^+ \qquad (1)$$

the O being derived from photolysis of CO_2 or water vapor in the atmosphere [4]; and (b) photochemical oxidation in UV light of either Fe^{2+} ions in acidic solutions [5,6]

$$Fe^{2+}_{(aq)} + 2H_2O \xrightarrow{\text{UV (<287 nm)}} FeOOH_{(s)}\downarrow + 2\ H^+ + 1/2\ H_{2(g)}\uparrow \qquad (2)$$

or FeOH+ complex ions in near-neutral pH or slightly alkaline solutions [4–7]

$$FeOH^+_{(aq)} + H_2O \xrightarrow{\text{UV light } \leq 366\text{ nm}} FeOOH_{(s)}\downarrow + H^+ + 1/2\ H_{2(g)}\uparrow \qquad (3)$$

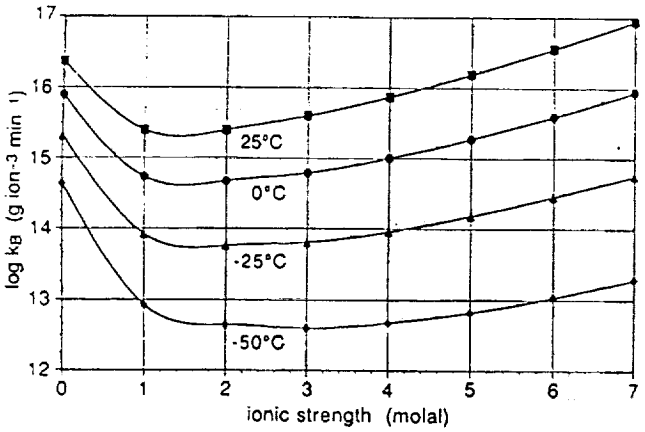

Fig. 1. Rate constants for the oxidation of dissolved Fe^{2+} ions as a function of ionic strength at different temperatures.

Note that gaseous H_2 is liberated in these photo-oxidation reactions (equations (2) and (3)), some of which could escape from the gravitational field of Mars, while O is retained by the martian regolith [8].

Before aqueous oxidation of Fe by reactions (1), (2), or (3) occurred on Mars, soluble ferrous iron had to exist in solution. These Fe^{2+} ions were produced by dissolution of silicates and sulfides that were initially present in basaltic rocks when they were exposed to permeating groundwater near the surface of Mars. Experimental data [2] show that in groundwater derived from the precipitation of acid rain (pH ≤ 4.5), basaltic minerals and glass dissolve rapidly, yielding a steady supply of aqueous Fe^{2+} ions. In less acidic and near-neutral pH groundwater, mineral dissolution would be much slower. For example, rates of dissolution of Fe from olivine and pyroxenes range from about 1400 ppm Fe m^{-2} yr^{-1} (pH 2 at 25°C) to 2×10^{-2} ppm Fe m^{-2} yr^{-1} (pH 6 at 0°C). In acidic ice-cold saline solutions (pH 4.5 at 0°C), dissolution rates are about 1 ppm Fe m^{-2} yr^{-1}.

Rates of Oxidation of Iron in Aerated Groundwaters: Rates of oxidation of aqueous Fe^{2+} ions by dissolved O are strongly influenced by acidity or pH, as well as salinity or ionic strength, temperature, and the concentration of dissolved O in aerated groundwater [2]. Rates of Fe^{2+} oxidation are slowest in acidic solutions, in contrast to dissolution rates of ferromagnesian silicates, but are much higher in near-neutral pH saline groundwater and brines. The rate-constant data illustrated in Fig. 1 show that the oxidation of dissolved Fe^{2+} initially decreases with rising ionic strength, but increases significantly in brine solutions. Figure 2 shows rates of oxidation of aqueous $Fe\%^{2+}$ in saline groundwaters saturated by atmospheric O corresponding to the present-day martian atmosphere ($P_{O2} = 10^{-5}$ bar) for a variety of temperatures and ionic strengths [2]. Rates of oxidation of dissolved Fe^{2+} in pH 6 groundwater range from about 500 to 1000 ppm Fe m^{-2} yr^{-1} in ice-cold saline solutions to about 100 ppm Fe m^{-2} yr^{-1} in low-temperature brine solutions. Such relatively low rates of oxidation of dissolved Fe on Mars contrast with the very high values for terrestrial rivers (1.8×10^7 ppm Fe m^{-2} yr^{-1} at pH 6 and 25°C) and for oxygenated deep ocean bottomwaters (5×10^6 ppm Fe m^{-2} yr^{-1} at pH 8.2 and 2°C). Thus, oxidation rates in slightly acidic brines that may might currently

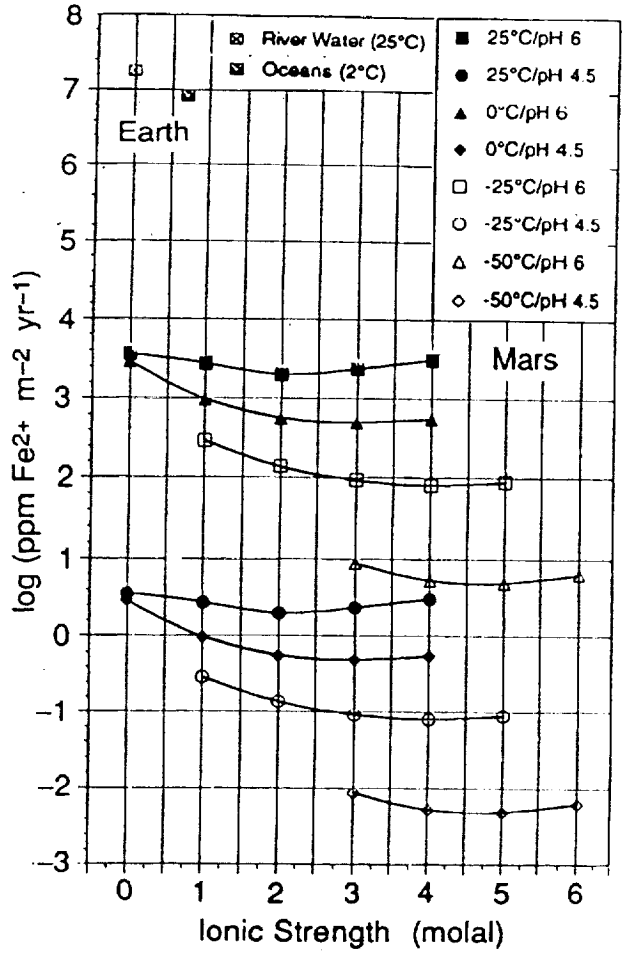

Fig. 2. Rates of oxidation of aqueous Fe^{2+} by dissolved atmospheric O as a function of ionic strength at different temperatures on Mars. Values for Fe^{2+} oxidation in terrestrial river water and oceans are also shown.

exist near the martian surface are about 10^5 times slower than those in the terrestrial hydrosphere. However, in summertime meltwaters in equatorial regions of Mars, rates of Fe^{2+} oxidation could be as high as 3000 ppm Fe m^{-2} yr^{-1}.

From a global viewpoint, the depth of weathering of surface basalts on Mars during dissolution and aqueous oxidation of Fe^{2+}-bearing minerals may be estimated as follows. Shergottites contain about 19 wt% FeO, or 3×10^{10} ppm Fe m^{-3}. Rates of oxidation of Fe^{2+} corresponding to 500–1000 ppm m^{-2} yr^{-1} indicate that weathering rates of shergottitic basalts on Mars were about 15–30 m b.y.$^{-1}$ when water flowed near the surface of the planet.

Deposition Rates in Aerated Water Basins on Mars: The annual deposition of hydrous ferric oxides in ocean basins on Mars may be calculated as follows. Oceanus Borealis is believed to have filled the northern plains of Mars episodically, covering an estimated area of 4×10^7 km^2 with an average depth of 1.7 km [9]. Assuming a rate of oxidation of aqueous Fe^{2+} in a cold, slightly acidic ocean to be in the range 500–1000 ppm Fe m^{-2} yr^{-1} (Fig. 2), the annual deposition of hydrous ferric oxides would have been ~2–4 × 10^{13}

g.Fe yr^{-1} in Oceanus Borealis. This quantity of Fe is comparable to the estimated deposition rate (2.25×10^{13} g.Fe yr^{-1}) in a typical Precambrian Fe formation on Earth [10]. The surges of water that periodically inundated the martian northern lowland plains in the past were probably initiated by increased volcanic activity that melted frozen regolith [9]. Such volcanism would also have provided fresh sources of basaltic glass and ferromagnesian silicate minerals that underwent submarine chemical weathering, thereby replenishing the supply of dissolved Fe^{2+} ions to be oxidized near the surface of intermittent martian oceans.

In addition to the circumpolar body of water in the northern hemisphere, other semipermanent locations of deep-water stratification may have provided sites for the deposition of hydrous ferric oxides on Mars. These include numerous impact basins (e.g., Hellas and Argyre) and several closed depressions in the Valles Marineris system [11]. The bright deposits littering the Argyre and Hellas Basins may comprise wind-blown dust derived from desiccated hydrous iron oxide-silica deposits that remained there after water had evaporated from these deep depressions.

Deposition Rates in UV Irradiated Surface Water: As indicated by equations (2) and (3), oxidation of aqueous ferrous iron to hydrous ferric oxides does not require dissolved atmospheric O. Dissolved ferrous iron may also be oxidized photochemically by solar UV radiation. In dilute, near-neutral pH solutions, rates of photo-oxidation of dissolved ferrous iron are increased by the presence of the complex $FeOH^+$ ion, which is sensitive to wavelengths in the 300–400-nm region [4,6]. Calculations of oxidation rates by solar UV have been made for the early Earth. In areas of vigorous upwelling in ocean basins containing 0.5–5.5 ppm total dissolved Fe, photo-oxidation could have precipitated hydrous ferric oxides at rates of $1–2 \times 10^6$ ppm Fe m^{-2} yr^{-1} [4,7,12], allowing for 50% loss of UV radiation through scattering and absorption by clouds and based on the present-day solar flux [4].

On early Mars, similar processes of photo-oxidation of dissolved Fe in surfacewaters could also have occurred, leading to the aqueous deposition of hydrous ferric oxide phases that have now been desiccated to nanophase hematite. However, since Mars is further away from the Sun than Earth, the lower solar UV flux incident on the martian surface would have induced slower deposition rates of the ferric oxides, perhaps smaller than 10^4 ppm Fe m^{-2} yr^{-1}.

Ferric Oxide Deposition on Present-Day Mars: Since frozen regolith currently prevents upwelling of Fe^{2+}-enriched subsurface aquifers, oxidation of aqueous Fe^{2+} by atmospheric O and solar UV radiation cannot occur, so dissolved Fe^{2+} ions may now persist beneath the martian surface. However, sublimation of permafrost and evaporation of daytime equatorial meltwaters exposed to the martian atmosphere would cause localized oxidation of dissolved ferrous iron, hydrolysis of Fe^{3+} ions, and flocculation of colloidal ferric-bearing clay silicate, oxide, and hydroxysulfate assemblages at freshly exposed surfaces on the planet. Such nanophase materials may constitute the particulate matter in local and global dust storms. During eolian transport, any unoxidized ferrous salts liberated from sublimed permafrost would be oxidized completely by exposure to atmospheric O, while desiccation of ferric hydrolysis products to Fe_2O_3 phases would be facilitated. Therefore, most of the nanophase hematite littering the martian surface is the ultimate oxidation product of dissolved Fe^{2+} ions that were derived from chemical weathering of basaltic ferromagnesian silicate minerals.

On the present-day arid martian surface, traces of O, OH, and HO_2 radicals formed by the photolysis of H_2O vapor in the atmosphere may have yielded low concentrations of H peroxide on the martian surface [13]. Experimental studies have demonstrated that rates of oxidation of dissolved Fe^{2+} by H_2O_2 are considerably higher than reactions involving atmospheric O [14,15]. Any Fe-bearing solutions percolating to the surface of Mars or resulting from melting of frost condensates would be immediately oxidized to ferric-bearing assemblages. Thus, thin veneers of ferric oxides may be continuously forming on the outermost arid surface of Mars.

Acknowledgments: Research supported by NASA grant NAGW-2220.

References: [1] Burns R. G. (1993) *JGR, 98,* 3365–3372. [2] Burns R. G. (1993) *GCA, 57,* in press. [3] Zent A. P. and McKay C. P. (1992) *LPI Tech. Rpt. 92-04,* 41–42. [4] Braterman P. S. and Cairns-Smith A. G. (1987) in *Precambrian Iron-Formations* (P. W. A. Appel and G. I. LaBerge, eds.), 215–242. [5] Cairns-Smith A. G. (1978) *Nature, 276,* 807–808. [6] Braterman P. S. et al. (1983) *Nature, 303,* 163–164. [7] Francois L. M. (1987) *Paleoceanog., 2,* 395–408. [8] McElroy M. B. and Kong T.-Y. (1976) *GRL, 3,* 569–572. [9] Baker V. R. et al. (1991) *Nature, 352,* 589–594; *Nature, 354,* 86–87. [10] Trendall A. F. (1973) *Econ. Geol., 68,* 1023–1034. [11] Spencer J. R. and Fanale F. P. (1990) *JGR, 95,* 14301–14313. [12] Anbar A. D. and Holland H. D. (1992) *GCA, 56,* 2595–2603. [13] Barth C. A. et al. (1992) in *Mars* (H. H. Kieffer et al., eds.), 1054–1089, Univ. of Arizona, Tucson. [14] Millero F. J. and Sotolongo S. (1989) *GCA, 53,* 1867–1873. [15] Millero F. J. et al. (1991) *J. Soln. Chem., 20,* 1079–109

MARSNET: A EUROPEAN NETWORK OF STATIONS ON THE SURFACE OF MARS. A. F. Chicarro, Space Science Department, ESA/ESTEC, 2200 AG Noordwijk, The Netherlands.

Introduction: Following an ESA preliminary study on the possible areas of European participation in the future international exploration of Mars [1] and an ESA call for ideas of new missions, MARSNET, a network of small surface stations, was selected for further in-depth scientific and technical assessment studies [2] as a potential European contribution to such exploration. Subsequently, the MARSNET phase A studies started in the autumn of 1991. The industrial kickoff took place in early January 1992, following the tender evaluation and the decision to select the Aérospatiale-led consortium including Dornier, Alcatel, Laben, and Etca to perform the industrial studies. The phase A studies ended in early 1993 [3]. However, critical items such as an instrument deployment device continue to be studied in the framework of ESA's Technology Research Program.

The MARSNET mission consists of a network of three semihard landers to be placed on the martian surface, several thousand kilometers apart, thus defining a regional/global seismological and meteorological network in the Tharsis region. The small stations would be targeted for landing at scientifically interesting sites in this region of Mars, which is the most likely area to still show tectonic activity; this will would allow the seismometers to acquire data for the determination of the internal structure of the planet. Landing site geology and geochemistry will also be studied.

Network Concept: Following early global survey missions such as Mariner 9 and Viking, and ongoing orbital and *in situ* missions like Mars Observer and Mars '94, focusing on the atmosphere

TABLE 1. MARSNET scientific payload.

Disciplines	Instruments	Acronyms	Mass
Geophysics of the interior	Seismometer	SEM	2.30
Geology	Panoramic camera	PCS	1.60
	Descent imager	DEI	0.20
	Close-up imager	CUI	0.30
Geochemistry and mineralogy	α-proton X-ray spectrometer	AXS	0.40
	Neutron detector	NED	0.15
Volatile studies	Differential thermal/ evolved gas analyzer	EGA	0.70
Iron studies	Mössbauer spectrometer	MÖS	0.40
Meteorology	Meteorological package	MEP	0.75
Atmospheric structure	Atmospheric structure experiment	ASE	0.30
Exobiology	Solar-UV dosimeter	SUV	0.40
Magnetic properties	Permanent magnet array	PMA	0.07
Instrument Deployment Device	To carry CUI, AXS, NED, EGA, and MÖS	IDD	1.80
Total (kg)			9.37

and surface of Mars, the subsequent natural evolutionary phase of Mars exploration would be to establish a network of small stations on the surface of Mars as an effective precursor to more detailed surface exploration.

The mission and scientific objectives of the network require the placing of a number of stations on the martian surface to perform seismological and meteorological measurements at sites of varied latitudes and altitudes to infer the internal structure of the planet and the atmospheric circulation and weather patterns. These long-term investigations would require an operational lifetime of at least one martian year (687 days). Other important scientific goals would be the morphology and geology of the landing sites, and the chemical and mineralogical analysis of martian volcanic and sedimentary surface rocks and soils, as well as the magnetic properties and volatile content of the surface materials. Also, atmospheric pressure and temperature profiles would be obtained during entry and descent, and surface and descent imagery would allow the correlation of the geological setting of each landing site to orbital imagery. The surface stations would also monitor the amount of solar-UV radiation reaching the martian surface in order to infer the present exobiological conditions on the planet, which may allow or prevent biochemical activity from occurring on the martian surface. The MARSNET mission would therefore contribute to provide a global perspective of Mars with simultaneous seismic and meteorological measurements at each landing site, as well as their chemical and geological characterization.

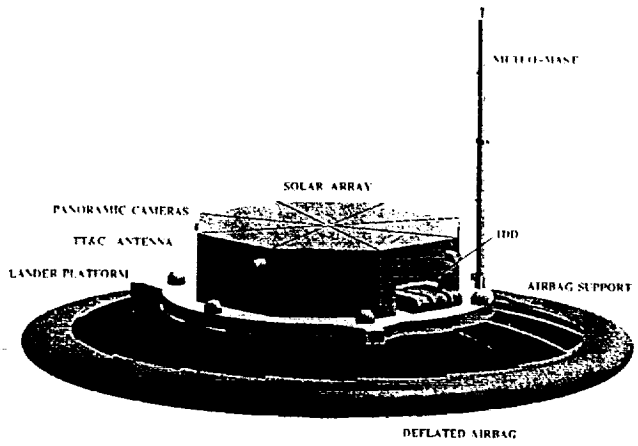

Fig. 1. MARSNET lander configuration on the martian surface showing the IDD.

Model Payload: Table 1 indicates the <10-kg model payload for each MARSNET surface station. A specific Instrument Deployment Device (IDD) will be needed in order to place the sensors of a number of instruments in contact with the martian rocks and soil. The IDD (Fig. 1) is a self-propelled mobile platform carrying sensors and electronics of the AXS, CUI, NED, MÖS, and EGA instruments. The length of each IDD element is 30 cm. A number of meteorological sensors will be placed on an 80-cm boom on top of the station. Each lander carries an identical scientific payload to obtain coherent measurements and to reduce costs.

A typical model payload to be carried onboard the surface stations that is compatible with the above-mentioned scientific objectives has been elaborated upon. It focuses on seismology, geochemistry, geology, and atmospheric physics. An outstanding feature of the model payload is manifested in its conformance with system mass constraints by utilizing state-of-the-art designs in terms of low mass, low power consumption, and a high level of integration.

Landing Sites: A number of baseline network landing sites are being considered. Each target site must be as homogeneous as possible within the 100-km × 20-km landing incertitude ellipse. However, sites of varied geology, chemical composition, and latitudes (within the Tharsis region) are necessary in order to satisfy the scientific requirements of geophysics, geochemistry, geology, and meteorology. Mission analysis constraints limit the number of potential areas of interest. The regions of Tempe Terra, Candor Chasma, and Daedalia Planum have been proposed.

A set of three landing sites (with an average separation of 3500 km) that would satisfy the scientific and technical requirements has been selected as a possible baseline network configuration. Therefore, MARSNET would provide a global scientific perspective of Mars and would also constitute part of a major international robotic precursor mission to future Mars sample return and manned exploration missions.

Lander Design: Each semihard lander would be carried onboard its own 2-m-diameter aeroshell and deployed at 10–15 km altitude for landing at about 25 m/s. Each lander (Fig. 1) would be approximately 1.2 m in diameter and 30 cm in height (excluding booms) and 67 kg in weight, including a scientific payload of about 10 kg. The surface stations would be powered by solar-cell arrays and batteries. Both communications via a relay orbiter at Mars and direct-to-Earth communications as backup are being studied for the landers. A scientific data rate of at least 2 Mb/day/station is expected.

Numerous design trade-offs have been performed, compatible with a design strategy aimed at a low-mass, low-power-consumption, maximum-inheritance, and low-cost approach. Resultant design characteristics reflected in the reference MARSNET probe/lander design are typically photovoltaic primary energy source (solar arrays), minimum booms/mechanisms, S-band communications,

passive descent subsystem (no active guidance or control), and landing system based on air vessels (no active propulsion). Further in-depth studies and critical analyses on such potentially critical areas as the descent and landing systems would consolidate and validate work already performed in supporting technology and the MARSNET phase A study. The feasibility of the concept has been adequately demonstrated to the present level, but further studies should be performed in the relevant critical technological areas.

Mission Scenario: The delivery of the three ESA MARSNET semihard landers could be performed by moderate- to high-performance expendable launch vehicles, such as Delta-II, Ariane-4, and Proton. The phase A study evaluated the two major mission scenarios for the transfer, delivery to Mars, and targeting of nominally three and possibly four probe/landers, which would then enter the martian atmosphere, descend, and land on the surface. Surface operations, during which a number of challenging and significant scientific investigations would be performed, is planned for a nominal duration of one martian year. The two major mission design scenarios are both based on a Delta-II 7925 expendable launch vehicle, but either could be performed with a similar class of expendable launch vehicle.

The MARSNET reference baseline mission design was that of the multiprobe carrier scenario, in which all landers are accommodated on one common cruise spacecraft (Mariner Mark-II class). The three entry modules could be launched toward Mars in appropriate reference launch windows (2001, 2003) and subsequent launch opportunities. The carrier spacecraft would then deliver and target the stations for atmospheric entry. The descent in the martian atmosphere would last for about 10 min. The distribution of the three MARSNET stations would take place from an approach hyperbola. The MARSNET probe/landers are targeted and separated sequentially during the Mars approach phase. All targeting maneuvers are performed by the cruise spacecraft. After separation, the entry probes containing the landers are passive with respect to communications until after landing.

The alternative was that of the single-probe carrier scenario, in which each lander is carried to Mars by a separate cruise module. Separation of the different cruise spacecraft modules from their launch accomodation structure will be at the time of separation from the launcher upper stage. After completion of the interplanetary cruise an unguided ballistic entry into the martian atmosphere from an hyperbolic approach has been chosen as the preferred solution for the final delivery of the landers. Each lander is contained in a blunt nosed sphere-cone aeroshell and thus uses passive aerobraking techniques with rigid decelerators to effect entry. During descent, further deceleration is achieved through the use of a two-parachute descent system, which stabilizes the descent module during the different phases and reduces the impact velocities to the design range catered for in the MARSNET design.

International Cooperation: NASA is also actively studying a network mission to Mars called MESUR (Mars Environmental SURvey). An existing understanding of future cooperation between the two agencies could develop into a joint ESA/NASA global Mars Network Mission, where ESA could provide, nominally, three surface stations (MARSNET) and NASA a number of additional ones (MESUR), therefore complementing each other in terms of scientific investigations and landing sites. A joint collaborative global Mars Network Mission is ideally suited to an appropriate division of effort and sharing of scientific return between the partners in the collaboration. Such a mission offers potentially high benefits to both the European and U.S. scientific communities.

Conclusions: The scientific exploration of Mars will give us new insights into the physical and chemical processes that took place in the primordial solar nebula, since the chemical composition of a planet depends on its location in the nebula during condensation. Most importantly, however, the study of Mars will deepen our understanding of the evolution of planets, including the Earth. Comparative planetology will thus provide significant clues for assessing current environmental challenges facing our planet.

References: [1] Chicarro A. F. et al. (1989) *Mission to Mars: Report of the Mars Exploration Study Team*, ESA SP-1117, 140. [2] Chicarro A. F. et al. (1991) *MARSNET: Report on the Assessment Phase Study*, ESA SCI(91)6, 103. [3] Chicarro A. F. et al. (1993) *MARSNET: Report on the Phase-A Study, European Space Agency*, ESA SCI(93)2, 119.

N94-33200

3091 ABS. ONLY

MARS ATMOSPHERIC DUST PROPERTIES: A SYNTHESIS OF MARINER 9, VIKING, AND PHOBOS OBSERVATIONS. R. T. Clancy[1], S. W. Lee[1], and G. R. Gladstone[2], [1]Laboratory for Atmospheric and Space Physics, University of Colorado, Boulder CO 80309, USA, [2]Southwest Research Institute, P.O. Drawer 28510, 6220 Culebra, San Antonio TX 78228, USA.

The longstanding model of Mars atmospheric dust, as derived by Toon et al. [1] on the basis of Mariner 9 IRIS observations and by Pollack et al. [2] on the basis of Viking lander observations, is characterized by a montmorillonite-like composition and a cross-section weighted mean radius of 2.5 μm (mode radius = 0.4 μm). The basis for this model was an analysis of Mariner 9 IRIS infrared (IR) spectra (5–50 μm) of the 1971 global dust storm, performed by Toon et al. [1]. Subsequently, Pollack et al. [2] analyzed Viking lander observations of visible (0.4–0.9 μm) sky brightness and transmission during the 1977 global dust storms. These observations were intrepreted as confirmation of the Toon et al. model of Mars atmospheric dust, with two important modifications. A nonspherical shape of the dust particles and an additional visible/ultraviolet absorbing component of dust were required to match these Viking lander observations. Pollack et al. suggested that a several percent component of magnetite in the Mars atmospheric dust could provide the observed visible absorption by the dust, since montmorillonite does not absorb visible or ultraviolet light efficiently.

Since these key studies, a number of important measurements ranging from analysis of Viking 9-μm dust opacities [3] to Phobos near-IR extinction observations of Mars dust have been obtained. Zurek [5] pointed out that the visible-to-IR dust opacity ratio obtained from the Viking studies (~2) was not consistent with the ratio predicted by the standard dust model of [1] (~1). Clancy and Lee [6] analyzed Viking IRTM emission-phase-function (EPF) sequences, which suggested smaller absorption (visible single scattering albedo near 0.92 vs. a value of 0.86 from Pollack et al.) and larger backscattering (single scattering assymetry parameter of 0.55 vs. the 0.79 from Pollack et al.) for Mars atmospheric dust. Phobos solar occultation measurements of dust extinction at wavelengths of 0.75–3.15 μm indicated particle sizes closer to 1 μm at 20 km altitude [4]. Most recently, Clark [7] interpreted groundbased near-IR spectra of Mars surface reflectance to place a very low limit (<1%) on the amount of montmorillonite-like clay materials.

In light of these findings and their conflict with the standard dust model, we have modified a doubling-and-adding code [8] to reanalyze the Mariner 9 IRIS spectra of Mars atmospheric dust as well as Viking IRTM EPF sequences in the 7-, 9-, and 20-μm channels. The code is capable of accurate emission/absorption/scattering radiative transfer calculations over the 5–30-μm wavelength region for variable dust composition and particle size inputs, and incorporates both the Viking IRTM channel weightings and the Mariner 9 IRIS wavelength resolution for direct comparisons to these datasets. We adopt atmospheric temperature profiles according to the algorithm of Martin [3] in the case of the Viking IRTM comparisons, and obtained Mariner 9 IRIS temperature retrievals from the 15-μm CO_2 band (as well as IRIS spectra of dusty periods, courtesy of J. Pearl and W. McMillan) for the case of the IRIS comparisons. We consider palagonite as the primary alternative to the montmorillonite composition of Mars atmospheric dust, based on several considerations. Palagonite absorbs in the ultraviolet and visible wavelength region due to its Fe content. Palagonite is also, in principal, consistent with the observed lack of clays on the Mars surface. Furthermore, palagonite does not display strong, structured absorption near 20 μm as does montmorillonite (in conflict with the IRIS observations). We were provided optical constants for a particular specimen of Hawaiian palagonite by T. Roush for the 5–30-μm wavelength region, and derived 0.3–5.0-μm constants for the same sample from Clark et al. [9].

We summarize the conclusions of our study as follows: (1) The Viking EPF visible and 9-μm sequences yield a visible-to-IR dust extinction ratio of ~2, consistent with the analysis of Martin [3]. This provides the first coincident, contemporaneous measurement of the visible-to-IR opacity ratio for Mars atmospheric dust. (2) Palagonite dust with a 1.2-μm cross-section weighted mean radius (mode radius = 0.15 μm) leads to visible single-scattering albedos consistent with their observed values at ultraviolet and visible wavelengths. Hence a single component composition for Mars atmospheric dust can explain all the existing observations of the dust within their uncertainties. (3) Such palagonite dust also leads to a much improved fit to the IRIS observations near 20-μm wavelengths. However, the particular sample of palagonite modeled does not fit the 8–9-μm region. (4) The ratio of 9- and 20-μm absorption for the palagonite or montmorillonite composition is very different for a 1.2- vs. a 2.5-μm mean cross-section weighted particle radius. (5) Palagonite dust with the 1.2-μm cross-section weighted mean radius also yields a visible-to-IR extinction ratio of 2, consistent with the measurements of this ratio, as well as the Phobos near-IR extinction observations. (6) A montmorillonite composition would require much smaller particle sizes than palagonite to obtain the same visible-to-IR opacity ratio. Hence a montmorillonite composition is much harder to accommodate with the observed visible-to-IR extinction ratio of Mars atmospheric dust.

We propose that a palagonite composition with particle sizes roughly one-half that of the Toon et al. [1] determination provide a much improved model to Mars atmospheric dust. Since palagonite is a common weathering product of terrestrial basalts, it would not be unreasonable for palagonite to be a major surface component for Mars. The lack of even a minor component of Al-rich clays on the surface of Mars [7] could be consistent with a palagonite composition for Mars dust if the conditions for basalt weathering on Mars were sufficiently anhydrous [10]. Variations in palagonite composition could also lead to the inability of the modeled palagonite to fit the details of the 9-μm absorption indicated by the IRIS observations [11].

References: [1] Toon O. B. et al. (1977) *Icarus, 30,* 663–696. [2] Pollack J. B. et al. (1979) *JGR, 84,* 2929–2945. [3] Martin T. Z. (1986) *Icarus, 66,* 2–21. [4] Drossart. P. et al. (1991) *Ann. Geophys., 9,* 754–760. [5] Zurek R. W. (1982) *Icarus, 50,* 288–310. [6] Clancy R. T. and Lee S. W. (1991) *Icarus, 93,* 135–158. [7] Clark R. N. et al. (1990) *JGR, 95,* 14463–14480. [8] Gladstone G. R. et al. (1984) Contract KM147-4-1041, Canada Department of the Environment. [9] Clark R. N. et al. (1990) *JGR, 95,* 14463–14480. [10] Clark R. N. (1993) personal communication. [11] Roush T. (1993) personal communication.

N94-33201

S11-91 ABS. ONLY

MAGMATIC VOLATILES AND THE WEATHERING OF MARS. B. C. Clark, Planetary Sciences Lab, Mail Stop B0560, Martin Marietta, Denver CO 80201, USA.

The sources for volatiles on Mars have been the subject of many hypotheses for exogenous influences including late accretion of volatile-enriched material, impact devolatilization to create massive early atmospheres, and even major bombardment by comets. However, the inventory of chemically active volatiles observable at the contemporary surface of Mars is consistent with domination by endogenous, subsequent planetary processes, viz., persistent magmatic outgassing.

Volcanism on Mars has been widespread in both space and time [1]. Notwithstanding important specific differences between the mantles of Earth and Mars, the geochemical similarities are such that the suite of gases emitted from martian volcanic activity should include H_2O, CO_2, S-containing gases (e.g., H_2S and/or SO_2), and Cl-containing gases (e.g., Cl_2 and/or HCl). Both H_2O and CO_2 exist in the atmosphere of Mars. Both are also present as surface condensates. However, spectroscopic observations of the martian atmosphere clearly show that the S- and Cl-containing gases are severely depleted, with upper limits of $\leq 10^{-7}$ the abundance of CO_2 [2]. Likewise, there is no evidence of polar condensates of compounds of these elements as there is for CO_2 and H_2O. Within the soil, on the other hand, there has been direct measurement of incorporated H_2O [3] and abundant compounds containing S and Cl [4]. Barring some as yet implausible geochemical sequestering process, the S/Cl ratio of about 6:1 in martian soils implies a limit of 5% on the contribution of matter of solarlike composition (e.g., carbonaceous chondrite or cometary material) to these volatiles [5]. Hence, exogenous sources are minor or not yet observed.

From analysis of elemental trends in martian soils, it has been recently shown that a simple two-component model can satisfy the Viking *in situ* measurements [6]. Component A includes Si and most or all the Al, Ca, Ti, and Fe. Component B, taken as 16 ± 3% by weight of the total, contains S and most or all the Cl and Mg. These results constrain several models of martian soil mineralogy but are consistent with a mixture of silicates (such as Fe-rich clays and accessory minerals [7]) and soluble salts [8]. The overall element profile is notably like shergottites [9,10], with significant incorporation of chemically reactive atmospheric gases from magmatic degassing.

Estimates for the total magma generated after crustal formation and the terminal stages of heavy bombardment have recently been updated. Although some 60× lower than the current areal rate of

extrusive lava resurfacing on Earth [1], the martian total is nonetheless equivalent to the release of ≥ 500 g/cm^2 averaged over the planet for every 0.1% (wt/wt) of volatile species released from magma. Quantitatively, this is sufficient to make up as much as 5% of the fine-grained regolith weathering product to a mean depth of 100 m. This reservoir of fine-grained material can be readily mobilized globally by episodic dust storms. With the relative absence of soil-consolidation factors, such as reworking by liquid water, tectonically driven metamorphism, and burial processes that are ubiquitous on Earth, survival of some material over significant portions of geologic time on Mars may have been possible. As fines are repeatedly transported over the surface, they have experienced weathering regimes from various geologic settings and epochs. Mixed fines could represent a planetwide sampling of the physical and chemical products from various surface, near-surface, and impactor materials.

Excess acidity in the fines can occur due to the preponderance of acidic volcanic emissions. Some minerals will be more susceptible to weathering than others, but reaction rates vary enormously as a function of temperature [11] and H_2O availability. Initial weathering rinds will typically form barriers to further conversion of source material. Resistant units such as rocks and bedrock outcrops would be subjected to a balance between surficial chemical weathering and physical removal by eolian abrasion. Because of saltation heights and wind-shadowing effects, three-dimensional geochemical gradients of weathering may be found on exposed surfaces on boulders such as those observed at the Viking 1 lander site.

Although carbonates and nitrates are widely expected in the martian regolith, current evidence is lacking or weak. Reworked fines may have been chemically scrubbed of any weathering product of either class of compounds since it has been demonstrated experimentally that volcanic SO_2 gas can undergo rapid heterogeneous-phase displacement reactions with susceptible solid substrates, even under simulated dry and cold martian conditions [12], to release CO_2 and NO_x back to the atmosphere.

On the other hand, magmas release additional volatiles that would not be recyclable because of their lower vapor pressures and/or chemical stability. A variety of data relevant to volatility would imply that weathering products may be highly enriched in elements such as Na, Cu, Zn, As, Se, Br, Rb, Cd, In, Sn, Sb, Hg, Tl, Pb, and Bi compared to rock compositions [13]. Many of the compounds formed by these elements may be soluble in H_2O, as data indicate for the S- and Cl-bearing compounds in martian fines, and hence be subject to transport processes that create duricrust and soil peds. The occurrences and distributions of these elements could provide key evidence of weathering history and magmatic degassing.

Where alteration products have been exposed to bulk liquid water, chemical sediment deposits with evaporite sequences should be found on Mars. Quasistable liquid brine pools might also have resulted. However, if the dominant soluble anion on Mars is SO_4^{2-}, then most strong freezing-point depressant salts would not be available for contemporaneous brine. Even if formed, subzero brines would have restricted mobility, because of high viscosity and reduced chemical activity of H_2O molecules compared to pure water.

Although it is widely believed that the missing H_2O is buried in the regolith as physical deposits of permafrost ice, it cannot be ruled out that significant portions, perhaps most, of this inventory has been incorporated into secondary minerals. A pervasive drawdown of atmospheric volatiles would result from chemical reaction with abraded and comminuted surface materials and may be central to probing the climatological evolution of Mars.

References: [1] Greeley and Schneid (1991) *Science, 254,* 996–998. [2] Owen T. (1992) in *Mars* (H. Kieffer et al. eds.), 818–834, Univ. of Arizona. [3] Biemann et al. (1978) *Icarus, 34,* 645–665. [4] Clark et al. (1982) *JGR, 87,* 11059–10067. [5] Clark B. (1987) *Icarus, 71,* 250–256. [6] Clark B. (1993) *GCA,* in press. [7] Banin et al. (1993) *JGR,* in press. [8] Clark B. and van Hart D. (1981) *Icarus, 45,* 370–378. [9] Baird A. K. and Clark B. C. (1981) *Icarus, 45,* 113–123. [10] Banin et al. (1992) in *Mars* (H. Kieffer et al. eds.), 594–625, Univ. of Arizona. [11] Burns R. (1993) *GCA,* in press. [12] Clark et al. (1979) *J. Molec. Evol., 14,* 91–102. [13] Clark and Baird (1979) *GRL,* 6 811–814

N94-33202

5/2-91 ABS ONLY

THERMAL AND HYDRAULIC CONSIDERATIONS REGARDING THE FATE OF WATER DISCHARGED BY THE OUTFLOW CHANNELS TO THE MARTIAN NORTHERN PLAINS. S. M. Clifford, Lunar and Planetary Institute, Houston TX 77058, USA.

The identification of possible shorelines in the martian northern plains suggests that the water discharged by the circum-Chryse outflow channels may have led to the formation of transient seas, or possibly even an ocean, covering as much as one-third of the planet. Speculations regarding the possible fate of this water have included local ponding and reinfiltration into the crust; freezing, sublimation, and eventual cold-trapping at higher latitudes; or the *in situ* survival of this now frozen water to the present day—perhaps aided by burial beneath a protective cover of eolian sediment or lavas. Although neither cold-trapping at higher latitudes nor the subsequent freezing and burial of flood waters can be ruled out, thermal and hydraulic considerations effectively eliminate the possibility that any significant reassimilation of this water by local infiltration has occurred given climatic conditions resembling those of today.

The arguments against the local infiltration of flood water into the northern plains are two-fold. First, given the climatic and geothermal conditions that are thought to have prevailed on Mars during the Late Hesperian (the period of peak outflow channel activity in the northern plains), the thickness of the cryosphere in Chryse Planitia is likely to have exceeded 1 km. As discussed by Clifford [1], a necessary precondition for the widespread occurrence of groundwater is that the thermodynamic sink represented by the cryosphere must already be saturated with ice. For this reason, the ice-saturated cryosphere acts as an impermeable barrier that effectively precludes the local resupply of subpermafrost groundwater by the infiltration of water discharged to the surface by catastrophic floods. Note that the problem of local infiltration is not significantly improved even if the cryosphere were initially dry, for as water attempts to infiltrate the cold, dry crust, it will quickly freeze, creating a seal that prevents any further infiltration from the ponded water above.

The second argument against the local infiltration of flood water into the northern plains is based on hydraulic considerations. As discussed by Carr [2] and Clifford [1], repeated impacts have likely brecciated the martian crust down to a depth of roughly 10 km. Given a value of permeability no greater than that inferred for the top 10 km of the Earth's crust (~10^{-2} darcies [1,3]), a timescale of

ABST cont (512

as much as a billion years or more for the martian groundwater system to achieve hydrostatic equilibrium, and the ~2–4 km elevation difference between the outflow channel source regions and the northern plains, the water confined beneath the frozen crust of the northern plains should have been under a significant hydraulic head. Thus, the existence of a hydraulic pathway between the ponded flood waters above the northern plains and the confined aquifer lying beneath it would not have led to the infiltration of flood water back into the crust, but rather the additional expulsion of groundwater onto the surface.

A more detailed discussion of the fate of flood waters discharged by the martian outflow channels is currently in preparation.

References: [1] Clifford S. M. (1993) *JGR, 98,* 10973–11016. [2] Carr M. H. (1979) *JGR, 84,* 2995–3007. [3] Brace W. F. (1980) *Int. J. Rock Mech. Min. Sci. Geochem. Abstr., 17,* 241–251.

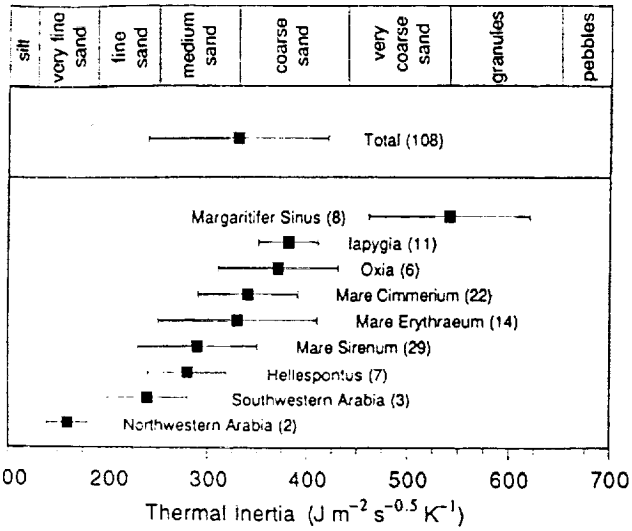

Fig. 1. Mean and standard deviation of thermal inertias for dark intracrater features in different regions. Numbers in parentheses indicate total craters examined. To convert thermal inertia to units of 10^{-3} cal cm^{-2} s$^{-0.5}$ K^{-1}, divide by 41.84.

REGIONAL SEDIMENTOLOGICAL VARIATIONS AMONG DARK CRATER FLOOR FEATURES: TOWARD A MODEL FOR MODERN EOLIAN SAND DISTRIBUTION ON MARS.

K. S. Edgett and P. R. Christensen, Department of Geology, Arizona State University, Tempe AZ 85287-1404, USA.

It has been known since 1972 that many martian craters (≤ 25 km diameter) have dark features on their floors, and that when seen at higher image resolution, some of the dark units are dune fields [1–3]. Interpretations of thermal inertia derived from Viking Infrared Thermal Mapper (IRTM) data have been used to suggest that many dark intracrater features, including those where dunes are not observed in images, contain some amount of sand or particles in the range 0.1–10 mm [4,5]. However, it has never been known if all these dark features consist of dunes.

We assembled a set of 108 carefully constrained Viking IRTM observations for dark crater-floor units. The data and selection criteria are described in detail elsewhere [6–9]. Studied in conjunction with Mariner 9 and Viking orbiter images of each crater, these data indicate that the dark crater-floor units in some regions have different thermal properties than those in other regions [7–9]. Figure 1 shows thermal inertia means and standard deviations for dark intracrater units in nine different regions. Thermal inertias were computed using the Viking thermal model of H. H. Kieffer and corrected for atmospheric CO_2 effects using the relationship for a dust-free atmosphere shown by Haberle and Jakosky [10]. The thermal inertias and interpreted particle sizes in Fig. 1 are regarded as upper limits, with lower limits (due to suspended dust in the atmosphere) perhaps 50–200 J m^{-2} s$^{-0.5}$ K^{-1} less than shown [10,11]. However, because the atmosphere had a nearly uniform dust opacity from L_s 344°–125° over the regions examined [12], the relative differences between regions in Fig. 1 are genuine [9].

The thermophysical differences illustrated in Fig. 1 [also see 7–9] are probably related to regional variations in the amount of surface covered by sand and perhaps dunes. In two of these regions, Hellespontus and Oxia, the thermal differences are consistent with an observed difference in the morphology of dunes comprising the dark features. In Hellespontus there are large transverse dunes while in Oxia there are fields of small barchans [2,9,13]. The regional differences are independent of the exact thermal inertia and particle size inferred for each, but sand (0.06–2 mm) is probably the dominant particle size [5,9,14].

In an unvegetated environment, the form and scale of eolian sand deposits are functions of sand availability, grain size distribution, wind energy and directional variability, the presence of topographic obstacles (e.g., crater walls), and climatic variations that might affect any of these factors [15]. In terms of sand-deposit morphology, grain size is probably not a significant control except among zibars [16]. Barchan and transverse dunes are typical of unidirectional wind regimes; their differences are largely considered a function of "sand supply": the amount of loose sand available for eolian transport in a region [17]. Barchans form in areas of low sand supply, though transverse dunes do not form exclusively in places of high sand supply [18]. Transverse dunes on Mars can be large deposits like those in Hellespontus or they can be small and difficult to identify without high-resolution images (an example occurs in Pettit Crater [19]).

To first order, the areal coverage of eolian sand (dunes, drifts, sheets) may be the main factor causing the observed regional differences in the thermal properties of low-albedo intracrater units [8,9]. The percentage of dune cover [8] may be similar among craters within a given region, but different between regions. The amount of sand transported and deposited is likely related to two main factors: sand supply and wind regime.

Sand sources that are regional in extent might include pyroclastic deposits laid down over a vast area, or perhaps fluvial and lacustrine strata. Detection of such sources will require high-resolution imaging or investigation on the planet's surface to find deposits or outcrops of volcaniclastic or fluviolacustrine sandstones from which dark sand might have eroded. Location of sand sources will also require remote multispectral observations to determine the mineralogy of the sediment and to trace wind-worked sand back to source areas.

as much as a billion years or more for the martian groundwater system to achieve hydrostatic equilibrium, and the ~2–4 km elevation difference between the outflow channel source regions and the northern plains, the water confined beneath the frozen crust of the northern plains should have been under a significant hydraulic head. Thus, the existence of a hydraulic pathway between the ponded flood waters above the northern plains and the confined aquifer lying beneath it would not have led to the infiltration of flood water back into the crust, but rather the additional expulsion of groundwater onto the surface.

A more detailed discussion of the fate of flood waters discharged by the martian outflow channels is currently in preparation.

References: [1] Clifford S. M. (1993) *JGR, 98*, 10973–11016. [2] Carr M. H. (1979) *JGR, 84*, 2995–3007. [3] Brace W. F. (1980) *Int. J. Rock Mech. Min. Sci. Geochem. Abstr., 17*, 241–251.

N94-33203

5/3 91 ABS ONLY

REGIONAL SEDIMENTOLOGICAL VARIATIONS AMONG DARK CRATER FLOOR FEATURES: TOWARD A MODEL FOR MODERN EOLIAN SAND DISTRIBUTION ON MARS.

K. S. Edgett and P. R. Christensen, Department of Geology, Arizona State University, Tempe AZ 85287-1404, USA.

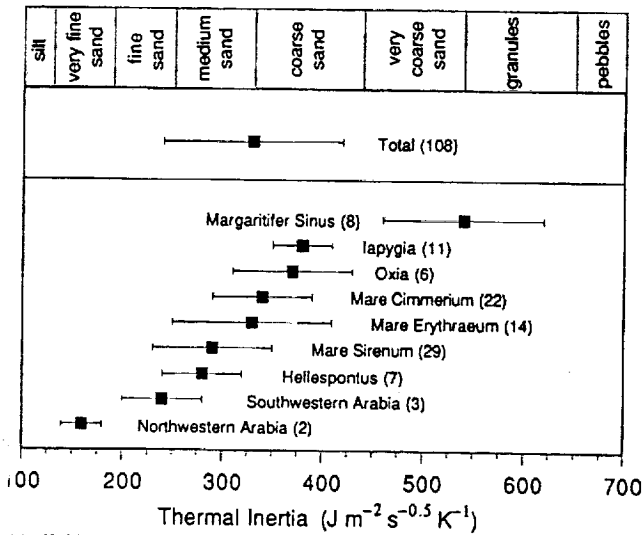

Fig. 1. Mean and standard deviation of thermal inertias for dark intracrater features in different regions. Numbers in parentheses indicate total craters examined. To convert thermal inertia to units of 10^{-3} cal cm^{-2} s$^{-0.5}$ K^{-1}, divide by 41.84.

It has been known since 1972 that many martian craters (≤ 25 km diameter) have dark features on their floors, and that when seen at higher image resolution, some of the dark units are dune fields [1–3]. Interpretations of thermal inertia derived from Viking Infrared Thermal Mapper (IRTM) data have been used to suggest that many dark intracrater features, including those where dunes are not observed in images, contain some amount of sand or particles in the range 0.1–10 mm [4,5]. However, it has never been known if all these dark features consist of dunes.

We assembled a set of 108 carefully constrained Viking IRTM observations for dark crater-floor units. The data and selection criteria are described in detail elsewhere [6–9]. Studied in conjunction with Mariner 9 and Viking orbiter images of each crater, these data indicate that the dark crater-floor units in some regions have different thermal properties than those in other regions [7–9]. Figure 1 shows thermal inertia means and standard deviations for dark intracrater units in nine different regions. Thermal inertias were computed using the Viking thermal model of H. H. Kieffer and corrected for atmospheric CO_2 effects using the relationship for a dust-free atmosphere shown by Haberle and Jakosky [10]. The thermal inertias and interpreted particle sizes in Fig. 1 are regarded as upper limits, with lower limits (due to suspended dust in the atmosphere) perhaps 50–200 J m^{-2} s$^{-0.5}$ K^{-1} less than shown [10,11]. However, because the atmosphere had a nearly uniform dust opacity from L_s 344°–125° over the regions examined [12], the relative differences between regions in Fig. 1 are genuine [9].

The thermophysical differences illustrated in Fig. 1 [also see 7–9] are probably related to regional variations in the amount of surface covered by sand and perhaps dunes. In two of these regions, Hellespontus and Oxia, the thermal differences are consistent with an observed difference in the morphology of dunes comprising the dark features. In Hellespontus there are large transverse dunes while in Oxia there are fields of small barchans [2,9,13]. The regional differences are independent of the exact thermal inertia and particle size inferred for each, but sand (0.06–2 mm) is probably the dominant particle size [5,9,14].

In an unvegetated environment, the form and scale of eolian sand deposits are functions of sand availability, grain size distribution, wind energy and directional variability, the presence of topographic obstacles (e.g., crater walls), and climatic variations that might affect any of these factors [15]. In terms of sand-deposit morphology, grain size is probably not a significant control except among zibars [16]. Barchan and transverse dunes are typical of unidirectional wind regimes; their differences are largely considered a function of "sand supply": the amount of loose sand available for eolian transport in a region [17]. Barchans form in areas of low sand supply, though transverse dunes do not form exclusively in places of high sand supply [18]. Transverse dunes on Mars can be large deposits like those in Hellespontus or they can be small and difficult to identify without high-resolution images (an example occurs in Pettit Crater [19]).

To first order, the areal coverage of eolian sand (dunes, drifts, sheets) may be the main factor causing the observed regional differences in the thermal properties of low-albedo intracrater units [8,9]. The percentage of dune cover [8] may be similar among craters within a given region, but different between regions. The amount of sand transported and deposited is likely related to two main factors: sand supply and wind regime.

Sand sources that are regional in extent might include pyroclastic deposits laid down over a vast area, or perhaps fluvial and lacustrine strata. Detection of such sources will require high-resolution imaging or investigation on the planet's surface to find deposits or outcrops of volcaniclastic or fluviolacustrine sandstones from which dark sand might have eroded. Location of sand sources will also require remote multispectral observations to determine the mineralogy of the sediment and to trace wind-worked sand back to source areas.

Regional wind regimes are important because the wind distributes sand over an area, removes material from a source, and forms deposits such as dunes. Sand has been or is being distributed in the classical albedo regions of Mars in different ways. In Hellespontus, for example, there appears to be a considerable volume of sand present, but it is entirely piled up into large transverse dunes. In Hellespontus, there appears to be little dark material that is not piled up in dunes. This is in contrast with craters in low-albedo regions like Mare Cimmerium or Margaritifer Sinus, where there are many extracrater dark deposits. The configuration of dunes in Hellespontus might have resulted from winds that were strong enough to strip loose sand from the surrounding areas and deposit the sand in craters.

In contrast, some of the sand from small barchans in Oxia has been removed from the craters to form dark streaks [20]. In places, the streaks coalesce to make larger, low-albedo units like Oxia Palus (9°N, 16°W). Barchans indicate that the amount of loose sand available for transport in Oxia is small relative to Hellespontus, yet the winds might have been more vigorous in order to facilitate the movement of sand in and out of craters and prevent the accumulation of fine, bright dust over the whole region. The coalescence of dark streaks forming Oxia Palus may provide a model for the formation of low-albedo regions like Mare Cimmerium, Mare Sirenum, or Margaritifer Sinus, where the winds may be stronger [21] and the sand supply might be greater than in Oxia, thus causing sand to be more widely distributed. Alternatively, the sources of sand in low-albedo regions might be more ubiquitous. Perhaps sediment beds are currently eroding and feeding the present-day dark eolian deposits found throughout the low-albedo regions.

Which of the two influences, broadly termed "wind regime" and "sand supply," has had the greatest influence on the nature of eolian sediment deposition and removal in different martian regions remains to be understood. One additional factor is the question of climatic change; for example, were the huge piles of sand in the Hellespontus craters deposited under climate conditions that were different from the present?

References: [1] Sagan C. et al. (1972) *Icarus, 17*, 346–372. [2] Cutts J. A. and Smith R. S. U. (1973) *JGR, 78*, 4139–4154. [3] Arvidson R. E. (1974) *Icarus, 21*, 12–27. [4] Peterfreund A. R. (1981) *Icarus, 45*, 447–467. [5] Christensen P. R. (1983) *Icarus, 56*, 496–518. [6] Edgett K. S. (1990) M.S. thesis, Arizona State Univ. [7] Edgett K. S. and Christensen P. R. (1991) *LPSC XXII*, 335–336. [8] Edgett K. S. and Christensen P. R. (1992) *LPSC XXIII*, 325–326. [9] Edgett K. S. and Christensen P. R. (1993) *JGR*, submitted. [10] Haberle R. M. and Jakosky B. M. (1991) *Icarus, 90*, 187–204. [11] Paige D. A. et al. (1993) *JGR*, submitted. [12] Martin T. Z. and Richardson M. I. (1993) *JGR, 98*, 10941–10949. [13] Thomas P. (1984) *Icarus, 57*, 205–227. [14] Edgett K. S. and Christensen P. R. (1991) *JGR, 96*, 22765–22776. [15] Pye K. and Tsoar H. (1990) *Aeolian Sand and Sand Dunes*, 218–220, Unwin and Hyman, London. [16] Lancaster N. (1989) *The Namib Sand Sea*, 111–112, A. A. Balkema, Rotterdam. [17] Wasson R. J. and Hyde R. (1983) *Nature, 304*, 337–339. [18] Rubin D. M. (1984) *Nature, 309*, 91–92. [19] Zimbelman J. R. (1986) *Icarus, 66*, 83–93. [20] Thomas P. et al. (1981) *Icarus, 45*, 124–153. [21] Greeley R. et al. (1993) *JGR, 98*, 3183–3196.

N94-33204

5/4 91 ABS. ONLY

AEROSOLS SCATTERING AND NEAR-INFRARED OBSERVATIONS OF THE MARTIAN SURFACE. S. Erard, IAS-Planetologia, viale dell'Universita 11, 00185 Roma, Italy.

Introduction: The presence of a scattered contribution in the atmosphere of Mars is a major problem for spectroscopic observations of the surface in the infrared since the main mineralogical absorptions have a typical depth of 1% and could be easily masked or subdued by atmosphere scattering. An estimate of the aerosol contribution between 0.77 and 2.6 μm was previously derived above Tharsis from ISM imaging spectroscopic data acquired from the Phobos 2 spacecraft in 1989 [1]. It is used here to investigate the effect of the scattering on the criteria that allow the mineralogical characterization of the surface.

Aerosols Contribution: Under low opacity and near-normal viewing geometry (the conditions of ISM observations) multiple atmospheric scattering can be neglected. Because the martian aerosols are very bright and strongly forward-scattering in the near-IR, the radiance factor can be further approximated as the sum of the surface reflectance and the backscattering [2]. This model was used to derive an estimate of the scattered spectrum, taking advantage of the overlap between two image cubes in the region of Pavonis Mons

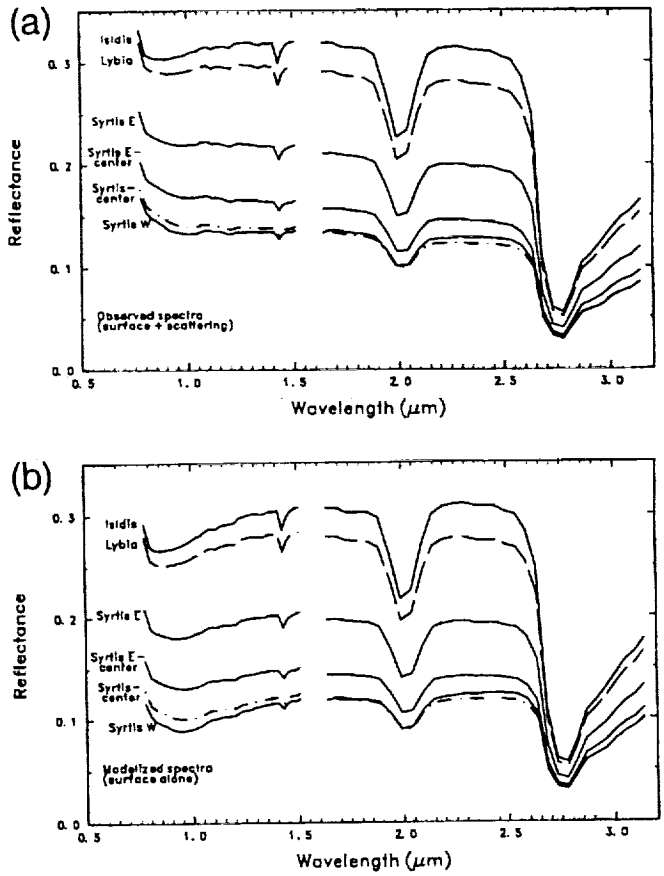

Fig. 1. Average spectra of the six main spectral units in the Syrtis Major-Isidis Planitia image-cube: (a) calibrated spectra; (b) after removal of the estimated scattering.

TABLE 1. Range of variation of the spectral criteria in the Syris-Isidis image cube.

	Surface + Scattering (Measured)			Surface Alone (Modeled)		
	Min	Max	Range/rms Noise	Min	Max	Range/rms Noise
Reflectance at 1.09 μm	0.115	0.33	1200	0.08	0.30	1200
Spectral slope reflectance units/μm	−0.025	0.0002	35	−0.010	0.020	30
2-μm pyroxenes (band depth)	0.97	1.00	20	0.98	1.01	20
0.9-μm Fe^{3+} (band depth)	0.965	1.055	50	0.955	1.055	60
1-μm Fe^{2+} (band depth)	0.0	0.40	85	0.0	0.70	150

[1]. The main hypotheses in this procedure are that (1) the aerosol contribution is assumed to be zero at 2.6 μm, (2) the photometric function of the surface is assumed independent of the wavelength, and (3) the difference between extinction and forward scattering is supposed to be small compared to backscattering. Although there is some uncertainty about the absolute level of the spectra, the result is reasonable in terms of opacity ($\tau \approx 0.23$ at 1.9 μm) and is consistent with the efficace radius of 1.2 μm derived from Phobos 2/ Auguste [3].

The image cube covering Syrtis Major and Isidis Planitia (400 × 3000 km^2), which is the more contrasted one, was used to test the effect of the scattering on the spectra. Statistical analysis of these 3000 spectra showed that the vertical scattering contribution can be considered uniform on the whole region, with a value of 0.75× the estimate derived on Tharsis, and no altimetric dependence. This correction is probably overestimated on the darkest areas.

Surface Properties: The six main spectral criteria related to the surface materials are the reflectance at 1.09 μm; the spectral slope, estimated here as the derivative between 1.84 and 2.35 μm; the strength of the 2-μm pyroxene band; an equivalent of the depth of the 0.88-μm ferric oxide band; and the surface of the Fe^{2+} band, integrated from 0.86 to 1.09 μm. They were computed on the whole image cube for the calibrated spectra and for the spectra corrected from scattering (estimate of the surface alone); their values are given in Table 1. The last three criteria were also used to establish a classification of the calibrated spectra [4]; the main spectral types are given in Fig. 1a. The spectra of the same pixels were averaged after subtraction of the aerosols contribution, and are given in Fig. 1b.

Discussion: The level of the scattered spectrum below 2 μm ranges from 0.02 to 0.05, which represents 5–15% of the albedo of the bright areas and 15–30% of that of the dark regions. This large contribution of scattering is similar to that infered for "clear atmosphere" from IRTM observations [5] and independent ISM analysis [6]. The negative spectral slope often ascribed to dark materials appears to be largely due to the aerosol scattering continuum, although intrinsic variations are recognized on the data. The opposition between the eastern and western parts of Syrtis Major is enhanced by the correction.

The three criteria measuring the main surface absorptions are relatively insensitive to the addition of a low-opacity scattered component. Although they are subdued and slightly shifted to longer wavelengths, their spatial distribution and relative contrast are not deeply modified. The Fe^{3+} and 2-μm pyroxene bands appear to be very insensitive to small variations of opacity. Conversely, the Fe^{2+} band area is reduced by almost a factor of 2, although the transformation is almost a linear stretch of the scale. This reduction may help explain why the mafic features are not always observed from the ground.

We measured the centers of the 1-μm band on the spectra of Fig. 1. On the corrected spectra they are systematicaly shifted by some tens of nanometers toward the short wavelengths, but the shift is not large enough to change dramatically the mineralogical interpretation of the surface: The absorptions are still compatible with hematite on bright regions (center at 0.86 μm) and with calcic pyroxenes in Syrtis Major (center at 0.94 μm), though probably less rich in Ca than previously inferred from ISM [7] (Ca/(Fe + Ca + Mg) ≈ 0.20 ± 0.08 instead of 0.275 ± 0.075). Very calcic pyroxenes could have their bands shifted up to 1.05 μm by the addition of a steep scattered component. In this case they could be mistaken for olivine, so no detection of this mineral could be validated unless made under very low opacity.

References: [1] Erard et al. (1993) *LPS XXIV*, 445. [2] Drossart et al. (1991) *Annal. Geophys.*, *9*, 754. [3] Korablev et al. (1993) *Icarus*, *102*, 76. [4] Erard et al. (1993) *LPS XXIV*, 443. [5] Clancy and Lee (1991) *Icarus*, *93*, 135. [6] Erard et al. (1992) *LPS XXIII*, 335. [7] Mustard et al. (1993) *JGR* 98 3387

5/5-91 ARS. ONLY

N94-33205

A MODEL FOR THE EVOLUTION OF CO_2 ON MARS.

R. M. Haberle[1], D. Tyler[2], C. P. McKay[1], and W. L. Davis[1], [1]NASA Ames Research Center, Moffett Field CA 94035-1000, USA, [2]San Jose State University, San Jose CA 95192, USA.

Our MSATT work has focused on the evolution of CO_2 on Mars. We have constructed a model that predicts the evolution of CO_2 on Mars from a specified initial amount at the end of the heavy bombardment to the present. The model draws on published estimates of the main processes believed to affect the fate of CO_2 during this period: chemical weathering, regolith uptake, polar cap formation, and atmospheric escape. Except for escape, the rate at which these processes act is controlled by surface temperatures that we calculate using a modified version of the Gierasch and Toon [1] energy balance model. The modifications account for the change in solar luminosity with time, the greenhouse effect, and an equatorial (as well as polar) energy budget. Using published estimates for the main parameters, we find no evolutionary scenario in which CO_2 is capable of producing a warm (global mean temperatures >250K) and wet (surface pressures >30 mbar) early climate, and then evolves to present

conditions with ~7 mbar in the atmosphere, <300 mbar in the regolith, and <5 mbar in the caps.

Such scenarios only exist if the early Sun was brighter than standard solar models suggest, if greenhouse gases other than CO_2 were present in the early atmosphere, or if the polar albedo is significantly lower than 0.75. However, these scenarios generally require the storage of large amounts of CO_2 (>1 bar) in the carbonate reservoir. If the warm and wet early Mars constraint is relaxed, then we find best overall agreement with present-day reservoirs for initial CO_2 inventories of 0.5–1.0 bar. We also find that the polar caps can have a profound effect on how the system evolves. If the initial amount of CO_2 is less than some critical value, then there is not enough heating of the poles to prevent permanent caps from forming.

Once formed, these caps control how the system evolves because they set the surface pressure and hence the thermal environment. If the initial amount of CO_2 is greater than this critical value, then caps do not form initially, but can form later on when weathering and escape lower the surface pressure to a point where polar heating is no longer sufficient to prevent cap formation and the collapse of the climate system. Our modeling suggests this critical initial amount of CO_2 is between 1 and 2 bar, but its true value will depend on all factors affecting the polar heat budget.

References: [1] Gierasch P. J. and Toon O. B. (1973) *J. Atmos. Sci., 30,* 1502–1508.

N94-33206

SIT 91 ABS ONLY

POSSIBLE TEST OF ANCIENT DENSE MARTIAN ATMOSPHERE. W. K. Hartmann[1] and S. Engel[2], [1]Planetary Science Institute, Tucson AZ 85705, USA, [2]Lunar and Planetary Lab, University of Arizona, Tucson AZ 85721, USA.

We have completed preliminary calculations of the minimum sizes of bolides that would penetrate various hypothetical martian atmospheres with surface pressures ranging from 6 to 1000 mbar for projectiles of various strengths (weak icy comet, carbonaceous bodies, coherent chondrite, iron). The calculations are based on a program kindly provided by C. Chyba [1]. These numbers are used to estimate the diameter corresponding to the turndown in the crater diameter distribution due to the loss of these bodies, analogous to the dramatic turndown at larger size already discovered on Venus due to this effect.

We conclude that for an atmosphere greater than a few hundred millibars, a unique downward displacement in the diameter distribution would develop in the crater diameter distribution at D ~ 0.5–4 km, due to loss of all but Fe bolides.

Careful search for this displacement globally, as outlined here, would allow us to place upper limits on the pressure of the atmosphere contemporaneous with the oldest surfaces, and possibly to get direct confirmation of dense ancient atmospheres.

We are currently searching for support to refine the calculations and conduct the necessary careful search in the cratering records.

References: [1] Chyba C. (1993) *Nature, 361,* 40.

N94-33207

SIT 91 ABS ONLY

GROUNDBASED MONITORING OF MARTIAN ATMOSPHERIC OPACITY. K. E. Herkenhoff[1] and L. J. Martin[2], [1]Mail Stop 183-501, Jet Propulsion Laboratory, California Institute of Technology, Pasadena CA 91109, USA, [2]Lowell Observatory, Flagstaff AZ 86001, USA.

The amount of dust in the martian atmosphere is variable in both space and time [1,2]. The presence of aerosols in Mars' atmosphere complicates quantitative analysis of martian surface properties [3–7]. Dust storms have been observed telescopically for almost 200 yr and are known to have major effects upon the structure and circulation of the martian atmosphere [8,9]. Great dust storms tend to occur during the southern spring and summer [2] and may be an important mechanism by which dust is transported into the polar regions [10]. It is widely believed that the martian polar layered deposits record climate variations over at least the last 10–100 m.y. [11–18], but the details of the processes involved and their relative roles in layer formation and evolution remain obscure [19]. The layered deposits are widely believed to be the result of variations in the proportions of dust and water ice deposited over many climate cycles [13–15]. However, the amount of dust currently transported into the polar regions is unknown, as are the effects of global climate changes on dust transport. In order to infer the climate history of Mars from geologic evidence including the polar layered deposits, the current cycling of dust through the martian atmosphere must be understood. In addition, future missions to Mars (including possible human exploration) will require better knowledge of the likelihood and severity of martian dust storms.

Zurek and Martin [2] found that "planet-encircling dust storms do not occur every Mars year, and . . . that there may have been periods of several successive years without such storms." The clarity of Mars images taken during recent oppositions suggests that the martian atmosphere has been less dusty recently than in previous years [20]. Hubble Space Telescope images of Mars show that the dust opacity was less than 0.06 in December 1990 [21]. Ingersoll and Lyons [22] proposed that martian great dust storms are chaotic phenomena, influenced by the amount of "background" dust in the atmosphere. However, their analysis was hindered by gaps in the historical record of martian dust opacity. Martian dust storms can be detected only when Mars is relatively close to Earth, so a complete seasonal or interannual history of dust storms is impossible to obtain from groundbased data alone. The optical depth of aerosols in the martian atmosphere between dust storms has been determined primarily from spacecraft data [23,24], but can also be inferred from groundbased observations [5]. Groundbased images of Mars show that atmospheric dust opacity significantly affects the photometric behavior of the planet. Lumme [5] modeled martian limb brightening using high-quality visible-light photographs taken on September 3, 1973. The optical thickness (0.16) and single-scattering albedo (0.55) at 435 nm that he derived are consistent with more recent results using Viking Orbiter violet-filter television data [4,6,25,26], indicating that groundbased data may be used to determine the scattering properties of the martian atmosphere. As shown below, Mars limb brightening data can be used to determine the opacity of aerosols in the martian atmosphere between dust storms.

We have developed a model for Mars surface and atmospheric scattering based on equations (1)–(6) in Hillier et al. [27]. This formulation was chosen for its speed of computation and because it accounts for the spherical geometry of atmospheric scattering at

high emission angles, i.e., near the planetary limb. The atmosphere is assumed to be optically thin in this model, so optical depths greater than 0.2 are not modeled using this formulation. Hapke's bidirectional reflectance function is used to model the surface scattering, assuming a phase function of the form P(a) = 1 + b cos(a), where a is the phase angle. Dust was assumed to be responsible for all the atmospheric scattering in this model (Rayleigh scattering in the martian atmosphere is insignificant in visible light).

The effects of turbulence in the terrestrial atmosphere ("seeing") upon groundbased Mars images were simulated by convolving a smearing function similar to that used by Lumme [5] with theoretical profiles. The results of this convolution indicate that changes in optical depth of 0.1 can be observed from Earth even with 2 arcsec seeing if the atmosphere is optically thin (small changes in opacity cannot be distinguished in the optically thick case). The shape of the photometric profile is not diagnostic of scattering in all cases, but the absolute reflectance can be used to infer the optical depth of dust in the atmosphere. Therefore, it should be possible to determine the optical depth of aerosols in an optically thin martian atmosphere using well-calibrated groundbased images of Mars. To test the viability of this method, we are comparing Viking data with nearly simultaneous groundbased photographs of Mars taken during the 1977–1978 apparition. The results of this comparison will be reported at the workshop.

References: [1] Martin L. J. and Zurek R. W. (1993) *JGR, 98,* 3221. [2] Zurek R. W. and Martin L. J. (1993) *JGR, 98,* 3247. [3] Arvidson R. E. et al. (1989) *JGR, 94,* 1573. [4] Herkenhoff K. E. and Murray B. C. (1990) *JGR, 95,* 1343. [5] Lumme K. (1976) *Icarus, 29,* 69. [6] Thorpe T. E. (1978) *Icarus, 36,* 204. [7] Thorpe T. E. (1982) *Icarus, 49,* 398. [8] Gierasch P. J. and Goody R. M. (1972) *J. Atmos. Sci., 29,* 400. [9] Haberle R. M. et al. (1982) *Icarus, 50,* 322. [10] Barnes J. R. (1990) *JGR, 95,* 1381. [11] Murray B. C. et al. (1972) *Icarus, 17,* 328. [12] Cutts J. A. et al. (1976) *Science, 194,* 1329. [13] Cutts J. A. (1979) *JGR, 84,* 2975. [14] Squyres S. W. (1979) *Icarus, 40,* 244. [15] Toon O. B. et al. (1980) *Icarus, 44,* 552. [16] Carr M. H. (1982) *Icarus, 50,* 129. [17] Howard A. D. et al. (1982) *Icarus, 50,* 161. [18] Plaut J. J. et al. (1988) *Icarus, 75,* 357. [19] Thomas P. et al. (1992) in *Mars* (H. H. Kieffer et al., eds.), 767–795, Univ. of Arizona, Tucson. [20] Martin L. J. et al. (1991) *Bull. A.A.S., 23,* 1217. [21] Clancy R. T. (1992) personal communication. [22] Ingersoll A. P. and Lyons J. R. (1991) *Bull. A.A.S., 23,* 1217. [23] Zurek R. W. (1982) *Icarus, 50,* 288. [24] Esposito L. W. et al. (1990) *Bull. A.A.S., 22,* 1076. [25] Thorpe T. E. (1977) *JGR, 82,* 4151. [26] Jaquin F. et al. (1986) *Icarus, 68,* 442. [27] Hillier J. et al. (1991) *JGR, 96,* 19203.

N94-33208

5IP-91 ABS. ONL

MARS ATMOSPHERIC LOSS AND ISOTOPIC FRACTIONATION BY SOLAR-WIND-INDUCED SPUTTERING AND PHOTOCHEMICAL ESCAPE.

B. M. Jakosky[1], R. O. Pepin[2], R. E. Johnson[3], and J. L. Fox[4], [1]Laboratory for Atmospherics and Space Physics, University of Colorado, Boulder CO 80309, USA, [2]School of Physics and Astronomy, University of Minnesota, Minneapolis MN 55455, USA, [3]University of Virginia, Charlottesville VA 22908, USA, [4]State University of New York, Stony Brook NY 11794, USA.

We examine the effects of loss of Mars atmospheric constituents by solar-wind-induced sputtering and by photochemical escape during the last 3.8 b.y. Sputtering is capable of efficiently removing all species from the upper atmosphere including the light noble gases; N is removed by photochemical processes as well. Due to diffusive separation (by mass) above the homopause, removal from the top of the atmosphere will fractionate the isotopes of each species with the lighter mass being preferentially lost. For C and O, this allows us to determine the size of nonatmospheric reservoirs that mix with the atmosphere; these revervoirs can be CO_2 adsorbed in the regolith or H_2O in the polar ice caps. We have constructed both simple analytical models and time-dependent models of the loss from and supply of volatiles to the martian atmosphere.

Both Ar and Ne require continued replenishment from outgassing over geologic time. For Ar, sputtering loss explains the fractionation of $^{36}Ar/^{38}Ar$ without requiring a distinct epoch of hydrodynamic escape (although fractionation of Xe isotopes still requires very early hydrodynamic escape). For Ne, the current ratio of $^{22}Ne/^{20}Ne$ represents a balance between loss to space and continued resupply from the interior; the similarity of the ratio to the terrestrial value is coincidental. For Ni, the loss by both sputtering and photochemical escape would produce a fractionation of $^{15}N/^{14}N$ larger than observed; an early, thicker CO_2 atmosphere could mitigate the N loss and produce the observed fractionation as could continued outgassing of juvenile N. Based on the isotopic constraints, the total amount of CO_2 lost over geologic time is probably of order tens of millibars rather than a substantial fraction of a bar. The total loss from solar-wind-induced sputtering and photochemical escape, therefore, does not seem able to explain the loss of a putative thick, early atmosphere without requiring formation of extensive surface carbonate deposits.

N94-33209

5IP 91 ABS. ONLY

SNC METEORITES AND THEIR IMPLICATIONS FOR RESERVOIRS OF MARTIAN VOLATILES.

J. H. Jones, Mail Code SN4, NASA Johnson Space Center, Houston TX 77058, USA.

The SNC meteorites and the measurements of the Viking landers provide our only direct information about the abundance and isotopic composition of martian volatiles [1,2]. Indirect measurements include spectroscopic determinations of the D/H ratio of the martian atmosphere [3]. Here I present a personal view of volatile element reservoirs on Mars, largely as inferred from the meteoritic evidence. This view is that the martian mantle has had several opportunities for dehydration and is most likely dry, although not completely degassed. Consequently, the water contained in SNC meteorites was most likely incorporated during ascent through the crust. Thus, it is possible that water can be decoupled from other volatile/incompatible elements, making the SNC meteorites suspect as indicators of water inventories on Mars.

Multiple Reservoirs of Volatiles on Mars: The covariation of $^{129}Xe/^{132}Xe$ with $^{84}Kr/^{132}Xe$ among the members of the SNC suite strongly implies that there are at least two volatile element reservoirs on Mars [4]. The first, best associated with the Chassigny meteorite, has a solar $^{129}Xe/^{132}Xe$ ratio of ~1 [4]. The second, best associated with shock glasses from the EETA79001 shergottite, has $^{129}Xe/^{132}Xe$ ~2 [4] and is within error of the Viking measurement of martian air [1]. Because Chassigny is a cumulate igneous rock that appears to have experienced minimal weathering [5,6] and interaction with crustal materials [7] (but see below!), it is assumed here that Chassigny's anhydrous, volatile-element component is derived

from the martian mantle. Conversely, the volatiles contained within the shock glasses of EETA79001 are thought to be derived from the martian atmosphere. The simplest alternative to this scenario is that the different subsets of SNC meteorites did not originate from the same planet [8].

The Mantle Reservoir: I advocate that the martian mantle has had little input from crustal or atmospheric sources and is most likely dry. The mantle of Mars is probably more depleted than the MORB mantle of the Earth [ε_{Nd} (Mars) = +20–25 vs. ε_{Nd} (MORB) = +10–12]. I also believe that the chemical and isotopic characteristics of the martian mantle were established very early. A corollary of this perspective is that most of the water contained in SNC meteorites is crustal.

A final (and more model-dependent) inference is that the martian mantle is relatively homogeneous and has been so over most of the planet's history. The logic, as presented by Jones [7], is somewhat convoluted: (1) Long-lived parent-daughter pairs, such as ^{238}U-^{206}Pb, ^{87}Rb-^{87}Sr, and ^{147}Sm-^{143}Nd, indicate that the ~180-m.y. shergottites [9] were produced from a mantle chemically similar to that which produced the nakhlites (and Chassigny) at ~1.25 b.y. (2) The crucial assumption behind this extrapolation from 1250 m.y. to 180 m.y. is that the parent-daughter ratio of the martian mantle that pertained between 4.5 aeons and 1.25 aeons also pertains subsequently. (3) The simplest way for this assumption to be true is if there was an early differentiation event that produced (a) enriched crust; (b) a homogeneous, highly depleted mantle; and (c) a metallic core. This depleted mantle was then tapped at various times, producing basalts over the history of the planet.

(Although the complexities arising from short and intermediate-lived nuclei, such as ^{146}Sm and ^{235}U, indicate that this model is somewhat oversimplified [7,10], it can nevertheless explain the ~4.5-aeon shergottite whole-rock Rb-Sr isochron [7]. And, as indicated above, the model can also isotopically relate the various SNCs to a common mantle source region, regardless of their individual crystallization ages.)

The large difference between the $^{129}Xe/^{132}Xe$ ratios of the crust and mantle is most plausibly attributed to the decay of ^{129}I ($t_{1/2}$ = 16 m.y.). If so, this iodine must have been "degassed" very early in the planet's history, consistent with the model given above, which was based on long-lived nuclei. There has presumably also been insignificant transport of Xe from the crust (or atmosphere) to the mantle, since mantle (Chassigny) Xe is isotopically indistinguishable from solar. This is consistent with the inference from Viking imaging that terrestrial-style plate tectonics and slab subduction has not been active on Mars for ~4 b.y. [11]. Consequently, it is inferred that the martian mantle and its volatiles have remained effectively isolated over most of the history of the planet. Accordingly, transport of volatiles has been chiefly from mantle to crust. The exception to this rule is water, since the martian mantle is thought to be dry.

Desiccation of the Martian Mantle: The SNC meteorites contain significant water [2] and it has often been assumed that that water is mantle-derived [12]. There are at least three reasons to suspect that this is not so: (1) Initially, before the formation of a core, there was presumably excess metal [13,14], which should have quantitatively reacted with oxidized phases, such as water or hydroxyl ions. (2) Following core formation, there was an early episode of crust formation. Consequently, the martian mantle should be depleted in incompatible, crust-forming elements, including water. (3) The water in terrestrial magmas is most probably not juvenile, but subducted, recycled water [15]. Since subduction does not appear to be an important process on Mars and since the Xe isotopic ratio of the mantle has remained unchanged relative to solar, it seems unlikely that volatile transport from crust to mantle has been significant (but see below).

An important piece of evidence in support of this view is the recent measurement of the D/H ratios of hydrous minerals in the SNC meteorites. At this writing, all measurements of water in SNCs are compatible with a single, isotopically heavy source with a D/H ratio of +4000‰ [16,17]. This value is so large that relatively massive loss of H from the planet, relative to D, is implied. Also, since this D/H ratio is in agreement with spectroscopic measurements of the martian atmosphere [3], the most likely source of SNC water is the crust or the atmosphere, which could have lost H to space.

Again, these inferences also imply that there has probably been a decoupling between water and other volatile/incompatible elements. For example, in the case of Chassigny, water is inferred to have been acquired during passage through the crust without addition of other volatiles such as Xe. Consequently, it seems difficult, using the SNCs, to make meaningful deductions about the water inventory of Mars.

Oxidation of the Martian Mantle: Has there been absolutely no cycling of water into the martian mantle over geologic time? Probably not. The phase assemblages of SNC meteorites imply that the redox state of the martian mantle is ~QFM, much like that of the Earth [5]. This O fugacity is considerably higher than is inferred from most models of core formation [13]. Consequently, the addition of small amounts of oxidized materials to the martian mantle have probably raised the mantle's O fugacity over geologic time. The lever arm here is quite large, as small amounts of such oxidants go a long way. Only 10 ppm of material with an intrinsic fo_2 of 10^{-3} is required to change a reduced mantle, with an fo_2 of 10^{-12}, to an oxidized one ($fo_2 = 10^{-8}$).

Atmospheric/Crustal Reservoir: The inferences from the Viking measurements and those based on the shock glasses of EETA79001 are amazingly consistent [18]. Consequently, it appears that we know the chemical and isotopic composition of the martian atmosphere quite well. This is in stark contrast to the convoluted and torturous machinations that have been required to decipher the SNCs and the story they have to tell. In brief, the martian atmosphere is dominated by CO_2, has a very large $^{40}Ar/^{36}Ar$ ratio of ~3000 (vs. ~300 for the Earth), a $^{129}Xe/^{132}Xe$ ratio of ~2 (vs. 0.98 for the Earth), a $^{15}N/^{14}N$ ratio of +600‰ (relative to terrestrial air), and a D/H ratio of ~+4000‰ (~5 times that of terrestrial ocean water). Thus, the atmosphere appears to be enriched in radiogenic components (^{40}Ar and ^{129}Xe), as well as in the heavier isotopes of stable elements (^{15}N and D). The enrichment of heavy stable isotopes is not well understood, although various atmospheric loss processes are likely to be responsible [19]. However, the enrichment of radiogenic isotopes is most plausibly attributed to crustal degassing over geologic time. Mantle degassing will presumably only dilute the effect of the crust-derived component. Thus, if the present atmosphere can be used as a guide, it appears that crustal degassing has dominated mantle degassing over the history of the planet.

Summary: There is currently evidence for two ancient, isolated, and quite distinct volatile element reservoirs on Mars. One is attributed to the martian mantle and is believed to be dry. The second has been shown to be much like the martian atmosphere and/

or the martian crust and is likely to be much wetter. SNC meteorites have probably gained their water by assimilation of crustal materials, and thus are probably poor indicators of the abundance of water on Mars.

References: [1] Bogard D. D. and Johnson P. (1983) *Science, 221*, 651–654. [2] Karlsson H. et al. (1992) *Science, 255*, 1890–1892. [3] Bjoraker G. L. et al. (1989) *Proc. 4th Intl. Conf. on Mars*, 69–70. [4] Ott U. (1988) *GCA, 52*, 1937–1948. [5] McSween H. Y. Jr. (1985) *Rev. Geophys., 23*, 391–416. [6] Treiman A. H., personal communication. [7] Jones J. H. (1989) *Proc. LPS 19th*, 465–474. [8] Ott U. and Begemann F. (1985) *Nature, 317*, 509–512. [9] Jones J. H. (1986) *GCA, 50*, 969–977. [10] Harper C. L. Jr. et al. (1993) *Science*, in press. [11] Phillips R. J. and Ivins E. R. (1979) *Phys. Earth Planet. Inter., 19*, 107–148. [12] Johnson M. C. et al. (1991) *GCA, 55*, 349–366. [13] Treiman A. H. et al. (1987) *Proc. LPSC 17th*, in *JGR, 92*, E627–E632. [14] Wänke H. and Dreibus G. (1988) *Phil. Trans. Roy. Soc. London, A325*, 545–558. [15] Sheppard S. M. F. (1977) *Stable Isotopes and High Temperature Geological Processes* (J. W. Valley et al., eds.), 165–183, *Rev. of Mineralogy, 16*. [16] Watson L. L. (1993) Presentation to the 56th annual Meteoritical Society meeting. [17] Kerridge J. F. (1988) *LPS XIX*, 599–600. [18] Pepin R. O. (1985) *Nature, 317*, 473–475. [19] Pepin R. O. (1992) *Annu. Rev. Earth Planet. Sci., 20*, 389–430.

S20-91 ABS ONLY

N94-33210

THE NORTHERN PLAINS MSATT MEETING, AND A CALL FOR A FIELD-ORIENTED SUCCESSOR TO MSATT.

J. S. Kargel, U.S. Geological Survey, Flagstaff AZ 86001, USA.

The Workshop on the Martian Northern Plains: Sedimentological, Periglacial, and Paleoclimatic Evolution (August 9–15, 1993) formally was devoted to a review of our knowledge of the martian northern plains and presentation of recent ideas pertaining to the geologic and climatic evolution of this interesting region. The meeting was held in Fairbanks to allow easy access to Mars-like terrains in central and northern Alaska. There is no place on Earth that is a close analog of the martian northern plains, but parts of Alaska come reasonably close in some respects, so we may expect that some of the processes occurring there are similar to processes that have occurred (or are hypothesized to have occurred) on Mars. The meeting was sited in Fairbanks because of (1) the accessibility of Mars-like landscapes, (2) the availability of logistical support facilities, and (3) the willingness of knowledgeable faculty at the University of Alaska to lead field trips.

The meeting organizers invited the participation of four scientists (T. Péwé, J. Begét, R. Reger, and D. Hopkins) with expertise in Alaskan geology, cold-climate geomorphology, and cold-climate physical processes. These scientists actively participated in the workshop and led us in two major field trips and a low-altitude overflight. Field Trip I (2 days) was to the Alaska Range and interior Alaska between Fairbanks and the Alaska Range; Field Trip II (1 day) was in the Fairbanks area; and the overflight (1 day) took us to Barrow (where we stopped and engaged in a brief field excursion), the Prudhoe Bay area, and the Brooks Range. The formal part of the meeting (2 days) was capped by an informal evening discussion, principally by the "terrestrial experts," that focused around a small selection of Mars slides that had engendered considerable discussion and controversy. A synopsis of this important discussion and of the field trips and overflight have been presented in the formal meeting summary [1].

Approximately 20 cameras recorded our field activities and the highlights of our overflight, resulting in some remarkable images of thermokarst, pingoes, ice-wedge polygons, sorted stone stripes and stone circles, gelifluction sheets, ice-cored moraine, eskers, alpine glaciers, the Arctic coast, and many other periglacial and glacial landforms. Field trip participants were introduced to some landforms that they had never observed previously (many had not even heard of them), most notably the nivation hollow and the cryoplanation terrace, both of which are periglacial features that are produced through the action of melting snow packs over permafrost, and both of which may have Mars analogs. The interaction of eolian, glacial, and periglacial processes, the results of which were observed in the the field, left indelible images in the minds and on the films of many participants. For instance, classic ventifacts on the summit of a moraine, and thick deposits of loess composed of dust that was originally derived from outwash plains, attested to the importance of wind modification or eolian genesis of many landforms and rock units that are an integral part of the regional glacial geologic assemblage. This series of observations of the interplay of wind and ice processes became a sharply imprinted reminder that multiple processes are likely to have operated in concert on Mars as well.

The involvement of Earth scientists was a major factor in the success of this field-oriented workshop. Many participants left the meeting with the conviction that interaction between the Mars and Earth science communities, as exhibited at the northern plains meeting, should continue, and that the combination of formal workshops with field studies is the nominal way for the deepest interaction to occur.

Call for Future Field-oriented Meetings of the Mars Science Community: It is widely acknowledged that Mars is an Earth-like planet (relative to other objects in the solar system). Accordingly, virtually all geomorphological interpretations of Mars are based, in part, on analogical inferences drawn directly from (or modified from) observations and interpretations of terrestrial geologic features. This is a justifiable basis from which to proceed in our studies of martian geological history, climate evolution, and atmospheric evolution, because there are insufficient data to build a geology of Mars from a totally "martian" perspective.

Some of the most dynamic recent controversies in Mars science have centered on geologic (or geomorphologic) interpretations of features that seem to speak differently to different observers. The controversies and the interpretations, of course, are in the minds of the observers, not in the rocks of Mars! The rocks surely have their stories to tell in all their fine detail, and it is the planetary geologists' job to decipher these stories. A roughly consistent geologic explanation of the martian surface has eluded Mars geologists, as a group, thus far. The problem is that, with the data we have, there are too many processes on Earth that might have formed many of the varied martian landforms. One can excuse the physical modelers when they sieze on the geologists' consistent descriptions of a very few types of landforms (e.g., sand dunes and volcanos) and frame very specific, and sometimes overly conservative, models around these limited observations and interpretations. Many geologists consider much of the recent Mars modeling to have very little relevance to the most dynamic episodes in martian geologic history; this is perhaps inevitable until the Mars geologists reach a consensus on a few of the major issues, and this is not likely to happen until new types of data, especially "ground truth," are obtained.

Our individual experiences shape our perceptions of martian geologic history. Because these experiences differ, and especially because Mars data are barely skin-deep, our concepts of martian history differ, often by ocean widths. It is necessary for Mars geologists to share the geological bases for our differing views with one another and with nongeologists in the Mars science community more than we have in the past. Just as with Earth scientists, it may be necessary to get out of the lecture hall and into the field. Ideally, we would all go to Mars, of course, but less than ideally, we should settle for Earth analog terrains as our field experiences. If expertly guided by Earth science specialists (who may or may not be members of the Mars science community), and if attended by representatives of all the subareas of Mars science, these field experiences may (1) teach the Mars community much about Mars, (2) educate the Mars community in the latest twists and turns and bruising battles in evolving thought of the Earth science community, and (3) inform Earth scientists of the latest shifts in thinking about Mars, including hypotheses and models that just might have bearing on matters pertaining to terrestrial geologic and climate evolution.

Probably all members of the Mars science community have something considerable to learn about somebody else's concepts of Mars. Of course, this is partly why we go to conferences and workshops. This is also the major reason why each of us should attend Mars-oriented field workshops, if such were available. At least in recent years, there has been no consistent framework in which anyone's field expertise could be shared with the wider Mars science community. Particularly now that it will be several more years before we can expect the next major infusion of Mars data, the time is right to establish a formal, Mars-oriented series of field workshops in which funded organizers would have a limited amount of money available for (1) preworkshop field work required for field trip planning, (2) organizing and conducting of the workshop and associated field trips, and (3) payment of expenses incurred by key invited personnel, who may include invited geological field experts, climate modeling specialists, and others who may be crucial to the success of the meeting (and who may or may not be members of the regular Mars science community).

The proposed field meetings do not need to be conducted in association with every topical meeting of the Mars science community, nor does every field trip have to be a multiday affair, complete with overflights. It would be relatively easy, if a few individuals are interested enough to put out a little effort, to organize day-long field trips to be conducted after or just prior to several meetings each year. Perhaps once each year there might be a more extensive field meeting, when the major purpose is to get scientists into the field in classic field areas that may pertain to Mars. The organizers of the northern plains MSATT meeting, and of the earlier Lake Bonneville field workshop (which was conducted in association with the Mars mappers' meeting in 1992), have found that it is all too easy to excite members of the Earth science community about Mars, and to obtain their expert leadership in the field. The Mars science community, as a community, should be taking full advantage of our existence on a very dynamic and, in some ways, a very Mars-like planet; we should not forget that there are many Earth science specialists who may want to share what they know about Earth so that we may learn more about Mars.

References: [1] Kargel et al., eds. (1993) *LPI Tech. Rpt. 93-04.*

TEMPORAL AND SPATIAL MAPPING OF ATMOSPHERIC DUST OPACITY AND SURFACE ALBEDO ON MARS. S. W. Lee[1], R. T. Clancy[1], G. R. Gladstone[2], and T. Z. Martin[3], [1]Laboratory for Atmospheric and Space Physics, University of Colorado, Boulder CO 80309, USA, [2]Southwest Research Institute, P. O. Drawer 28510, 6220 Culebra, San Antonio TX 78228, USA, [3]Mail Stop 169-237, Jet Propulsion Laboratory, 4800 Oak Grove Dr., Pasadena CA 91109, USA.

The Mariner 9 and Viking missions provided abundant evidence that eolian processes are active over much of the surface of Mars [1,2]. Past studies have demonstrated that variations in regional albedo and wind streak patterns are indicative of sediment transport through a region [3,4], while thermal inertia data [derived from the Viking Infrared Thermal Mapper (IRTM) dataset] are indicative of the degree of surface mantling by dust deposits [5–9]. The visual and thermal data are therefore diagnostic of whether net erosion or deposition of dust-storm fallout is taking place currently and whether such processes have been active in a region over the long term. These previous investigations, however, have not attempted to correct for the effects of atmospheric dust loading on observations of the martian surface, so quantitative studies of current sediment transport rates have included large errors due to uncertainty in the magnitude of this "atmospheric component" of the observations.

We are making use of the method developed by T. Z. Martin to determine dust opacity from IRTM thermal observations [10,11]. We have developed a radiative transfer model that allows corrections for the effects of atmospheric dust loading on observations of surface albedo to be made. This approach to determining "dust-corrected surface albedo" incorporates the atmospheric dust opacity, the single-scattering albedo and particle phase function of atmospheric dust, the bidirectional reflectance of the surface, and accounts for variable lighting and viewing geometry. The most recent dust particle properties [12,13] are utilized. The spatial and temporal variability of atmospheric dust opacity strongly influences the radiative transfer modeling results. This approach allows the atmospheric dust opacity to be determined at the highest spatial and temporal resolution supported by the IRTM mapping data; maps of "dust-corrected surface albedo" and atmospheric opacity can be constructed at a variety of times for selected regions. As a result, we obtain information on the spatial and temporal variability of surface albedo and atmospheric opacity and inferences of the amount of dust deposition/erosion related to such variability.

Analyses of IRTM mapping observations of the Syrtis Major region, covering a time span of more than a martian year, will be presented.

References: [1] Veverka J. et al. (1977) *JGR, 82*, 4167–4187. [2] Thomas P. et al. (1981) *Icarus, 45*, 124–153. [3] Lee S. W. et al. (1982) *JGR, 87*, 10025–10042. [4] Lee S. W. (1986) *LPI Tech. Rpt. 87-01*, 71–72. [5] Kieffer H. H. et al. (1977) *JGR, 82*, 4249–4295. [6] Christensen P. R. (1982) *JGR, 87*, 9985–9998. [7] Christensen P. R. (1986) *JGR, 91*, 3533–3545. [8] Christensen P. R. (1986) *Icarus, 68*, 217–238. [9] Jakosky B. M. (1986) *Icarus, 66*, 117–124. [10] Martin T. Z. (1986) *Icarus, 66*, 2–21. [11] Martin T. Z. (1993) *JGR*, in press. [12] Clancy R. T. and Lee S. W. (1991) *Icarus, 93*, 135–158. [13] Clancy R. T. et al. (1993) *Abstracts for the MSATT Workshop on Atmospheric Transport on Mars.*

522-91 ABS. ONLY

HOW WELL WAS TOTAL OZONE ABUNDANCE INFERRED WITH MARINER 9? B. L. Lindner, Atmospheric and Environmental Research, Inc., 840 Memorial Drive, Cambridge MA 02139, USA.

Ozone is a key to understanding atmospheric chemistry on Mars. Over 20 photochemical models of the martian atmosphere have been published, and O_3 is often used as a benchmark for these models [1–3]. O_3 abundance has been inferred from instrumentation on several spacecraft, with the most complete coverage provided by Mariner 9 [3,4]. The Mariner 9 UV spectrometer scanned from 2100 to 3500 Å with a spectral resolution of 15 Å and an effective field of view of approximately 300 km² [4]. The only atmospheric absorption in the 2000–3000-Å wavelength region was previously assumed to come from the Hartley band system of ozone [4], which has an opacity of order unity at winter polar latitudes [3]. Therefore the amount of ozone was inferred by fitting this absorption feature with laboratory data of ozone absorption, as shown in Fig. 1 [4]. Mars O_3 shows strong seasonal and latitudinal variation, with column abundances ranging from 0.2 μm-atm at equatorial latitudes to 60 μm-atm over northern winter polar latitudes [4] (1 μm-atm is a column abundance of 2.689×10^{15} molecules cm^{-2}). However, the O_3 abundance is never great enough to significantly affect atmospheric temperatures [5] or surface temperatures and frost amounts [6]. Figure 2 shows some of the previously inferred O_3 abundances [7].

A radiative transfer computer model is used to reexamine the Mariner 9 UV spectra. Assuming a constant mixing ratio for O_3 and no chemical or radiative interaction between O_3 and clouds/dust, Fig. 3 shows that when typical amounts of dust and cloud are present, significant underestimation of O_3 abundance occurs. A factor of 3 times as much O_3 is needed to generate the same spectrum the spacecraft would measure for a cloudy, dusty atmosphere as for a clear atmosphere. If the scattering properties of martian clouds and dust were well known, their appearance would not be a problem, as a model would be capable of retrieving the O_3 abundance. However, these properties are not well known, which raises doubts about the effectiveness of the UV reflectance spectroscopy technique for measuring O_3 abundance on Mars. The simulations shown in Fig. 3 are repeated for a range in solar zenith angle (50°–90°); ground albedo (0.3–0.8); altitude distribution of O_3; satellite viewing geometries; and cloud, dust, and O_3 abundances. A factor of 3 underestimation is typical, with greater underestimation for high ground albedo or high dust opacities. Even if scattering by clouds is properly accounted for (as previously done with Mariner 9 data reduction in [4]), masking by dust can easily result in factor-of-2 underestimation. Results are not strongly dependent on solar zenith angle.

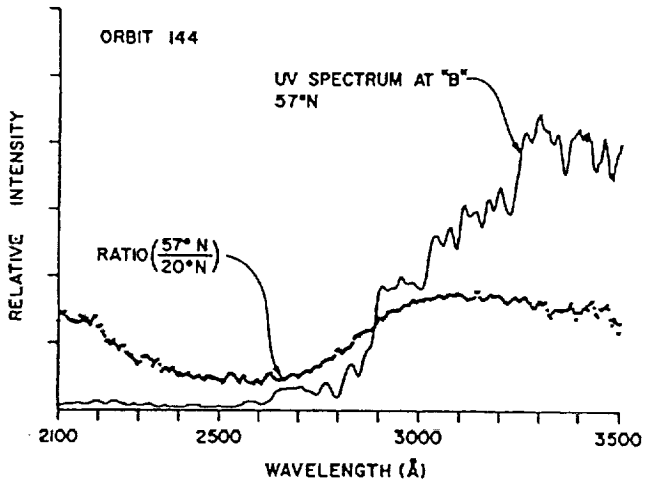

Fig. 1. Ultraviolet spectrum measured by Mariner 9 at 57°N latitude on orbit 144 [7]. To enhance the O_3 absorption feature, this spectrum was divided by one obtained at 20°N latitude on orbit 144, where O_3 abundances are minimal [7].

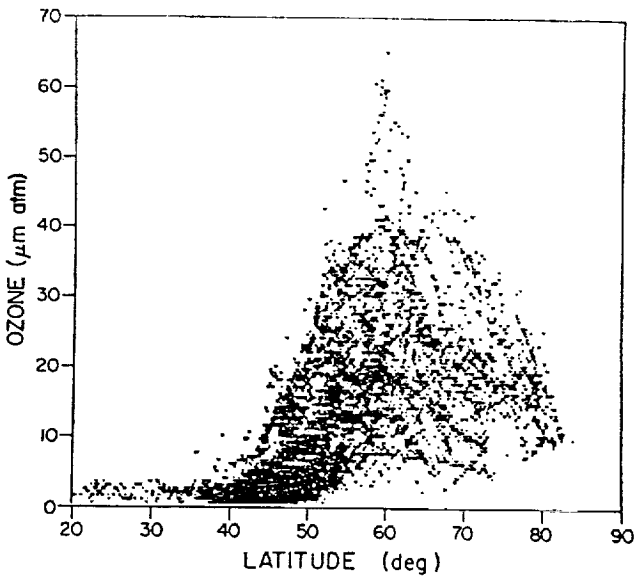

Fig. 2. Measurements of the O_3 column abundance previously inferred from the Mariner 9 UV spectrometer data during the northern winter, $L_s = 330°–360°$, in the northern hemisphere [4].

Spatial and temporal variability in temperature and water vapor have been claimed to account for the scatter of the data points in Fig. 2 [8]. A decrease in temperature results in a decrease in water vapor, if saturated as expected at prevalent temperatures. A decreased water vapor abundance decreases the availability of odd hydrogen (H, OH, and HO_2), which converts CO and O into CO_2 catalytically, decreasing the abundance of O needed to form O_3. However, water vapor is a small source of odd hydrogen in the winter polar atmosphere compared to H_2, and may not account for most of the variability in Fig. 2 [3]. Masking by clouds and dust may also account for some of the observed O_3 variability, because the nature and opacity of the clouds and dust at winter polar latitudes change significantly spatially and temporally. As the maximum O_3 abundance resides near the surface [3], spacecraft must be able to observe through the entire cloud and dust abundance in order to measure the total O_3 column abundance. If reflectance spectroscopy is used, as on Mariner 9, then the cloud and airborne dust must be traversed twice, first by the incoming solar flux down to the surface, and then once again upon reflection from the surface out to the spacecraft. In addition, the large solar zenith angles at winter polar latitudes mean several times the vertical opacity of cloud and dust must be traversed. Indeed, part of the observed latitudinal variation in O_3 abundance in Fig. 2 may be due to the inability of the spacecraft

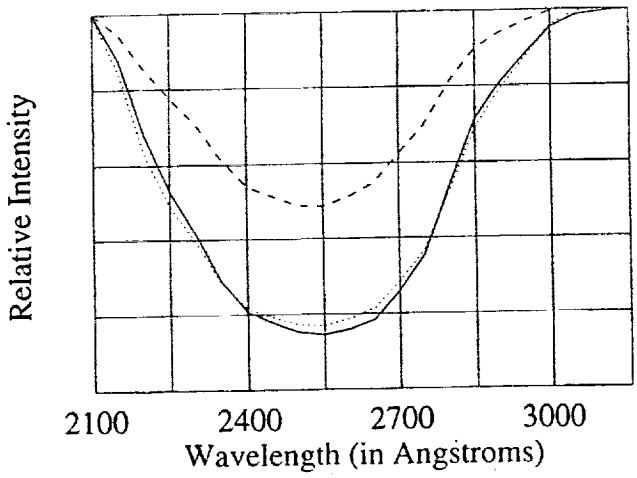

Fig. 3. Synthetic spectra as would be observed by spacecraft for atmospheres with no cloud or dust and 30 μm-atm O_3 (solid line), vertical opacities of dust and cloud of 0.3 and 1.0, respectively, and 30 μm-atm of O_3 (dashed line), and vertical opacities of dust and cloud of 0.3 and 1.0, respectively, and 100 μm-atm of O_3 (dotted line). All cases assume a solar zenith angle of 75° (typical for winter polar observations), and a polar cap albedo of 0.6.

to observe through the increasing effective optical depths as one goes poleward.

By using a photochemical model that included multiple scattering of solar radiation, Lindner [3] showed that the absorption and scattering of solar radiation by clouds and dust should actually increase O_3 abundances at winter polar latitudes. Hence, regions with high dust and cloud abundance could contain high O_3 abundances (heterogeneous chemistry effects have yet to be fully understood [2,9]). It is quite possible that the maximum O_3 column abundance observed by Mariner 9 of 60 μm-atm is common. In fact, larger quantities may exist in some of the colder areas with optically thick clouds and dust. As the Viking period often had more atmospheric dust loading than did that of Mariner 9, the reflectance spectroscopy technique may even have been incapable of detecting the entire O_3 column abundance during much of the Mars year that Viking observed, particularly at high latitudes. The behavior of O_3 is virtually unknown during global dust storms, in polar night, and within the polar hood, leaving large gaps in our understanding.

Acknowledgments: I thank K. Stamnes for providing the radiative transfer program, and NASA's MSATT Program for support.

References: [1] Shimazaki T. (1989) *J. Geomag. Geoelectr., 41*, 273–301. [2] Krasnopolsky V. A. (1993) *Icarus, 101*, 313–332. [3] Lindner B. L. (1988) *Planet. Space Sci., 36*, 125–144. [4] Barth C. A. et al. (1973) *Science, 179*, 795–796; Lane A. L. et al. (1973) *Icarus, 18*, 102–108. [5] Lindner B. L. (1991) *Icarus, 93*, 354–361; Lindner B. L. (1993) *Publ. Astron. Soc. Japan*, submitted. [6] Lindner B. L. (1990) *JGR, 95*, 1367–1379; Lindner B. L. (1992) *GRL, 19*, 1675–1678; Lindner B. L. (1993) *JGR, 98*, 3339–3344. [7] Barth C. A. (1985) in *The Photochemistry of Atmospheres. Earth, Other Planets, and Comets* (J. Levine, ed.), Academic, Florida. [8] Barth C. A. and Dick M. L. (1974) *Icarus, 22*, 205–211. [9] Atreya S. K. and Blamont J. E. (1990) *GRL, 17*, 287–290.

THE EFFECT OF POLAR CAPS ON OBLIQUITY. B. L. Lindner, Atmospheric and Environmental Research, Inc., 840 Memorial Drive, Cambridge MA 02139, USA.

Rubincam [1] has shown that the martian obliquity is dependent on the seasonal polar caps. In particular, Rubincam analytically derived this dependence and showed that the change in obliquity is directly proportional to the seasonal polar cap mass. Specifically, Rubincam showed

$$d\psi/dt = 3 \times 10^{-10}\, M(t)/M(0) \quad \text{degrees/Earth year} \qquad (1)$$

where ψ is the obliquity and M is the mass of the seasonal polar caps, with time t of 0 being the present. This expression assumes uniformly thick spherical caps with identical angular radii of 45°. However, even if a very different polar cap mass distribution is used, Rubincam estimates the total uncertainty in the constant in equation (1) to be less than a factor of 2. Using the current mass of the seasonal polar cap as typical over geologic time, Rubincam calculates that the amount that the obliquity would secularly change is only 1.4°. Considering that the current obliquity of Mars is 25°, Rubincam concludes that seasonal friction does not appear to have changed Mars' climate significantly.

Using a computer model for the evolution of the martian atmosphere, Haberle et al. [2,3] have made a convincing case for the possibility of huge polar caps, about 10× the mass of the current polar caps, that exist for a significant fraction of the planet's history. Given the large uncertainties in input parameters and in the model itself, the results must be regarded as speculative. Also, the Haberle et al. results have been unable to favor or rule out a large polar cap scenario vs. a small polar cap scenario.

Nonetheless, since Rubincam showed that the effect of seasonal friction on obliquity is directly proportional to polar cap mass, a scenario with a ten-fold increase in polar cap mass over a significant fraction of the planet's history would result in a secular increase in Mars' obliquity of perhaps 10° (using equation (1)). Hence, the Rubincam conclusion of an insignificant contribution to Mars' climate by seasonal friction may be incorrect. Furthermore, if seasonal friction is an important consideration in the obliquity of Mars, this would significantly alter the predictions of past obliquity as presented by Ward [4–6], Murray et al. [7], Ward et al. [8], Rubincam [9], Chao and Rubincam [10], Bills [11], Ward and Ruby [12], Touma and Wisdom [13], and Laskar and Robutel [14]. That in turn would significantly alter the predictions of past climate, which are based on obliquity predictions [15–20]. The mechanics of the polar cap system also depend on obliquity [21–26]. If obliquities were often much smaller than at present, that could have implications for past atmospheric composition [27].

Given the enormity of the implications, the effect of the polar caps on the obliquity of Mars should be given more attention and study. Perhaps further modeling of obliquity could be used to rule out the possibility of large polar caps for extended times, which would assist modeling of atmospheric evolution. Similarly, modeling of atmospheric evolution should be given more attention and study because of the implications for obliquity history, and therefore climate history.

Acknowledgments: The author is indebted to the NASA MSATT program for support (Contract No. NASW-4614).

References: [1] Rubincam D. P. (1992) *JGR, 97*, 2629–2632. [2] Haberle R. M. et al. (1992a) *LPI Tech. Rpt. 92-08, Part 1*, 10–11. [3] Haberle R. M. et al. (1992b) *Bull. A.A.S., 24*, 1015–1016. [4] Ward W. R. (1973) *Science, 181*, 260–262. [5] Ward W. R. (1974) *JGR, 79*, 3375–3386. [6] Ward W. R. (1979) *JGR, 84*, 237–241. [7] Murray B. C. et al. (1973) *Science, 180*, 638–640. [8] Ward W. R. et al. (1979) *JGR, 84*, 243–259. [9] Rubincam D. P. (1990) *Science, 248*, 720–721. [10] Chao B. F. and Rubincam D. P. (1990) *JGR, 95*, 14755–14760. [11] Bills B. G. (1990) *JGR, 95*, 14137–14153. [12] Ward W. R. and Ruby D. J. (1991) *Icarus, 94*, 160–164. [13] Touma J. and Wisdom J. (1993) *Science, 259*, 1294–1297. [14] Laskar J. and Robutel P. (1993) *Nature, 361*, 608–612. [15] Sagan C. et al. (1973) *Science, 181*, 1045–1049. [16] Ward W. R. (1974) *JGR, 79*, 3387–3395. [17] Toon O. B. et al. (1980) *Icarus, 44*, 552–607. [18] Fanale F. P. et al. (1982) *Icarus, 50*, 381–407. [19] Pollack J. B. and Toon O. B. (1982) *Icarus, 50*, 259–287. [20] Francois L. M. et al. (1990) *JGR, 95*, 14761–14778. [21] Leighton R. B. and Murray B. C. (1966) *Science, 153*, 136–144. [22] James P. B. and North G. R. (1982) *JGR, 87*, 10271–10283. [23] Lindner B. L. (1990) *JGR, 95*, 1367–1379. [24] Lindner B. L. (1992) *GRL, 19*, 1675–1678. [25] Lindner B. L. (1993) *JGR, 98*, 3339–3344. [26] Wood S. E. and Paige D. A. (1992) *Icarus, 99*, 1–14. [27] Lindner B. L. and Jakosky B. M. (1985) *JGR, 90*, 3435–3440.

N94-33214

5274-91 ABS

ESCAPE OF MARS ATMOSPHERIC CARBON THROUGH TIME BY PHOTOCHEMICAL MEANS. J. G. Luhmann[1], J. Kim[2], and A. F. Nagy[3], [1]Institute of Geophysics and Planetary Physics, University of California, Los Angeles CA 90024-1567, USA, [2]KARI, Seoul, Korea, [3]Space Research Laboratory, University of Michigan, Ann Arbor MI 48109, USA.

Luhmann et al. [1] recently suggested that sputtering of the martian atmosphere by reentering O^+ pickup ions could have provided a significant route of escape for CO_2 and its products throughout Mars' history. They estimated that the equivalent of C in a ~140-mbar CO_2 atmosphere should have been lost this way if the Sun and solar wind evolved according to available models. Another source of escaping C (and O) that is potentially important is the dissociative recombination of ionospheric CO^+ near the exobase [2]. We have evaluated the loss rates due to this process for "ancient" solar EUV radiation fluxes of 1, 3, and 6× the present flux in order to calculate the possible cumulative loss over the last 3.5 Gyr. (Earlier estimates of loss by McElroy [2] used the present-day rates and thus represent underestimates.) The inputs and assumptions for this calculation are the same as used by Zhang et al. [3] for an evaluation of historical O escape by dissociative recombination of ionospheric O_2^+. We find loss rates of C that are at least comparable to the sputtering loss rates, thereby potentially accounting for another 100 mbar or more of Mars' original atmosphere.

References: [1] Luhmann J. G. et al. (1992) *GRL, 19*, 2151–2154. [2] McElroy M. B. (1972) *Science, 443*. [3] Zhang M. H. G. et al. (1993) *JGR, 98*, 10915–10923.

525-91 ABS.ONLY

MIGHT IT BE POSSIBLE TO PREDICT THE ONSET OF MAJOR MARTIAN DUST STORMS? L. J. Martin[1], P. B. James[2], and R. W. Zurek[3], [1]Lowell Observatory, Flagstaff AZ 86001, USA, [2]University of Toledo, Toledo OH 43606, USA, [3]Jet Propulsion Laboratory and California Institute of Technology, Pasadena CA 91109, USA.

This was done very successfully by the late "Chick" Capen in 1971, but we now believe that the chance of having a planet-encircling storm in any given Mars year is less than 50% [1]. Capen suggested that these storms begin around the time of perihelion. More recent storms have extended this season to nearly one-third of a martian year, during the same interval that the south polar cap is receding [2]. There is no observational evidence that storms of this size have occurred outside of that period, although smaller dust storms have been observed throughout most of the martian year. The circumstances that allow a limited storm to become a runaway or encircling storm are not well understood. Seasonal effects are apparently just one aspect of these circumstances, but apparently a critical one. Dust activity seen by Viking near the edges of the receding cap and data showing that the cap may be receding at a faster rate prior to these storms suggest that the seasonal south cap may be influencing dust activity.

We have also determined that the north polar hood recedes during major dust storms, but it is not clear whether impending storms might have an effect upon this atmospheric phenomenon. Viking images do show local storm clouds near the hood prior to the first 1977 planet-encircling dust storm, but the hood is such a dynamic feature that minor changes may not be meaningful. We are, however, continuing to analyze these data.

Several datasets indicate that Mars' atmosphere was less clear before the first 1977 encircling storm, although we cannot discount the possibility that this was merely a seasonal change. Data from other Mars years are less detailed and comprehensive, but the 1977 Viking data from both imaging [3] and infrared [4] suggest that dust in the atmosphere was increasing prior to the storm. Peter Boyce found that, prior to the 1971 planet-encircling storm, there was "violet haze" present on Mars. He attributed this to the impending storm, which may have been correct, but this condition, which could be due in part to atmospheric dust on Mars, is not uncommon at times when no storm is on the way. This may also be true for other indicators of increasing atmospheric dust mentioned above.

Capen also believed that smaller, precursor storms occurred before a planet-encircling storm. This generally seems to be the case, although the data are not conclusive. These earlier storms certainly provide a good vehicle for raising dust into the the atmosphere and regional dust storms may be a sign of an impending larger storm. However, many of these storms occur without any subsequent dust activity, even during the dust storm "season."

Investigations of dust-storm observations show that that the Hellas Basin is the most active area on Mars for all sizes of storms [2]. This area is probably their primary dust source.

Earth-based observations suggest that, during the expansion phase of planet-encircling storms, diurnal cycles often begin at Hellas, presumably with a new load of dust, as mountain climbers return to a base camp for more supplies to be cached along their route. Each day the storms carry an increasing supply of dust farther to the west, until Hellas is reached from the east, completing the

circuit of the globe. This scenario probably requires that the dust supply in Hellas was adequate to provide for a large daily removal during the two-week period that it takes for these storms to encircle Mars. It may be that storms that died out earlier did so because there was not enough dust in Hellas at that time.

Hellas is a traditional name for a bright albedo feature now known as Hellas Planitia. Not everyone is aware, however, that this area is not always bright, and sometimes is not even lighter than its surroundings. Hellas was bright during the Viking and Mariner 9 missions, which, of course, took place during dust-storm years. During Mariner 9 and after the global storm, the basin floor was covered with so much dust that almost no detail showed. In recent years, during which no encircling storms have been observed, Hellas has become less prominent and smaller as an albedo feature. We assume that this means that it contained less dust and possibly not enough to support a runaway dust storm. The albedo of this basin should be closely monitored, especially during the season of the south polar cap's recession.

Predicting major dust storms seemed easier when we knew less about them. We can probably expect this trend to continue. The possible indicators of impending storms discussed above may be helpful, however, and perhaps should be taken seriously in the event that all signs are positive at once.

Martin's research is primarily supported by NASA grants NAGW-2257 and NAGW-3311. HST observations are supported by Space Telescope Institute grant 2379 to the University of Toledo, with subcontracts that include the Lowell Observatory. James is the Principal Investigator for the HST General Observer Team for Mars imaging and a collaborator for the above NASA grants.

References: [1] Zurek R. W. and Martin L. J. (1993) *JGR, 98,* 3247–3259. [2] Martin L. J. and Zurek R. W. (1993) *JGR, 98,* 3221–3246. [3] Martin L. J. and Richardson M. I. (1993) *JGR, 98,* 10941–10949. [4] Martin L. J. et al. (1992) *LPI Tech. Rpt. 92-02,* 99–100.

STUDIES OF ATMOSPHERIC DUST FROM VIKING IR THERMAL MAPPER DATA. T. Z. Martin, Jet Propulsion Laboratory, California Institute of Technology, Pasadena CA 91109, USA.

Following earlier work to map the dust opacity of the Mars atmosphere [1], a number of separate studies have been performed employing the radiometric measurements of the Viking IR Thermal Mappers: (1) extension of global opacity mapping to the entire Viking mission period; L_s 84° in 1976 until L_s 210° in 1979—a span of 1.36 Mars years—with 5° L_s resolution [2]; (2) isolation of opacity behavior at the inception of the two major storms 1977a and 1977b [2]; (3) determination of the effects of topography on the opacities [3]; (4) computation of the mass of dust raised by both local and global dust events [4,5]; and (5) mapping of local dust storm opacity using individual IRTM sequences to provide "snapshots" [5].

These efforts have resulted in a new perspective on the atmospheric dust distribution during the Viking mission, as well as quantitative measures useful in the modeling of likely behavior at other times, and improved boundary conditions for circulation models of Mars. Among the significant findings are these: (1) Confirmation of the persistent dust present in Hellas, as seen frequently in Earthbased observations. A new storm was detected there prior to the 1977a event; however, Hellas seemed less obscured during the 1977a storm than its surroundings. (2) Opacity mapping confirms other evidence that the 1977a and 1977b storms commenced in southern midlatitudes and grew laterally. (3) Minimal opacity increases at the southernmost latitudes provide evidence against significant poleward dust transport during the major 1977 storms. (4) Continued high opacity in equatorial latitudes during later stages of the 1977b storm, consistent with findings from Mariner 9, supports the hypothesis that dust is lofted by diurnal tides [6]. (5) Dust raising appears to be ubiquitous in high northern latitudes during northern spring and summer. This is evidence for significant surface wind stress. (6) Considerable differences in opacity exist between the first and second Mars years observed by Viking, with clearer conditions in the latter. (7) As expected, topography influences observed opacities during relatively clear periods, but the correlation disappears during major storms. (8) Approximately 10^{12} kg of dust were raised at the peak of the 1977b storm, corresponding to 800 kg/km^2. The variation of atmospheric dust loading can be portrayed by computing total dust mass as a function of time from the set of 5° L_s opacity maps (see Fig. 1). (9) The well-known L_s 226° (1977) local dust storm raised about 1.6×10^8 kg of dust.

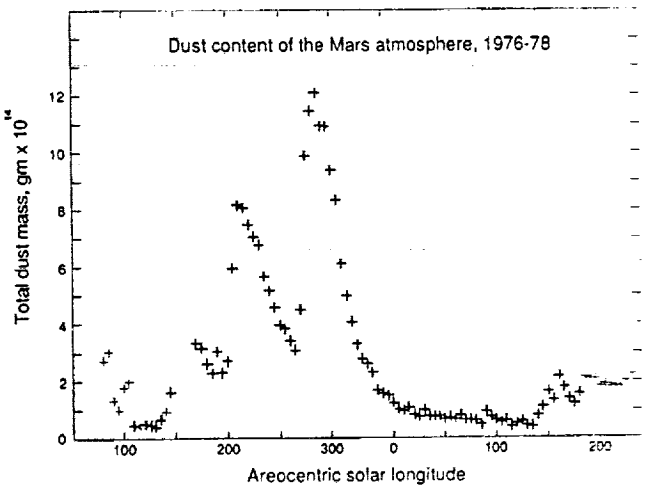

Fig. 1.

While the temporal and spatial coverage of the mapping was not ideal for tracking the development of dust storms, the opacities derived from IRTM data offer good characterization of the general character of martian atmospheric changes. The value of doing both synoptic "snapshots" and systematic coverage is demonstrated.

The research described in this paper was carried out by the Jet Propulsion Laboratory, California Institute of Technology, under a contract with the National Aeronautics and Space Administration.

References: [1] Martin T. Z. (1986) *Icarus, 66,* 2. [2] Martin T. Z. and Lachin A. (1992) *Bull. AAS, 24,* 1009. [3] Martin T. Z. and Richardson M. I. (1993) *JGR, 98,* 10941. [4] Martin T. Z. (1993) *LPI Tech. Rpt. 93-05,* in press. [5] Martin T. Z. and Lachin A. (1993) *Bull. AAS,* in press. [6] Anderson E. and Leovy C. (1978) *J. Atmos. Sci., 35,* 723.

N94-33217

S27-91 ABS

GLOBAL COLOR VIEWS OF MARS. A. S. McEwen, L. A. Soderblom, T. L. Becker, E. M. Lee, and R. M. Batson, U.S. Geological Survey, Flagstaff AZ 86001, USA.

About 1000 Viking Orbiter red- and violet-filter images have been processed to provide global color coverage of Mars at a scale of 1 km/pixel. Individual image frames acquired during a single spacecraft revolution ("rev") were first processed through radiometric calibration, cosmetic cleanup, geometric control, reprojection, and mosaicking [1]. We have produced a total of 57 "single-rev" mosaics. Phase angles range from 13° to 85°. All the mosaics are geometrically tied to the Mars Digital Image Mosaic (MDIM), a black-and-white base map with a scale of 231 m/pixel [2].

The largest challenge in producing a global mosaic from Viking images with useful color and albedo information for the surface was the photometric normalization, including removal of atmospheric effects. First we selected a subset of single-rev mosaics that provide the best global coverage (least atmospheric obscuration and seasonal frost). A Minnaert photometric normalization was applied to normalize the variations in illumination and viewing angles. Image data acquired at illumination or emission angles larger than 77° were trimmed off, as these data are strongly affected by atmospheric scattering. A model image of condensate haze was created from the violet images, consisting of 60% of the violet-filter reflectance greater than 0.05, followed by smoothing over 20-km scales. The haze model was then subtracted from both the violet- and red-filter images. The residual polar caps were excluded from haze removal. This procedure is "conservative" in the sense that it errs on the side of undercorrecting for the haze. Finally, these normalized mosaics were combined with seam removal [3] into global mosaics. Global coverage is about 98% complete in the red-filter mosaic and 95% complete in the violet-filter mosaic. A green-filter image was synthesized from an average of the red- and violet-filter data to complete a three-color set. The Viking Orbiters acquired actual green-filter images covering about 60% of the martian surface.

Two final datasets have been produced: "cosmetic" and "scientific" versions. For the cosmetic version, gaps were filled by interpolation, the violet-filter images were given a divide filter to remove residual atmospheric hazes, and digital airbrushing was applied to the north polar region. The divide filter consists of dividing the value of each pixel by the average value over a 200-km^2 area surrounding each pixel. The north polar region contains the largest gaps and poorest color data due to the typical atmospheric conditions and the geometry of the Viking orbits. For large areas near the north pole with red-only coverage, the violet-filter coverage was synthesized using a function fit to actual Mars red- and violet-filter data. For the scientific versions, data gaps are left blank and the divide filtering and digital airbrushing were not applied. About 30% of the violet-filter data is obscured by hazes to an extent that makes the data unreliable for quantitative analyses of the surface color. We plan to mosaic the available green-filter images in the near future.

The final mosaics have been reprojected into several map projections: Sinusoidal Equal-Area (global), Lambertian Equal-Area (east- and west-hemisphere views), Polar Stereographic (one-half planet views of the northern and southern hemispheres), Mercator (equatorial region), and Orthographic views centered on six different positions. The Orthographic views are most like those seen by a distant observer looking through a telescope. All versions exist both with and without latitude-longitude overlays.

The color balance selected for these images was designed to be close to natural color for the bright reddish regions such as Tharsis and Arabia, but the data have been "stretched" such that the relatively dark regions appear darker and less reddish than their natural appearance. This stretching allows us to better see the color and brightness variations on Mars, which are related to the composition or physical structure of the surface materials. Note that these images are also unnatural because atmospheric effects have been (mostly) removed and because we see the summertime appearance of both polar caps simultaneously.

Five major surface units can be mapped from the global mosaics: (1) bright red regions such as Tharsis, Arabia, and Hellas, which have properties consistent with surface deposits of fine-grained dust such as that carried aloft by dust storms [4]; (2) dark regions, which have properties consistent with coarse-grained sand and rock fragments [4]; (3) intermediate brightness regions, which may represent rough, indurated surfaces [5]; (4) the bright north polar residual cap, which consists of water ice mixed with dust [6]; and (5) the very bright south polar residual cap, which probably consists of CO_2 ice [7].

The global color mosaics have been merged with the MDIM in a set of 30 quadrangles covering Mars at a scale of 462 m/pixel. These products show both the surface morphology as seen from imaging at low Sun elevation angles and the color and albedo information best seen at high Sun elevations. The datasets were merged by the following steps: (1) extract red and violet color data (cosmetic versions) for a quadrangle and make red/violet ratio; (2) reproject red and red/violet ratio to the same map projection and scale as the MDIM quadrangle; (3) choose match points and warp the color images to improve the geometric registration; (4) add the red and MDIM files to create a merged red; (5) divide the merged red by the red/violet ratio to make a merged violet; and (6) average the merged red and violet files to create a synthetic merged green image.

References: [1] McEwen A. S. and Soderblom L. A. (1993) *LPS XXIV*, 955–956. [2] Batson R. M. and Edwards K. (1990) *NASA TM-4210*, 573. [3] Soderblom L. A. et al. (1978) *Icarus, 34*, 446–464. [4] Christensen P. R. and Moore H. J. (1992) in *Mars* (H. H. Kieffer et al., eds.), 686–729. [5] Kieffer H. H. et al. (1981) *Proc. LPSC 12B*, 1395–1417. [6] Kieffer H. H. et al. (1976) *Science, 194*, 1341–1344. [7] Kieffer H. H. (1979) *JGR, 84*, 8263–8288.

N94-33218

S28-91 ABS. ON

THE DISTRIBUTION OF MARTIAN GROUND ICE AT OTHER EPOCHS. M. T. Mellon[1] and B. M. Jakosky[2], [1]Laboratory for Atmospheric and Space Physics, Department of Astrophysical, Planetary, and Atmospheric Sciences, [2]Department of Geological Sciences, University of Colorado, Boulder CO 80309-0392, USA.

The theoretical study of ground-ice stability for the present epoch has shown that ice within the martian regolith is stable poleward of about ±40° latitude with about 20°–30° of variation from one longitude to the next in the northern hemisphere (due to variations in the surface thermal properties). The depth of stability in this region was found to range from a couple of tens of centimeters to about a meter, being closer to the surface nearer to the pole. It was also found that atmospheric water vapor (at Viking-measured abun-

dances) was capable to diffusing into the regolith and condensing as pore ice within the top few meters in these regions of stability. The timescale of condensation of ice from atmospheric water was found to be comparable to that of the evolution of the martian orbit, indicating the need to include past orbital changes in the prediction of the present distribution of ground ice. In the present work we include the past orbital evolution of Mars and examine the changes in ice stability as well as the condensation, sublimation, and diffusion of atmospheric water in an exchange with the regolith.

The martian obliquity has undergone significant oscillations in its recent past. During periods of high obliquity the solar energy would have been distributed such that the equatorial and midlatitude regions would have been colder than at present and the polar regions would have been warmer. Warmer polar regions would result in the sublimation of more polar cap water into the atmosphere and thus higher atmospheric water abundances. This combination of effects would have resulted in ground ice being stable globally. During periods of low obliquity the opposite would have occurred, where the equatorial and midlatitude regions were warmer and the polar regions were colder, resulting in less atmospheric water and ground-ice stability only in the polar regions.

The results of our modeling of the regolith thermal behavior and the molecular diffusion of water vapor within the regolith and in exchange with the atmosphere have shown significant quantities of ground ice can form at all latitudes within the top 50 cm to 1 m of the regolith during periods of high obliquity. The amount of ice that forms can be as much as the regolith pores can hold. During low obliquity most or all of this ice sublimes and diffuses away. Below this depth a longer-term stability is observed at some latitudes where ice steadily increases in concentration regardless of the orbital oscillations that occur.

These changes in the pattern of ice stability may affect the surface morphology at all latitudes. Periodic saturation and dessication of the regolith may produce some type of frost-heave-related features such as solifluction or stone sorting. The presence of ice in conjunction with seasonal thermal cycles may produce small-scale (a few meters) ice-wedge polygons or other forms of segregated ice.

N94-33219

529-91 ABS. ONLY

MINERALOGICAL DIVERSITY (SPECTRAL REFLECTANCE AND MÖSSBAUER DATA) IN COMPOSITIONALLY SIMILAR IMPACT MELT ROCKS FROM MANICOUAGAN CRATER, CANADA. R. V. Morris[1], J. F. Bell III[2], D. C. Golden[1], and H. V. Lauer Jr.[3], [1]Code SN4, NASA Johnson Space Center, Houston TX 77058, USA, [2]NASA Ames Research Center, Moffett Field CA 94035, USA, [3]Lockheed ESC, Houston TX 77058.

Introduction: Meteoritic impacts under oxidizing surface conditions occur on both Earth and Mars. Oxidative alteration of impact melt sheets is reported at several terrestrial impact structures including Manicouagan [1], West Clearwater Lake [2], and the Ries Basin [3,4]. A number of studies [e.g., 5–7] have advocated that a significant fraction of martian soil may consist of erosional products of oxidatively altered impact melt sheets. If so, the signature of the Fe-bearing mineralogies formed by the process may be present in visible and near-IR reflectivity data for the martian surface.

What mineral assemblages form in impact melt sheets produced under oxidizing conditions and what are their spectral signatures? We report here spectral and Mössbauer data for 19 powder samples of impact melt rock from Manicouagan Crater. Experimental procedures are discussed elsewhere [8,9].

Results and Discussion: *Previous chemical and petrographic studies.* One of the important conclusions of chemical studies of Manicouagan impact melt rocks [1] is that there is no significant difference in the bulk composition with respect to either vertical or horizontal sampling of the impact melt sheet (230 m thick and 55 km

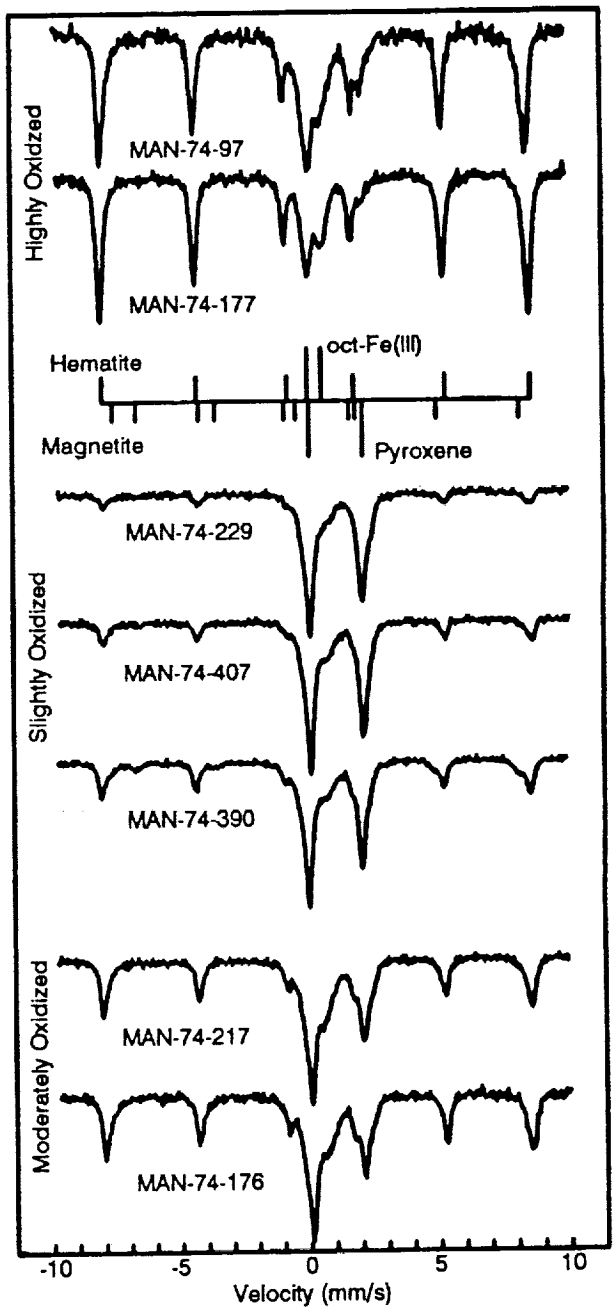

Fig. 1.

wide). Although chemical compositions are similar, the oxidation state of Fe is highly variable: $FeO/(FeO + Fe_2O_3)$ varies from 0.142 to 0.639. However, there is still no significant difference in chemical composition when the samples are grouped according to $FeO/(FeO + Fe_2O_3)$. The 12 samples with the lowest values have the same average composition as the 12 samples with the highest values. All samples are at least somewhat oxidized as [1] estimate a prealteration value of 0.77.

The mineralogy of the impact melt rocks [1] includes plagioclase, sanidine, Ca-rich pyroxene, pigeonite (in various stages of inversion to hypersthene), quartz, titanoferrous magnetite, and apatite. Approximate pyroxene compositions are $Wo_{40}En_{42}Fs_{18}$ and $Wo_4En_{53}Fs_{43}$. Alteration (oxidation and/or hydration) products of glass, mafic minerals (mainly olivine and Ca-poor pyroxene), and oxides are smectite, hematite, and possibly hydrous ferric oxides [1]. The alteration is thought to have occurred shortly after the impact when oxidizing vapors and/or solutions (probably of external origin) reacted with the impact melt, which was below its solidus temperature but still relatively hot.

Mössbauer and Reflectivity Spectra: *Highly oxidized samples ($FeO/(FeO+Fe_2O_3) < 0.250$).* Representative Mössbauer and reflectivity spectra are shown in Figs. 1 and 2. The Mössbauer spectra are dominated by a hematite (α-Fe_2O_3) sextet; the asymmetry of the lines implies impurities (probably Ti) are present. There is no evidence for a goethite (α-FeOOH) sextet. A doublet resulting from octahedrally coordinated ferric iron and a small doublet resulting from ferrous iron in pyroxene are also present. The origin of the ferric doublet cannot be uniquely assigned at present. It could result from pseudobrookite solid solutions (from ilmenite oxidation) or from ferric iron in a silicate phase such as pyroxene or smectite. Nanophase ferric oxides and lepidocrocite (γ-FeOOH) are unlikely because, respectively, the doublet was not removed by extraction with DCB and not magnetically split by 16 K. The reflectivity spectra are dominated by the signature of hematite (band minimum or plateau center near 840 nm, relative reflectivity maximum near 750 nm, and inflections near 620 and 520 nm [e.g., 10]).

What is the origin of the hematite? The Mössbauer and reflectivity spectra of MAN-74-177 are virtually identical to those published by [11] for Hawaiitic tephra sample HWMK11. As discussed by [11], this sample is completely oxidized (presumably by heating to a high temperature) and contains hematite grains with highly variable Ti contents. The larger hematite grains are Ti rich and were attributed to thermal oxidation and phase separation of precursor Ti-magnetites. Fine hematite grains are distributed throughout the glass matrix, are Ti poor, and were formed from exclusion of silicate phases (including glass) during thermal oxidation. Phinney et al. [2] describe a similar situation for the reddish impact melt rocks from West Clearwater Lake. Straub et al. [12] report the for-mation of nanophase hematite during the thermal decomposition of pyroxene. Thus, it is reasonable to conclude that hematite formation in the highly oxidized Manicouagan impact melt samples proceeded by thermally induced magnetite oxidation and silicate decomposition.

Slightly oxidized samples ($FeO/(FeO+Fe_2O_3) > 0.500$. Hematite is still present but in significantly lesser amounts than in the heavily oxidized samples (Figs. 1 and 2). Magnetite is present in MAN-74-390. The ferrous doublet from pyroxene is the dominant feature in the Mössbauer spectra. The two-band signature typical of ferrous iron in orthopyroxene and type-B clinopyroxene [13] is

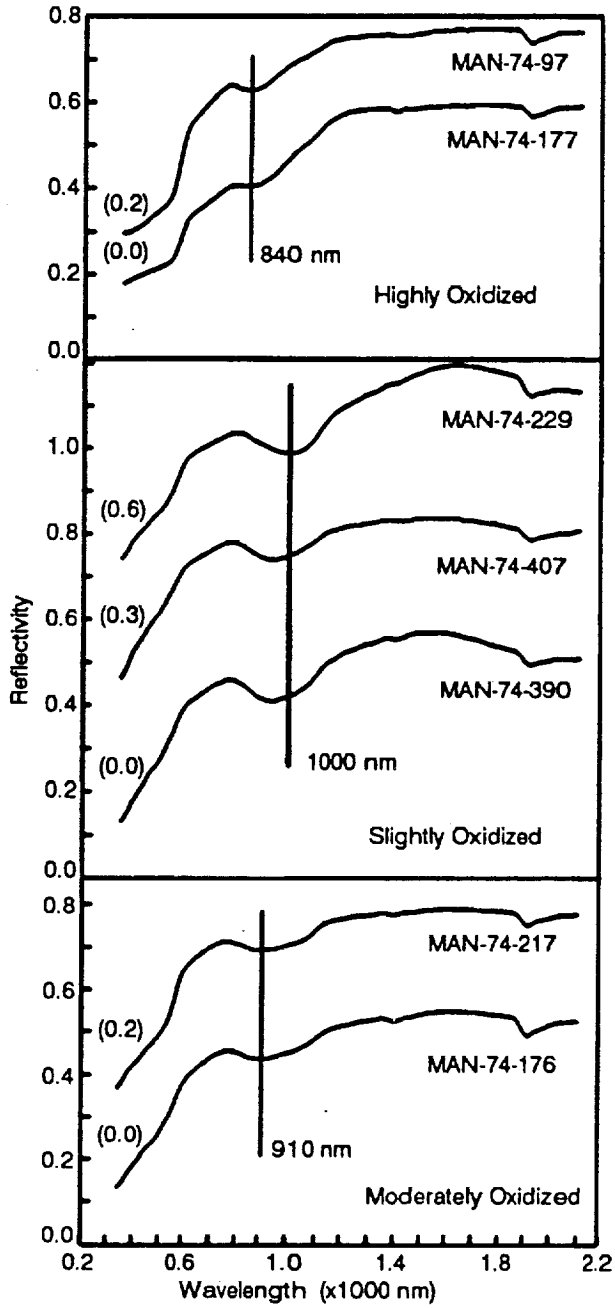

Fig. 2.

clearly evident in the reflectivity spectra. The position of the first band is well defined and varies from ~940 nm to 1000 nm, which implies more than one pyroxene is present. The positions are consistent with the high- and low-Ca pyroxenes [13] observed petrographically [1]. Positions of the second bands are not definable because they are partially obscured by H_2O bands near 1900 nm and our data do not extend to long enough wavelength.

Moderately oxidized samples $0.500 > (FeO/(FeO+Fe_2O_3) > 0.250$. Mössbauer and reflectivity spectra for two samples having

intermediate values of FeO/(FeO + Fe_2O_3) are shown in Figs. 1 and 2. Their Mössbauer spectra show more comparable amounts of hematite and pyroxene than the heavily and slightly oxidized samples. The reflectivity data for both have a band minimum near 910 nm, which could result from (1) a composite of hematite (840–870-nm) and pyroxene (940-nm) bands; (2) a different pyroxene characterized by a 910-nm band; (3) a composite band derived from a pyroxene ferrous band and a pyroxene ferrous-ferric charge transfer band; and (4) another ferric mineral (e.g., goethite) having a band in this region. Alternative (4) is excluded by the Mössbauer data specifically for the case of goethite. None of the other alternatives can be excluded. However, a pyroxene 910-nm band usually implies a second band near 1800 nm [13], which we would probably observe, and [12] did not observe ferrous-ferric charge transfer transitions in two-band pyroxenes they subjected to thermal oxidation in air. Thus, there is some evidence to favor the interpretation involving composite hematite-pyroxene bands. This is particularly the case for MAN-74-217, where the 750-nm relative reflectivity maximum and 620- and 520-nm inflections are evidence for a strong spectral contribution from hematite.

Implications for Interpretation of Martian Spectral Data: Visible and near-IR martian bright-region spectral data (400 to ~2000 nm) returned from groundbased telescopes and the Phobos-2 encounter are characterized by a shallow band minimum in the near-IR whose position varies between approximately 850 and 1000 nm [14,15]. It is reasonable to assign these endmember band positions to hematite and pyroxene respectively [8,14,15]. Assignment of band positions near 910 nm is more equivocal. Murchie et al. and Geissler et al. [14,16] favor another ferric phase (like goethite) as the interpretation for Phobos-2 bands in the region of 910 nm, although they do not exclude composite hematite-pyroxene bands. The results of this study show for naturally occurring materials that composite hematite-pyroxene bands have minima in the 910-nm region. Thus, many of the anomalous Phobos-2 spectra can be explained by assemblages whose endmembers (hematite and pyroxene) are accepted to be present on Mars. Furthermore, our results show that a mineralogically diverse suite of rocks can be generated at essentially constant composition, which implies that variations in martian surface mineralogy do not necessarily imply variations in chemical composition.

References: [1] Floran et al. (1978) *JGR, 83*, 2737. [2] Phinney et al. (1978) *LPS IX*, 2659. [3] Pohl et al. (1977) *Impact and Explosion Cratering*, 343. [4] Newsom et al. (1986) *Proc. LPS 17th*, in *JGR, 91*, E239. [5] Newsom (1980) *Icarus, 44*, 207. [6] Kieffer and Simonds (1980) *Rev. Geophys. Space Phys., 18*, 143. [7] Allen et al. (1982) *JGR, 87*, 10083. [8] Morris et al. (1989) *JGR, 94*, 2760. [9] Morris et al. (1993) *GCA*, in press. [10] Morris et al. (1985) *JGR, 90*, 3126 [11] Golden et al. (1993) *JGR, 98*, 3401. [12] Straub et al. (1991) *JGR, 96*, 18819. [13] Cloutis and Gaffey (1991) *JGR, 96*, 22809. [14] Murchie et al. (1993) *Icarus*, in press. [15] Bell et al. (1990) *JGR, 95*, 14447. [16] Geissler et al. (1993) *Icarus*, in press.

MARTIAN SPECTRAL UNITS DERIVED FROM ISM IMAGING SPECTROMETER DATA.

S. Murchie[1], J. Mustard[2], and R. Saylor[3], [1]Lunar and Planetary Institute, Houston TX 77058, USA, [2]Brown University, Providence RI 02912, USA, [3]Western Kentucky University, Bowling Green KY 42101,USA.

Introduction: Based on results of the Viking mission, the soil layer of Mars has been thought to be fairly homogeneous and to consist of a mixture of as few as two components, a "dark gray" basaltic material and a "bright red" altered material [1,2]. However, near-infrared reflectance spectra measured recently both telescopically and from spacecraft indicate compositional heterogeneity beyond what can be explained by just two components [3,4]. In particular, data from the ISM imaging spectrometer [4,5], which observed much of the equatorial region at a spatial resolution of ~22 km, indicate spatial differences in the presence and abundance of Fe-containing phases, hydroxylated silicates, and H_2O [4.6–8]. We have used the ISM data to define, characterize, and map soil "units" based on their spectral properties. The spatial distributions of these "units" were compared to morphologic, visible color, and thermal inertia features recognized in Viking data.

Analysis: We investigated ISM data "windows" that cover eastern Tharsis, Valles Marineris, Arabia, Syrtis Major, Isidis, and Amenthes. These areas contain examples of most of the variations in color, reflectance, and thermal inertia recognized in Viking data [2]. The windows were registered with the digital topographic map of Mars using spacecraft pointing information and correlation of topographic relief features with variations in depth of the 2.0-μm atmospheric CO_2 absorption. The ISM data were reduced to a suite of "parameter" images that describe key sources of spectral variability, including reflectance, strength of a narrow absorption at 2.2 μm attributed to metal-OH, depth of the 3.0-μm H_2O absorption, depth of the broad 2-μm absorption attributed to Fe in pyroxene, and NIR spectral slope. Representative spectra were extracted for regions displaying different spectral characteristics to validate these differences and to characterize the shape and position of the 1-μm and 2-μm absorptions due to ferric and ferrous iron.

The parameterized ISM data were then classified using principal components analysis. Three principal components were found capable of accounting for most of the observed variations in NIR spectral properties. Spatial variations in the contributions or "loadings" of the principal components define coherent regions of soils having distinctly different spectral properties.

Results: The observed martian soils can be divided into broad groupings (Table 1) based on systematic, spatially coherent differences in their spectral attributes. The two largest groupings correspond with materials that are "bright red" and "dark gray" at visible wavelengths. "Normal bright soil" exhibits a high albedo, an intermediate 3.0-μm absorption, a relatively strong 2.2-μm absorption, and a flat spectral slope; "normal dark soils" exhibit a strong 2-μm pyroxene absorption and a relatively weak 3.0-μm absorption. Each group can be subdivided further based on position and shape of the ferric iron absorption in bright regions, and in dark regions, spectral slope, strength of the 3.0-μm absorption, and position and shape of the 1-μm and 2-μm absorptions due to Fe in pyroxene. "Transitional" soils, which occur largely at borders of "normal" bright and dark soils, are intermediate to "normal" bright and dark soils in most respects but have a negative spectral slope.

TABLE 1. Properties and geologic correlations of ISM spectral units.

Arbitrary Unit Designation	3-μm "Water" Band Depth	2-μm "Pyroxene" Band Depth	Spectral Slope	2.2-μm "M-OH" Band Depth	Center of Ferric Band	Geologic Correlations
Low Albedo						
Normal dark I	Weak	Strong/v. strong	Intermed.	Weak/absent	—	Parts of plateau plains, floor of Valles Marineris
Normal dark II	Weak	Intermed./strong	Negative/v. negative	Weak/absent	—	Parts of plateau plains
Normal dark III	Intermed.	Intermed./strong	Negative	Weak/absent	—	Plateau plains in Arabia
High Albedo						
Normal bright I	Intermed./strong	Weak/absent	Flat	Strong	0.85 μm	Low-thermal-inertia regions of Tharsis; parts of Amenthes
Normal bright II	Intermed./strong	Weak/absent	Very Flat	Strong	0.92 μm	Low-thermal-inertia regions of Arabia
Transitional	Intermed./strong	Weak	Intermed./v. negative	Intermed./strong	—	Libya Montes; parts of Amenthes; bright-dark borders
Anomalous						
Hydrated dark	Strong	V. strong	Flat/very flat	Weak/absent	—	Layered material in Melas, Eos. Ch.
Intermediate	Intermed.	Intermed.	Flat/intermed.	Weak/absent	—	Layered material in Hebes, C. Candor Ch.
Hydrated bright I	V. strong	Weak/absent	Flat	Strong/ v. strong	~0.86 μm	Basin fill of Isidis
Hydrated bright II	V. strong	Intermed.	Very flat	Intermed.	—	"Dark red" plains in Western Arabia
Hydrated bright III	V. strong	Weak/absent	Very flat	Intermed.	0.89 μm?	"Dark red" plains in Lunae Planum
Hydrated bright IV	V. strong	Weak	Negative/v. negative	Weak/absent	—	Layered material in E. W Candor Ch.

The remainder of the data, about 15% of the observed surface, are "anomalous" and can be divided into as many as six additional groupings, which are distinct spectrally from "normal" bright, "normal" dark, and "transitional" soils. Parts of Lunae Planum and western Arabia with a "dark red" visible color are intermediate to "normal" bright and dark soils in some respects, but, unlike "transitional" areas, they have a flat spectral slope and they exhibit a stronger 3.0-μm absorption than do either "normal bright" or "normal dark" soils. Low-albedo layered materials in Valles Marineris have a stronger 2-μm pyroxene absorption than most dark regions, yet also a stronger 3-μm absorption than most bright regions. High-albedo layered materials are very heterogeneous, with some regions characterized by a higher albedo and very strong 3.0-μm absorption, and others exhibiting an intermediate albedo and a 2-μm pyroxene absorption. Isidis resembles "normal bright soil" in most respects, but has a much stronger 3.0-μm absorption.

Discussion: "Normal bright soils" are correlated spatially with low-thermal-inertia regions interpreted as accumulations of "dust" by airfall [2,9,10]. The ferric absorption at 0.85 μm throughout the Tharsis region and in Amenthes is indicative of hematite, but the absorption at 0.92 μm throughout Arabia indicates the presence of one or more additional Fe phases, possibly goethite or ferrihydrite [8,11]. This difference implies that all low-thermal-inertia regions cannot be airfall derived from a single, well-mixed reservoir, and that regional lithologic differences have survived eolian mixing. The intermediate albedo and absorption strengths in "transitional" soils appear to a first order to be consistent with mixture of local "normal" bright and dark components; their negative spectral slope is consistent with a bright component either coating or mixed intimately with a darker substrate [12,13].

In contrast, "anomalous" soils are mostly intermediate to high albedo, but lie outside the low-inertia regions. They exhibit greater spectral heterogeneity than "normal" bright and dark soils, they are distinctive from "transitional" soils, and they are correlated spatially with independently identified high-thermal-inertia features and geologic units. As such they may represent indurated materials and/or exposures of specific geologic deposits. For example, intermediate-albedo "dark red" soils in Lunae Planum and Arabia correspond to high thermal inertia surfaces previously interpreted as cemented duricrust [2]. Their strong 3.0-μm absorptions suggest enrichment in a water-bearing phase, perhaps hydrated salts that act as the duricrust's "cement" [cf. 14]. The Isidis unit also corresponds with a thick, unconformable, basin-filling deposit [15] having anomalously high thermal inertia [2,10]. This unit's high inertia and strong 3.0-μm absorption would also be consistent with induration of soil by water-bearing cement, but its high albedo and relatively strong 2.2-μm absorption indicate a different compositon of cemented particulates than in "dark red" soils.

The "intermediate," "hydrated dark," and "hydrated bright" units in Valles Marineris correspond with different plateaus of eroded layered materials. Previous analysis of ISM data covering these deposits has also shown that their absorptions due to Fe vary in position and strength, indicating the presence of pyroxenes of different composition [6,7] and local enrichments of ferric minerals [16]. This heterogeneity in the layered materials' spectral properties supports previous inferences based on stratigraphic relations that layered materials were emplaced under differing environmental regimes [17,18].

References: [1] Arvidson R. et al. (1982) *JGR, 87*, 10149. [2] Christensen P. and Moore H. (1992) in *Mars* (H. Kieffer et al.,

eds.), 686, Univ. of Arizona, Tucson. [3] Bell J. (1992) *Icarus, 100,* 575. [4] Erard S. et al. (1991) *LPS XXI,* 437. [5] Bibring J.-P. et al. (1990) *LPS XX,* 461. [6] Murchie S. et al. (1992) *LPS XXIII,* 941. [7] Mustard J. et al. (1993) *LPS XXIV,* 1039. [8] Murchie S. et al. (1993) *Icarus,* in press. [9] Palluconi F. and Kieffer H. (1978) *Icarus, 45,* 415. [10] Christensen P. (1986) *Icarus, 68,* 217. [11] Morris R. et al. (1985) *JGR, 90,* 3126. [12] Singer R. and Roush T. (1983) *LPS XIV,* 708. [13] Morris R. and Neely S. (1982) *LPS XIII,* 548. [14] Merenyi E. et al. (1992) *LPS XXIII,* 897. [15] Grizzaffi P. and Schultz P. (1989) *Icarus, 77,* 358. [16] Geissler P. et al. (1993) *Icarus,* in press. [17] Witbeck N. et al. (1991) *U.S.G.S. Misc. Inv. Ser. Map I-2010.* [18] Komatsu G. et al. (1993) *JGR. 98.* 11105.

S31-91 ABS. ONLY

EDDY TRANSPORT OF WATER VAPOR IN THE MARTIAN ATMOSPHERE. J. R. Murphy[1,2] and R. M. Haberle[1], [1]SJSU Foundation, [2]NASA Ames Research Center, Moffett Field CA 94035, USA.

Viking orbiter measurements of the martian atmosphere suggest that the residual north polar water-ice cap is the primary source of atmospheric water vapor, which appears at successively lower northern latitudes as the summer season progresses [1]. Zonally symmetric studies of water vapor transport indicate that the zonal mean meridional circulation is incapable (due to its weakness at high latitudes) of transporting from north polar regions to low latitudes the quantity of water vapor observed [2]. This result has been interpreted as implying the presence of nonpolar sources of water, namely subsurface ice and adsorbed water, at northern middle and subtropical latitudes. Another possibility, which has not been explored, is the ability of atmospheric wave motions, which are not accounted for in a zonally symmetric framework, to efficiently accomplish the transport from a north polar source to the entirety of the northern hemisphere. The ability or inability of the full range of atmospheric motions to accomplish this transport has important implications regarding the questions of water sources and sinks on Mars: if the full spectrum of atmospheric motions proves to be incapable of accomplishing the transport, it strengthens arguments in favor of additional water sources.

Preliminary results from a three-dimensional atmospheric dynamical/water vapor transport numerical model will be presented. The model accounts for the physics of a subliming water-ice cap, but does not yet incorporate recondensation of this sublimed water. Transport of vapor away from this water-ice cap in this three-dimensional framework will be compared with previously obtained zonally symmetric (two-dimensional) results to quantify effects of water vapor transport by atmospheric eddies.

References: [1] Jakosky and Farmer (1982) *JGR, 87,* 2999–3019. [2] Haberle and Jakosky (1990) *JGR, 95,* 1423–1437.

S32-91 ABS.

IRTM BRIGHTNESS TEMPERATURE MAPS OF THE MARTIAN SOUTH POLAR REGION DURING THE POLAR NIGHT: THE COLD SPOTS DON'T MOVE. D. A. Paige[1], D. Crisp[2], M. L. Santee[2], and M. I. Richardson[1], [1]Department of Earth and Space Sciences, UCLA, Los Angeles CA 90024, USA, [2]Jet Propulsion Laboratory, Pasadena CA 91106, USA.

The Viking Infrared Thermal Mapper (IRTM) polar winter season observations in the 20-μm channel showed considerable temporal and spatial structure, with minimum brightness temperatures well below the surface CO_2 frost point of ~148 K [1,2]. Brightness temperatures as low as 134 K in the south and 128 K in the north were observed. To date, these low brightness temperatures have not been uniquely explained. In the 1976 paper, Kieffer et al. [1] suggested three mechanisms: (1) low surface emissivities, (2) presence of high-altitude clouds, and (3) depressed solid-vapor equilibrium CO_2 frost kinetic temperatures due to reduced atmospheric CO_2 partial pressures at the surface. Hess [3] cast doubt on mechanism (3) by showing that vertical and horizontal gradients in average molecular weight of the polar atmosphere could only be stable under special circumstances.

In 1979, Ditteon and Kieffer [4] published infrared transmission spectra of thick, solid CO_2 samples grown in the laboratory. The results showed that in wavelengths away from the strong CO_2 absorption features, the transmissivity of their samples was quite high, and concluded that the low brightness temperature observations could be explained by low surface frost emissivity. Warren et al. [5] have used Ditteon and Kieffer's laboratory data in conjunction with scattering models to show that the spectral emissivities of martian CO_2 frosts could take on almost any value from 0 to 1 depending on CO_2 grain size, dust and water ice content, or viewing angle.

Hunt [6] showed that the polar night brightness temperatures could be explained by the radiative effects of CO_2 clouds. Using the results of a one-dimensional atmospheric model in conjunction with IRTM observations, Paige [7,8] showed that the spatial and temporal occurrence of low brightness temperatures are consistent with the notion that they are due to CO_2 clouds. Subsequently, Pollack et al. [9] published the results of Global Circulation Model (GCM) experiments that showed that CO_2 should condense in the atmosphere over the winter pole and that this condensation is enhanced by the presence of dust.

In the 1977 paper, Kieffer et al. [2] published midwinter brightness temperature maps that showed some evidence of temporal variation. These temporal variations have since been interpreted by others as illustrating dynamic motions of the lowest of the low brightness temperature regions. However, Kieffer et al. [2] state that the possible motion of individual features cannot be established from the analysis presented in the 1977 paper.

In this study, we have examined a series of IRTM south polar brightness temperature maps obtained by Viking Orbiter 2 during a 35-day period during the southern fall season in 1978 (L_s 47.3 to 62.7, Julian Date 2443554 to 2443588). These maps represent the best spatial and temporal coverage obtained by IRTM during a polar-night season that have not been analyzed in previous studies. The maps show a number of phenomena that have been identified in previous studies, including day-to-day brightness temperature variations in individual low-temperature regions [1], and the tendency for

IRTM 11-μm channel brightness temperatures to also decrease in regions where low 20-μm channel brightness temperatures are observed [7,8]. The maps also show new phenomena, the most striking of which is a clear tendency for the low-brightness temperature regions to occur at fixed geographic locations. During this season, the coldest low brightness temperatures appear to be concentrated in distinct regions, with spatial scales ranging from 50 to 300 km. There are approximately a dozen of these concentrations, with the largest centered near the location of the south residual polar cap. Other concentrations are located at Cavi Angusti, and close to the craters Main, South, Lau, and Dana. Broader, less-intense regions appear to be well correlated with the boundaries of the south polar layered deposits, and the Mountains of Mitchell. We have thus far detected no evidence for horizontal motion of any of these regions.

The fact that the low brightness temperature regions do not appear to move and are correlated with the locations of surface features suggests that they are not artifacts of the IRTM instrument or its viewing geometry, but the result of processes occurring on the surface or in the lower atmosphere. Presently, we do not know whether other low brightness temperature regions that have been observed during the southern winter or during the northern fall and winter exhibit similar spatial and temporal behavior. We intend to better understand the cause(s) and implications of these phenomena through modeling and further analysis of the Viking and Mariner 9 datasets.

References: [1] Kieffer H. H. et al. (1976) *Science, 193*, 780–786. [2] Kieffer H. H. et al. (1977) *JGR, 82*, 4249–4291. [3] Hess S. L. (1979) *JGR, 84*, 2969–2973. [4] Ditteon R. and Kieffer H. H. (1979) *JGR, 84*, 8294–8300. [5] Warren S. G. et al. (1990) *JGR, 95*, 14717–14741. [6] Hunt G. E. (1980) *GRL, 7*, 481–484. [7] Paige D. A. (1985) Ph.D. thesis, California Institute of Technology. [8] Paige D. A. and Ingersoll A. P. (1985) *Science, 228*, 1160–1168. [9] Pollack J. B. et al. (1990) *JGR, 94*, 1447–1473.

533-91 ABS. 01 **N94-33223**

NUMERICAL SIMULATION OF THERMALLY INDUCED NEAR-SURFACE FLOWS OVER MARTIAN TERRAIN.

T. R. Parish[1] and A. D. Howard[2], [1]Department of Atmospheric Science, University of Wyoming, Laramie WY 82071, USA, [2]Department of Environmental Sciences, University of Virginia, Charlottesville VA 22903, USA.

Introduction: The near-surface martian wind and temperature regimes display striking similarities to terrestrial desert counterparts [1,2]. The diurnal radiative cycle is responsible for establishment of a pronounced thermal circulation in which downslope (katabatic) flows prevail during the nighttime hours and weak upslope (anabatic) conditions prevail during the daytime. The low-level wind regime appears to play an important role in modifying the surface of the polar regions [3]. Viking imagery of the north polar cap shows evidence of eolian characteristics such as dunes, frost streaks, and wind-scour features. The direction of the prevailing wind can in cases be inferred from the orientation of surface features such as frost streaks and ice grooves.

For the past several years a numerical modeling study has been in progress to examine the sensitivity of thermally induced surface winds on Mars to the patterns of solar insolation and longwave radiative. The model used is a comprehensive atmospheric mesoscale equation system that has been employed previously for simulation of Antarctic katabatic winds [4]. The model equations are written in terrain-following sigma coordinates to allow for irregular terrain [5]; prognostic equations include the flux forms of

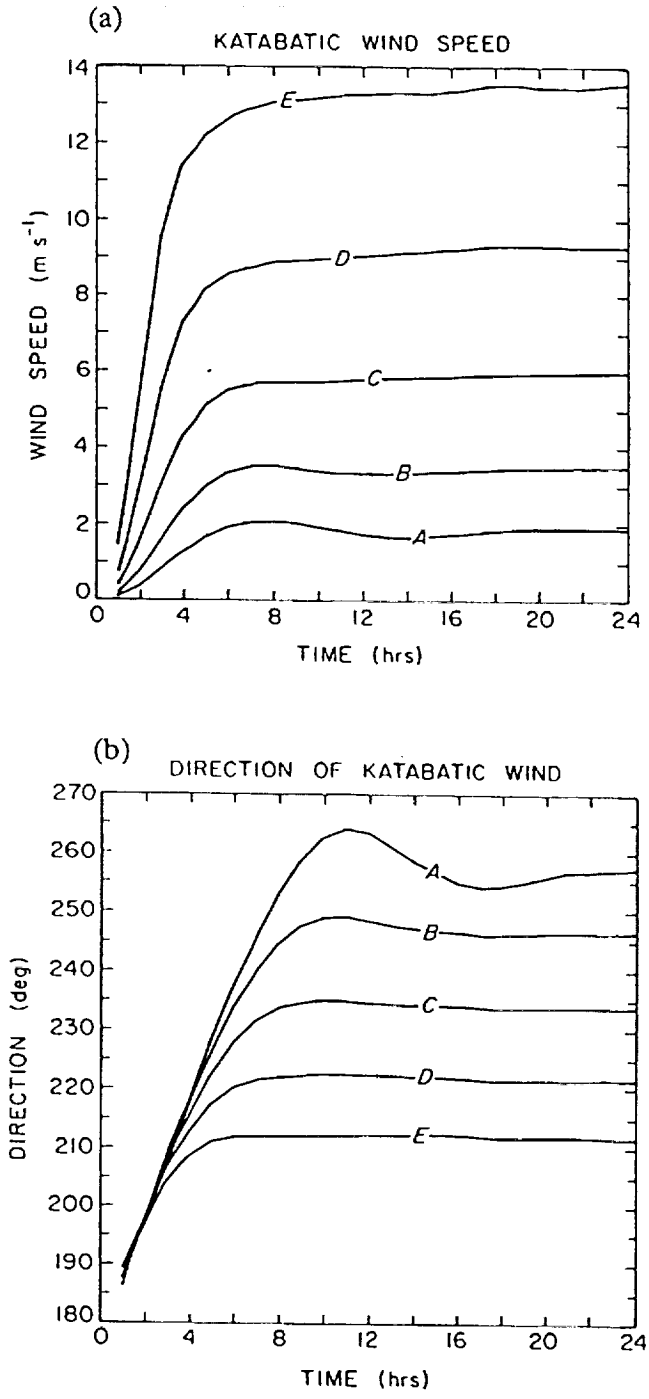

Fig. 1. Time evolution of (a) wind speed and (b) wind direction at the lowest sigma level (20 m) after 24-hr integration of constant slope runs for terrain slopes of 0.0005, 0.001, 0.002, 0.004, and 0.008, corresponding to curves A, B, C, D, and E respectively.

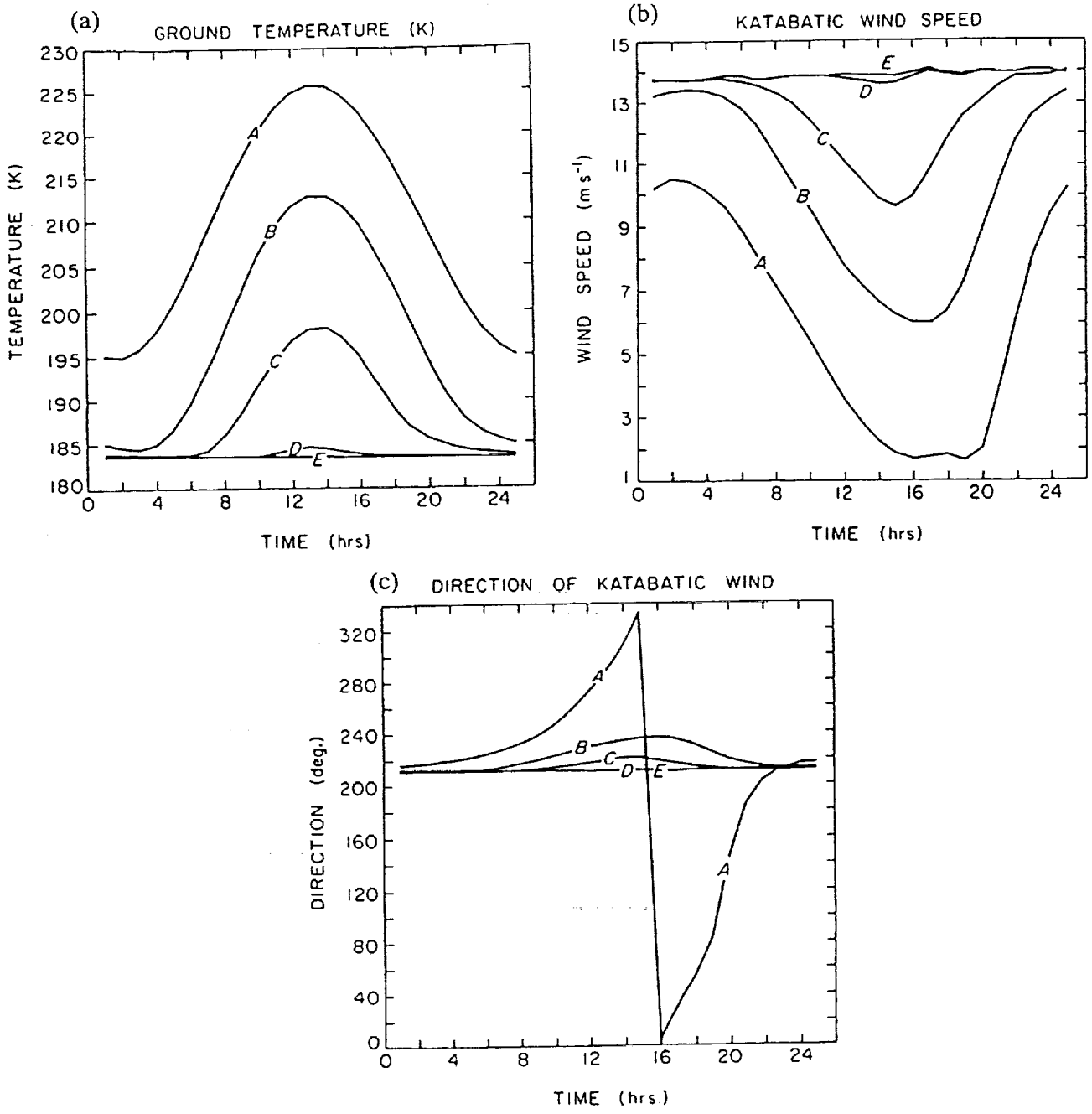

Fig. 2. Diurnal variation of (a) ground temperature, (b) wind speed, and (c) wind direction at the lowest sigma level for the solar cycle simulations over the 0.008 slope for solar declination angles of 24°, 12°, 0°, −12°, and −24°, corresponding to curves A, B, C, D, and E respectively.

the horizontal momentum equations, temperature, and continuity. A surface-energy budget equation is also incorporated in which the surface temperature is determined. Explicit parameterization of both solar insolation and longwave radiation is included. Turbulent transfer of heat and momentum in the martian atmosphere is assumed to follow the similarity expressions in the surface boundary layer on Earth [6-8]. The vertical grid consists of 15 levels (σ = 0.998, 0.99, 0.98, 0.97, 0.96, 0.94, 0.92, 0.90, 0.85, 0.775, 0.70, 0.60, 0.50, 0.30, 0.10). The high resolution in the lower atmosphere is necessary to capture details of the boundary layer flows. The lowest level corresponds to a height of approximately 20 m above the ground, the second level to 100 m.

Probably the greatest uncertainty in model simulations of thermally driven martian flows is the specification of the terrain. While detailed topographic information is available for certain regions, only a fairly broadscale representation is possible over the martian

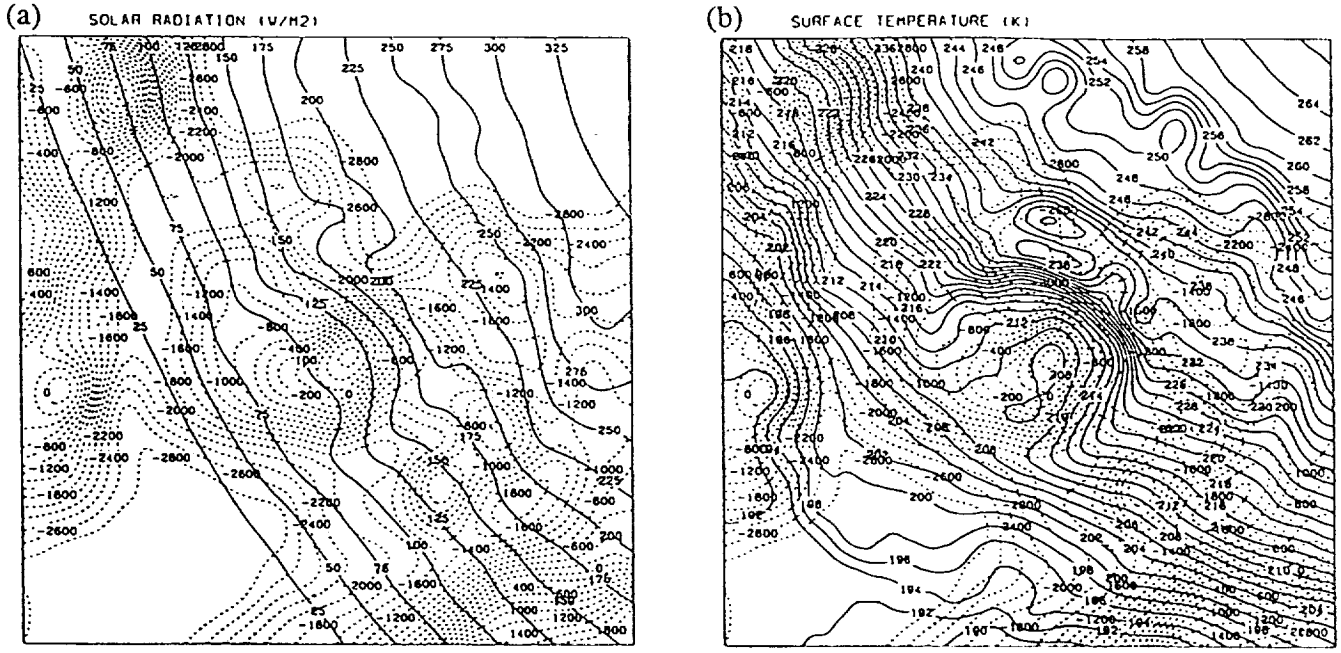

Fig. 3. Intensity of solar radiation (W m^{-2}) (a) reaching the surface and (b) corresponding to surface temperatures from numerical simulation of diurnal cycle over martian north polar cap.

north polar cap. For three-dimensional simulations, terrain heights for the martian north polar region have been obtained from the U.S. Geological Survey map, which have been digitized onto a 57 × 57 grid with a spacing of 75 km.

Model Results: *Two-dimensional simulations of thermally induced flows.* A series of numerical experiments have been conducted that focus on the relationship between katabatic wind intensity and terrain slope. The model runs are valid for high-latitude (75°), nocturnal conditions similar to midwinter on the north polar cap in which no solar radiation reaches the ground. A horizontal grid consisting of 20 points with a grid spacing of 20 km was used. The results of five 24-hour uniform slope runs are presented here. In each experiment, the model atmosphere was started from rest to isolate the katabatic wind. An initial lapse rate of 3°C km^{-1} was used with a surface temperature of approximately 220 K at the vertical reference level.

In all cases, the katabatic wind reached a quasisteady state within the first 12 martian hours. The resulting evolution of the wind speed and wind direction at the lowest sigma level (approximately 20 m above the surface) for the five martian katabatic wind simulations after 24 hr are shown in Fig. 1. Curves A–E correspond to terrain slopes of 0.0005, 0.001, 0.002, 0.004, and 0.008 respectively. The intensity of the katabatic wind (Fig. 1a) appears sensitive to the terrain slope. For steeper slopes, the flow remains directed more downslope (downslope direction is 180°), which implies the horizontal pressure gradient force remains considerably greater than the Coriolis acceleration.

To test the sensitivity of the martian slope flows to solar forcing, numerical experiments have been conducted in which the full cycle of solar forcing is replicated over sloping terrain. Results for a constant slope of 0.008 at 75° latitude will be described.

Five numerical simulations have been conducted covering the seasonal range of solar declination angles (24°, 12°, 0°, −12°, and −24°); the model equations are integrated for three complete martian days to allow the model to settle into a stable diurnal oscillation. The results presented here are taken from day 2; only minor variations were seen beyond the first diurnal cycle. It is assumed that the polar cap is composed of "dirty" ice with an albedo of 0.50. All simulations start from a rest state. Thus the influence of large-scale pressure gradients in the free atmosphere is neglected. This implies that all atmospheric motions arise due to the longwave radiative cooling or solar heating of the sloping terrain. No solar insolation is allowed for the first 12 hr of model integration time to allow the drainage flows to become established before model sunrise.

Figure 2 illustrates the diurnal course of the surface temperature, wind speed, and wind direction over the 0.008 slope martian terrain for solar declinations of 24°, 12°, 0°, −12°, and −24°, corresponding to curves A, B, C, D, and E, respectively. The Sun never sets during the midsummer period and never rises for the winter case. The ground temperature (Fig. 2a) undergoes diurnal oscillations of 30 K in summer; the magnitude of the oscillation decreases with the approach of the autumn; the diurnal ground temperature oscillation amounts to 15 K at the equinox. Maximum temperatures appear an hour or so after local noon. Wind speeds at the first sigma level (Fig. 2b) show marked diurnal trends during summer and equinox periods. Maximum wind speeds occur in the early morning hours coinciding with a minimum in the solar insolation in midsummer or just before sunrise in other simulations. Note that the simulated midsummer katabatic wind maximum of approximately 10.5 ms^{-1} (reached in the early morning hours) is 3 ms^{-1} less than seen for the other cases. This reflects the insolation from the midnight Sun, which retards development of the katabatic wind. Wind directions

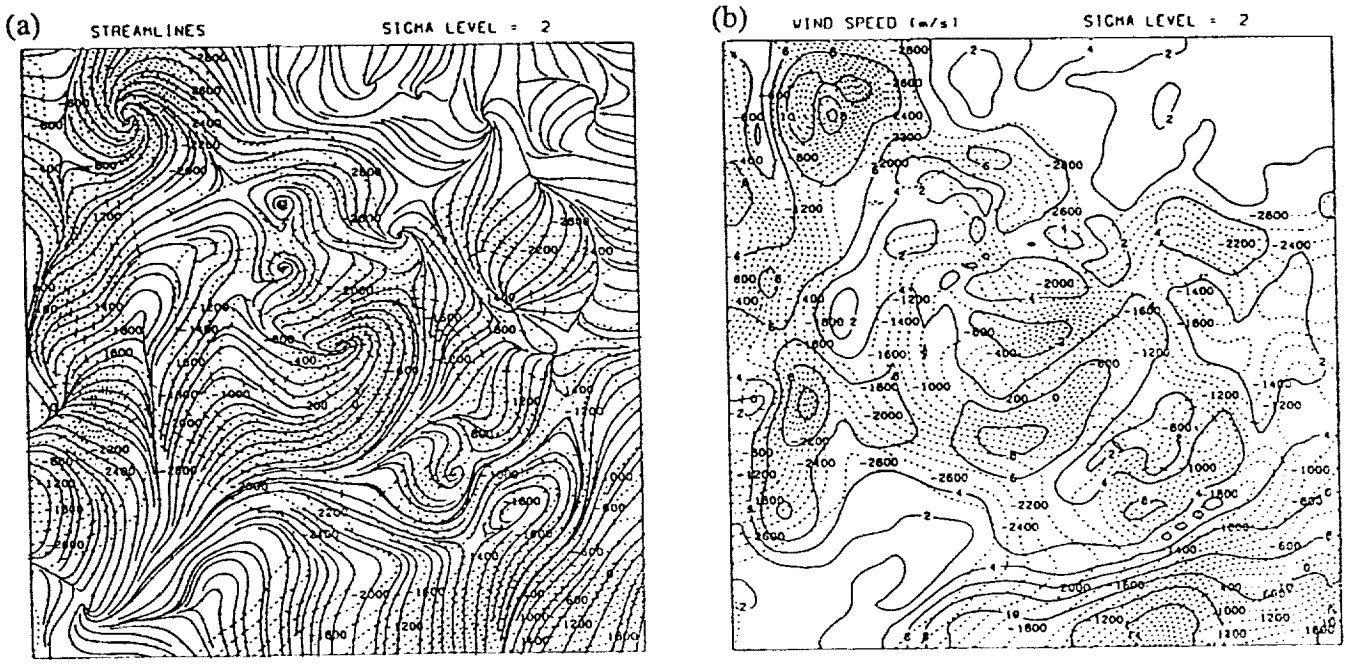

Fig. 4. Model simulations of (a) streamlines and (b) wind speeds of slope flows at the second sigma level for diurnal cycle experiment.

at the first sigma level throughout the diurnal course for the five numerical simulations are shown in Fig. 2c. The downslope direction is 180° for these simulations. The Coriolis force acts to deflect the katabatic wind some 30° to the right of the fall line of the terrain for the winter katabatic wind case. The wind directions show surprisingly little variation with time except for the midsummer declination angle of 24° (curve A). Note that upslope flow is modeled during the early afternoon hours of the summer case. The effect of solar insolation appears to retard but not overcome the katabatic forcing in all but the summertime case. This emphasizes the robust nature of the martian katabatic circulation.

Three-dimensional simulations of the near-surface flows over the martian north polar cap. Numerical simulations have also been conducted incorporating solar insolation over the irregular terrain of the northern martian latitudes. For these simulations, the model equations have been integrated for a period of three martian days to ensure that the wind and temperature regimes have had ample time to adjust to the cycle of solar heating. It was found that the second- and third-day results of the model integration were nearly identical. Here the third-day results of one such experiment will be presented. In this experiment, the solar declination is assumed to be 25°, representative of midsummer conditions. It is assumed that the atmosphere is dust-free. As before, the model is initialized about a state of rest to isolate the thermally induced slope flows in the lower atmosphere. Values of albedo and thermal inertia were taken from Paige [9].

Figure 3 illustrates the solar insolation received at the surface and corresponding surface temperatures. Local noon at this time is along the 60° meridian in Fig. 1. Note that significant spatial variations in the intensity of solar radiation reaching the surface are found near the polar cap in response to albedo differences. Surface temperatures range from 265 K along the southern edge of the domain at local noon to around 190 K in the nighttime section of the model domain.

Anabatic motions become established in response to the solar heating of the sloping terrain. Figure 4 illustrates the streamlines and wind speeds at the second sigma level for the time of the local solar forcing shown in Fig. 3. Note that especially along the local noon meridian, the streamline patterns are dramatically altered by the solar insolation as compared to pure katabatic flow. Upslope wind conditions are simulated at middle to high latitudes from morning through midafternoon. As seen in the previous simulation, the strongest winds are associated with the steepest terrain. Upslope flows reach approximately 7 ms^{-1} in places along the local noon meridian. The intensity of the upslope flows appears to be weaker than the nocturnal katabatic winds. This is in agreement with numerous terrestrial observations such as over the Antarctic ice sheet. The katabatic wind speeds simulated over the nighttime sector centered are only slightly weaker than pure katabatic winds (not shown), emphasizing the rapid response of the wind field to the radiative-induced temperature changes near the surface.

Summary: Numerical simulations of the martian near-surface wind regime using a mesoscale atmospheric model have shown that the thermally induced near-surface winds are analogous to terrestrial circulations. In particular, katabatic wind displays a striking similarity to flows observed over Antarctica. Introduction of solar radiation strongly perturbs the slope flows; anabatic conditions develop in middle to high latitudes during the daytime hours due to the solar heating of the sloping terrain. There appears to be a rapid transition from the katabatic to the anabatic flow regimes, emphasizing the primary importance of radiative exchanges at the surface in specifying the horizontal pressure gradient force.

References: [1] Hess S. L. et al. (1977) *JGR, 82,* 4559–4574. [2] Sutton J. L. et al. *J. Atmos. Sci., 35,* 2346–2355. [3] Howard A. D. (1981) *NASA TM-82385,* 333–335. [4] Parish T. R. and Waight K. T. (1987) *Mon. Wea. Rev., 115,* 2214–2226. [5] Anthes R. A. and Warner T. T. (1978) *Mon. Wea. Rev., 106,* 1045–1078. [6] Brost R. A. and Wyngaard J. C. (1978) *J. Atmos. Sci., 35,* 1427–1440. [7] Busch N. E. et al. (1976) *J. Appl. Meteor., 15,* 909–919. [8] Businger J. A. et al. (1971) *J. Atmos. Sci. 28,* 181–189. [9] Paine D. A. (1992) *LPS XXIII,* 1013.

S34-91 ABS. ON

APRON HEIGHTS AROUND "STEPPED MASSIFS" IN THE CYDONIA MENSAE REGION: DO THEY RECORD THE LOCAL PALEOBATHYMETRY OF "OCEANUS BOREALIS"?

T. J. Parker and D. S. Gorsline, Department of Geological Sciences, University of Southern California, Los Angeles CA 90089-0740, USA.

Over the past several years a number of investigators have described geomorphic evidence for and paleoclimatic significance of large standing bodies of water or ice sheets within the northern lowland plains of Mars [e.g., 1–14]. The details of the timing, emplacement mechanisms, and sizes of these bodies differ markedly from one group of investigators to another, however. For example, Jöns [1,2] envisioned a "mud ocean" covering much of the northern plains, with sediment slurries derived from a variety of peripheral sources, including the fretted terrains and outflow channels. Lucchitta et al. [4] pictured an ice-covered ocean, fed by large circum-Chryse ice streams, analogous to those in Antarctica. Parker et al. [10,11] indicated two or more highstands of a sea or ocean that, most recently, would have been charged by catastrophic floods, but may have existed more or less permanently during Noachian and Hesperian time. Interestingly, the shorelines of Jöns' "mud ocean," Lucchitta et al.'s ice-covered ocean, and Parker et al.'s most recent sea, or "interior plains" [11], coincide almost precisely around the northern lowlands, though the details of the mechanisms by which key boundary morphologies are thought to have been produced differ. Baker et al. [12] pictured a plainswide ocean emplaced by the major outflow channels relatively late in martian history, and coined the term "Oceanus Borealis" for this ocean.

Taking a more conservative approach to the question of standing water in the northern plains, Rotto and Tanaka [14] have relied on volume estimates of maximum discharge from the circum-Chryse outflow channels, which they feel limits any standing water to one or a few large, ephemeral lakes. The locations of these lakes are based on the identification of broad, shallow topographic basins on the present martian topographic maps [15]. Similarly, Scott et al. [13] have indicated evidence for several large lakes across the northern plains, some exhibiting connecting spillways, that were fed by a variety of channel sources peripheral to the plains. Delineation of these lakes is based on a similar assessment of the topography, but also included the identification of shore morphology.

All the above studies would have benefited greatly from the advent of the high-resolution topography afforded by the Mars Observer Laser Altimeter [16], which would have produced global topographic maps beginning in early 1994. For example, basin volume estimates in Parker et al. [11] are loosely based on the available topography with its very large vertical errors. These estimates, when compared to estimates by others of the water discharged by the Chryse outflow channels, suggest the possibility that the volumes required to fill the basin may be at or beyond the high end of the estimated volumes available from the channels. High-resolution topography is needed to sort out the common modifiers of shoreline elevation, such as tectonism, isostatic rebound, and sediment desiccation and compaction, that probably altered the topography of the northern plains after the putative surface water was lost, so that the original topography can be reconstructed. Until a reflight of the laser altimeter or some similar instrument, elevations derived using the currently available high-resolution topographic tools—photoclinometry and shadow measurements—cannot be accurately tied to the global datum. It is not possible, therefore, to be certain that basin volumes based on the current global topography provide better than a crude approximation of the volume of ancient standing bodies of water in the northern plains. Until they do, such estimates cannot, by themselves, either point to nor preclude the presence of surface water or ice within the northern plains prior to the latest catastrophic floods; the uncertainties are still too large relative to the flood volume estimates.

Can photoclinometry and shadow measurements be used to determine the volume of the basin without having to link the measurements to a global datum? Since the boundary, or shoreline of the basin cannot be tied to the datum and typically has no useful local relative height to measure, what is needed are a number of measurements of the height of the paleoshoreline(s) distributed across the basin—soundings, in effect.

Parker et al. [9,11] described a type of small knob in the northern plains that resembles terrestrial and lunar steptoes (volcanic apron) and terrestrial wave-cut islands, and applied the nongenetic term "stepped massifs" to the martian knobs. If these are upland outliers that had been abraded through wave action in an unfrozen ocean, or through ice-shoving in an ice-covered ocean, then the height of the apron above the surrounding plains could provide a measure of the local basin depth in the vicinity of the knob. Since stepped massifs are distributed over broad expanses in several places in the northern plains, it should be possible to measure the variation in basin depth regionally. With the exception of those regions where the available image scale is insufficiently small, it should be possible to measure the heights of the aprons to within a few tens of meters.

As a feasibility test of this approach, photoclinomettic profiles are being compiled from Viking Orbiter images of the Cydonia Mensae region, which includes images with high Sun elevations (necessary to avoid shadows) and images with low Sun elevations (to enable the use of shadow measurements as an independent check) at high resolution (40–100 m/pixel). Both asymmetric and symmetric photoclinometic profile models are being used, and the results cross checked with one another to minimize the errors. An apron-height map, potentially a paleobathymetric map of part of the margin of "Oceanus Borealis," will be compiled of this data to determine whether variations in apron height are consistent with a lacustrine interpretation.

References: [1] Jöns H.-P. (1985) *LPS XVI,* 414–415. [2] Jöns H.-P. (1986) *LPS XVII,* 404–405. [3] Jöns H.-P. (1990) *Geol. Rundsch., 79,* 131–164. [4] Lucchitta B. K. et al. (1986) *Proc. LPSC 17th,* in *JGR, 91,* E166–E174. [5] McGill G. E. (1985) *LPS XVI,* 534–535. [6] McGill G. E. (1986) *Geophys. Res. Let., 13,* 705–708. [7] McGill G. E. and Hills L. S. (1992) *JGR, 97,* 2633–2647. [8] Parker T. J. et al. (1987) *LPI Tech. Rpt. 87-01,* 96–98. [9] Parker T. J. et al. (1987) *Rept. Planet. Geol. Prog. 1986,* NASA TM-89810,

502–504. [10] Parker T. J. et al. (1989) *Icarus, 82,* 111–145. [11] Parker T. J. et al. (1993) *JGR, 98,* 11061–11078. [12] Baker V. R. et al. (1991) *Nature, 352,* 589–594. [13] Scott D. H. et al. (1992) *LPI Tech. Rpt. 92-02,* 132–133. [14] Rotto S. T. and Tanaka K. L. (1991) *LPI Tech. Rpt. 92-02,* 124–125. [15] U.S.G.S. (1989) *Atlas of Mars,* 1:15,000,000 Topographic Series, Map I-2030, 3 sheets. [16] Zuber M. T. et al. (1992) *JGR 97* 7781–7797.

535 91 ABS ONLY

N94-33225

THE pH OF MARS. R. C. Plumb[1,2], J. L. Bishop[2], and J. O. Edwards[2], [1]Worcester Polytechnic Institute, Worcester MA 01609, USA, [2]Brown University, Providence RI 02912, USA.

The Viking Labeled Release (LR) experiments provided data that can be used to determine the acid-base characteristics of the regolith. Constraints on the acid-base properties and redox potentials of the martian surface material would provide additional information for determining what reactions are possible and defining formation conditions for the regolith. A number of chemical models [1] and simulation experiments [2–8] attempted to explain the LR results. A recent chemical model suggests that nitrates are present, as well as a carbonate with a solubility similar to that of calcite [9].

During the LR experiments after the oxidation process was complete (~5 days) the magnitude of the LR signal was controlled by the distribution of $^{14}CO_2(g)$ between the gas phase and the moist solids in the LR cell. That distribution was controlled by chemical equilibria that are sensitive to acid-base conditions. Levin and Straat [10] demonstrated that the second injection reabsorption occurs as a result of a shift in chemical equilibria involving $CO_2(g)$, water, and soil. Calculations devised to determine the pH of Mars must include (1) the amount of soluble acid species or base species present in the LR regolith sample and (2) the solubility product of the carbonate with the limiting solubility [11].

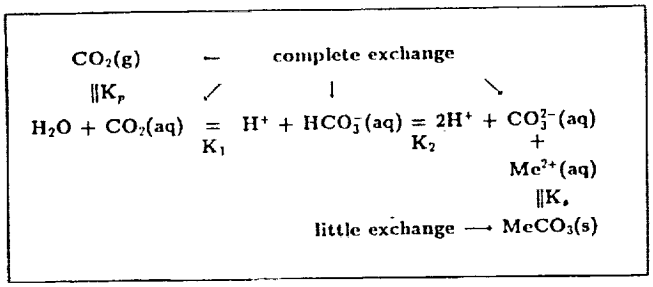

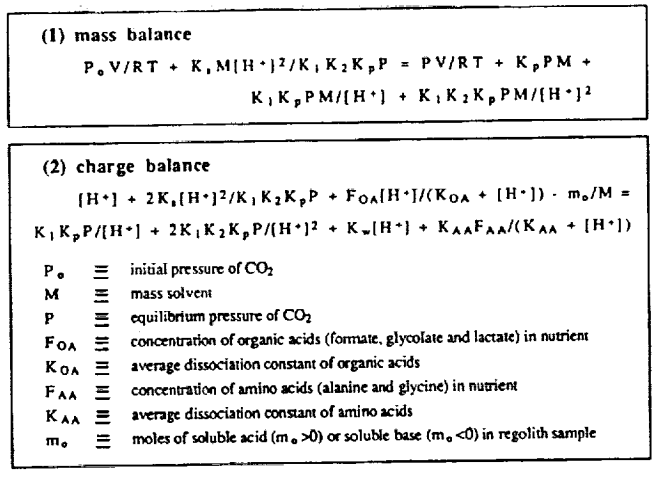

Fig. 1. Chemical and isotopic exchange equilibria in labeled release experiment.

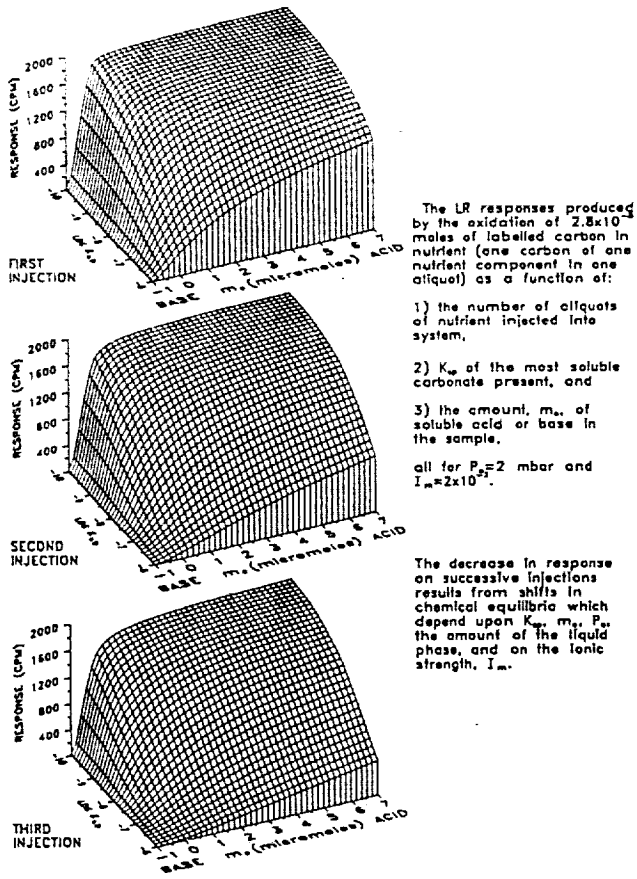

Fig. 2.

Results and Discussion: The equilibria for CO_2 in a heterogeneous system are shown in Fig. 1. This equilibrium system as represented is completely general. Several metal carbonates may be present. $MeCO_3(s)$ refers to the particular metal carbonate that is the most soluble of those that do not dissolve completely. Less soluble carbonates, if present, do not enter into the equilibria; more soluble carbonates dissolve completely and are not present as solids in the system after wetting. The limiting case of no metal carbonates present corresponds to a vanishingly small K_s, i.e., a K_s that does not enter into the equilibria.

Exchange of $^{14}CO_2$ among the soluble species and $CO_2(g)$ occurs rapidly, but the $MeCO_3(s)$ does not enter into the exchange pool, except for the surface layer, which is a negligibly small quantity.

It was observed in the Viking studies that successive injections of nutrient decreased the magnitude of the response. This is what

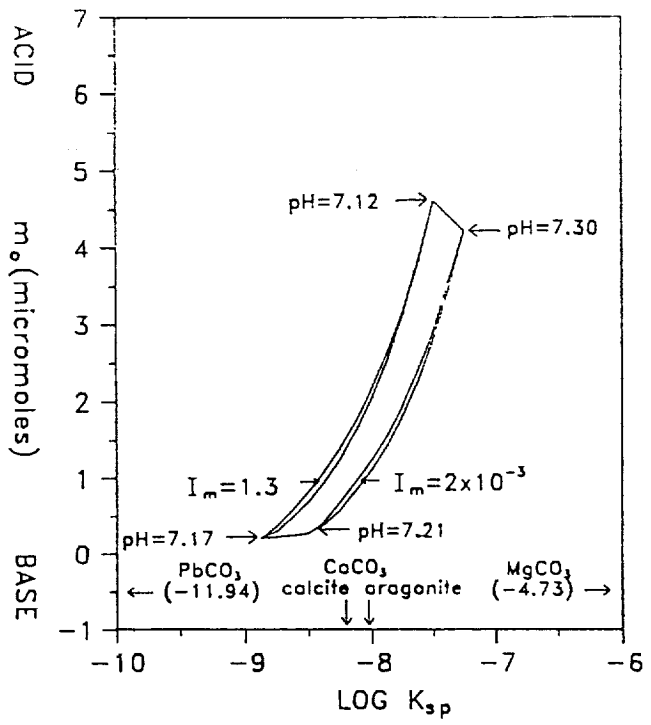

Fig. 3. The zone of compositions that would produce the 21.5–22.5% LR reabsorption upon both the second and third injections. The ionic strength of wet martian regolith is unknown; a range of 2×10^{-3} to 1.3 has been assumed. The pressure of atmospheric CO_2 trapped in the cells after loading, thermal equilibration and venting is estimated to have been 2 mbar. The pHs are the values that would be observed if 0.5 mL samples of regolith were sealed in 10 mL volumes with martian atmosphere at 6 mbar and wet with 0.5 mL of deionized H_2O at 25°C.

one would expect from consideration of the equilibria involved. Qualitatively, the addition of more liquid into the system would have two effects. First, the amount of CO_2(aq) would increase because the amount of liquid phase increases, causing a decrease in the amount of labeled CO_2(g). Second, and more important, more $MeCO_3$(s) dissolves, increasing the exchange pool and causing the fraction of the $^{14}CO_2$(g) in the gas phase to decrease.

The equilibria and the decreased responses on successive injections are described quantitatively by the (1) mass balance and (2) charge balance equations. Allowance has been made for ionic strength using assumed limits and for activity coefficients at various ionic strengths as calculated using the Davies equation. Thermodynamic equilibrium constants have been adjusted to 283 K. The effects of K_s and of the amount m_o of soluble acid or base present in the sample are shown in Fig. 2.

There is a narrow zone of composition that will produce the observed reabsorption effect for a particular injection. The similar magnitudes of successive injection reabsorption limits the zone of acceptable compositions still further. The zones for two extreme ionic strengths are shown in Fig. 3. Since the ionic strength is unknown, compositions between these zones must also be considered as possible.

Conclusions: This theoretical analysis has been confirmed experimentally by quantitative simulations of the reabsorption effects [9]. The kinetics of the LR oxidation reaction provide additional evidence that $CaCO_3$(s) must be present.

This analysis shows that $CaCO_3$ (either as calcite or aragonite) has the correct K_{sp} to have produced the Viking LR successive injection reabsorption effects. Thus $CaCO_3$ or another $MeCO_3$ with very similar solubility characteristics must have been present on Mars. A small amount of soluble acid, but no more than 4 µmol per sample, could also have been present. We conclude that the pH of the regolith is 7.2 ± 0.1. This is the value that would be observed if 0.5 mL sample of regolith were sealed in a 10-mL volume with a martian atmosphere at 6 mbar and wetted with 0.5 mL of deionized H_2O at 25°C. The variation in pH values is very small, which is a consequence of carbonate buffering.

Acknowledgments: This model was devised and the calculations were carried out by R. Plumb before his death. Bishop and Edwards have abstracted his work and submitted it in his memory in light of his deep interest in the chemistry of Mars. The work by Plumb on the chemistry of Mars was supported by NASA.

References: [1] Klein (1979) *J. Molec. Evol., 14*, 161–165. [2] Oyama and Berdahl (1977) *JGR, 82*, 4669–4676. [3] Ponnamperuma et al. (1977) *Science, 197*, 455–457. [4] Ballou et al. (1978). [5] Oyama and Berdahl (1979) *J. Molec. Evol., 14*, 199–210. (1978). [6] Huguenin et al. (1979) *J. Molec. Evol., 14*, 103–132. [7] Levin and Straat (1981) *Icarus, 45*, 494–516. [8] Banin and Rishpon (1979) *J. Molec. Evol., 14*, 133–152. [9] Plumb et al. (1989) *Nature, 338*, 633–635. [10] Levin and Straat (1979) *J. Molec. Evol., 14*, 167–183. [11] Plumb (1992) *LPI Tech. Rpt. 92-02*, 117.

N94-33226

536 91 ABSTRACT

THE MINERALOGIC EVOLUTION OF THE MARTIAN SURFACE THROUGH TIME: IMPLICATIONS FROM CHEMICAL REACTION PATH MODELING STUDIES.

G. S. Plumlee[1], W. I. Ridley[1], J. D. De Braal[2], and M. H. Reed[2], [1]Mail Stop 973, U.S. Geological Survey, Denver Federal Center, Denver CO 80225, USA, [2]Department of Geological Sciences, University of Oregon, Eugene OR 97403, USA.

This report summarizes results to date of the MSATT-sponsored project, "Chemical Reaction Path Modeling at the Martian Surface Through Time." We have used chemical reaction path calculations to model the minerals that might have formed at or near the martian surface (1) as a result of volcano- or meteorite impact-driven hydrothermal systems [1]; (2) as a result of weathering at the martian surface during an early warm wet climate [2,3]; and (3) as a result of near-zero [4] or sub-zero °C brine-regolith reactions in the current cold climate.

Fundamentals of Chemical Reaction Path Modeling: Computer-driven chemical reaction-path modeling [5] quantitatively predicts the changes in water chemistry, amounts of minerals precipitated or dissolved, and amounts of gases formed as the result of specified geochemical processes such water-rock reactions, fluid mixing, or fluid boiling. The modeling is based upon equilibrium chemical thermodynamics, and takes into account both chemical reactions (through equilibrium constants) and mass balance relations between all solid, aqueous, and gaseous phases in a specified

water-rock-gas system. A wide variety of reaction-path calculations can be performed to address potential variations in starting conditions and other factors that influence particular chemical processes. The chemical speciation and reaction path programs SOLVEQ and CHILLER [5,6] were used in this project.

It is important to note the limitations of the reaction-path modeling. First, the validity of modeling results are highly dependent on thequality of the thermodynamic data upon which the modeling is based. Thermodynamic data determined through laboratory experiments are generally the most accurate; experimentally derived data, especially those for reactions involving aqueous species, are best-developed at or near 25°C, are somewhat less available at hydrothermal temperatures above 50°–100°C, and are not well developed at near-zero or sub-zero °C temperatures. When experimentally derived data are not available, they are generally estimated instead by various techniques or are extrapolated from experimentally derived data at 25°C. Another limitation of the reaction-path modeling is that minerals predicted to be thermodynamically stable for a given set of geochemical conditions may not actually precipitate in nature due to kinetic factors. For example, minerals such as chalcedony, kaolinite, aluminum hydroxides, and ferrihydrite are kinetically stable and much more likely to precipitate at 25°C than thermodynamically stable quartz, illites, smectites, other aluminosilicate minerals, hematite, and goethite [7]. The relative chemical effects of such kinetic controls on mineral precipitation can be evaluated in the modeling by carrying out runs in which kinetically inhibited minerals are allowed to precipitate, and runs in which these minerals are suppressed, thereby allowing kinetically more stable but thermodynamically less stable minerals to precipitate.

Chemical Modeling of Possible Martian Hydrothermal Processes: Hydrothermal systems associated with volcanos and impact events have been proposed to play important roles in the development of the martian regolith and the valley networks [8–10]. Our chemical modeling results [1] indicate that such hydrothermal processes would produce a variety of alteration minerals and mineral precipitates that can be readily searched for using remote sensing techniques. For example, condensation of SO_2- and CO_2-rich volcanic gases in the throats of martian volcanos would probably generate highly acidic (pH < 1.5) fluids capable of altering the volcanic wallrocks to zoned silica-alunite-anhydrite-hematite-nontronite-smectite-carbonate assemblages. If the gases condensed into hydrothermal waters circulating within the volcanos, then such acid alteration assemblages could extend well away from the immediate vicinity of the volcano throats. If interactions between the hydrothermal fluids and volcanic gases were negligible, then hydrothermal systems circulating within the volcanos would alter the basaltic volcanics to quartz-pyrite-carbonate-epidote-albite alteration assemblages. Hydrothermal fluids that reacted with the regolith (such as permafrost meltwaters generated by a meteorite impact) were likely acidic (pH 3–5) and saline, and produced nontronite, anhydrite, kaolinite, Mg-smectite, Mg-chlorite, and quartz alteration assemblages within the regolith. Near-surface quenching of hydrothermal fluid outflows from impact- or volcano-driven hydrothermal systems should have produced extensive silica- and/or carbonate-rich precipitates analogous to the silica sinter and travertine terraces formed by terrestrial geothermal systems.

Chemical Modeling of Weathering in an Early Warm Wet Climate: In the reaction-path calculations modeling weathering in an early warm wet climate [2], a range of initial water compositions was used to account for reasonable variations in ambient partial pressures of atmospheric CO_2 and O_2, and possible variations in the input of acidic volcanic gases such as SO_2 and HCl. Our results indicate that weathering processes in an early warm wet climate (temperature = 25°C) with at least some free atmospheric O would have altered basalts to mixtures of ferric and manganese hydroxides, chalcedony, kaolinite, apatite (or other phosphate minerals), dolomite, and calcite. Smectite clays are predicted to be thermodynamically stable in many of the weathering reaction paths considered; such clays may have formed if kinetic barriers to their nucleation were overcome. Acid rain (resulting either from high atmospheric CO_2 or influx into the atmosphere of acid volcanic gases such as HCl and SO_2) would have enhanced the extent of the weathering reactions and increased the proportions of minerals such as carbonates and gypsum in the weathering assemblages. Reaction paths modeling the limited evaporation of waters that had previously reacted with basalt predict the formation of gypsum, calcite, dolomite, sodium and potassium feldspars, dawsonite (a hydrated sodium-aluminum carbonate mineral), and phosphate minerals. Calculations modeling more extensive evaporation generally do not predict the precipitation of common halides such as halite or sylvite. Rather, unusual minerals such as Cl-bearing apatite (see below) or MgOHCl are predicted to form. We are currently evaluating whether the predicted lack of precipitation of halite and sylvite is geochemically and kinetically reasonable. Waters initially high in dissolved sulfate and chloride (such as acid rain) require substantially less evaporation to reach saturation with gypsum (and other readily soluble salts) than waters that derive their sulfate and chloride solely from the rocks. These results lend support to the premise that acid rain may have helped generate the high sulfate and chloride values measured in the martian regolith.

Our calculations show that weathering of P-bearing basalts would probably result in the transport of aqueous phosphate, the formation of phosphate alteration minerals such as apatite or crandallite, and the possible evaporative enrichment of phosphate in the regolith. Based on these results, we speculated in an earlier report [2] that Cl-bearing apatite could serve as a residence for chloride in the regolith. Recent infrared reflectance studies (T. V. V. King, 1992, oral communication) do not support the presence of Cl-apatite in detectable amounts in the martian regolith; however, further work is needed to evaluate if the chloride could be tied up in some other phosphate phase.

Regolith Weathering by Aqueous Solutions in a Cold Climate: We are currently modeling potential interactions of martian regolith and basaltic rocks with near-zero °C waters or sub-zero °C brines that may have been or are currently stable at or near the martian surface [3,4]. Model groundwaters at 0.1°C in equilibrium with the current martian atmospheric CO_2 and O_2 pressures are predicted to be acidic (pH 6) and oxidizing, while model groundwaters that have no contact with the atmosphere are predicted to be very alkaline (pH 11) and reducing. Calculations modeling weathering of a Shergotty basalt composition by the near-zero (0.1°C) groundwaters predict alteration assemblages that consist of Mg-nontronite, $MgCO_3{*}3H_2O$, chalcedony, kaolinite, trona ($Na_3CO_3HCO_3{*}2H_2O$), spurrite ($Ca_5[SiO_4]2CO_3$), potassium feldspar, alunite, and MgOHCl, in order of decreasing abundance. If the nontronite and potassium feldspar were kinetically inhibited from precipitating, then the alteration

assemblages are predicted to contain abundant Fe-, Mn-, and Al-hydroxides in addition to the dolomite, chalcedony, and kaolinite. Subsequent evaporation of the groundwaters after reaction with basalt is predicted to form, with progressive evaporation, dolomite, $MgCO_3*3H_2O$, apatite (or other phosphate minerals), calcite, dawsonite, and gypsum. Halite and sylvite are not predicted to form, even with extensive evaporation. Reactions of the regolith with groundwaters near 0°C are predicted to result in acidic waters and alteration assemblages containing abundant Fe- and Al-hydroxides (or smectites), Mn-hydroxides, and kaolinite.

The portion of the project in which we model sub-zero brine-regolith interactions has required extensive modifications to the computer programs that carry out the reaction-path calculations and the thermodynamic database that serves as the basis for the calculations. Modeling calculations below 0°C are still in progress.

Summary: Although the chemical reaction-path calculations carried out to date do not define the exact mineralogical evolution of the martian surface over time, they do place valuable geochemical constraints on the types of minerals that formed from an aqueous phase under various surficial and geochemically complex conditions. Based on these results, we believe that further chemical reaction-path modeling efforts are needed as new remote sensing data and other lines of evidence are acquired on possible surficial mineralogies. By integrating such geochemical modeling calculations with remote sensing studies, more realistic and geochemically valid models for the evolution of the martian surface through time can be developed.

References: [1] Plumlee G. S. and Ridley W. I. (1991) *LPI Tech. Rpt. 92-02*, 118–119. [2] Plumlee G. S. et al. (1992) *LPI Tech. Rpt. 92-04, Part 1*, 31–32. [3] DeBraal J. D. et al. (1992) *LPS XXIII*, 287–288. [4] DeBraal J. D. et al. (1992) *LPI Tech. Rpt. 92-04, Part 1*, 10–11. [5] Reed M. H. (1982) *GCA, 46*, 513–528. [6] Spycher N. F. and Reed M. H. (1989) *Econ. Geol., 84*, 328–359. [7] Nordstrom D. K. et al. (1990) *Am. Chem. Soc. Symposium Series, 416*, 398–413. [8] Newsom H. E. (1992) *LPI Tech. Rpt. 92-04, Part 1*, 27–29. [9] Brakenridge G. R. et al. (1985) *Geology, 13*, 859–862. [10] Gulick V. C. (1991) *LPI Tech. Rpt. 92-02*, 63–64.

N94-33227

S3 T 91 ABS. 6A

CONTROLS ON THE CO_2 SEASONAL CYCLE. J. B. Pollack[1], F. Forget[1,3], R. M. Haberle[1], J. Schaeffer[2], and H. Lee[2], [1]NASA Ames Research Center Moffett Field CA 94035-1000, USA, [2]Sterling Software, Inc., Palo Alto CA, USA, [3]University of Paris, FRANCE.

The meteorology experiment on the Viking landers carried out accurate measurements of the surface pressure over the course of several martian years [1]. These data show substantial variations in pressure on seasonal timescales that are characterized by two local minima and two local maxima. These variations have widely been attributed to the seasonal condensation and sublimation of CO_2 in the two polar regions. It has been somewhat of a surprise that the amplitude of the minimum and maximum that is dominated by the CO_2 cycle in the north was much weaker than the corresponding amplitude of the south-dominated extrema. Another surprise was that the seasonal pressure cycle during years 2 and 3 of the Viking mission was so similar to that for year 1, despite the occurrence of two global dust storms during year 1 and none during years 2 and 3.

We have attempted to model the observed seasonal pressure variations with an energy balance model that incorporates dynamical factors from a large number of general circulation model runs in which the atmospheric dust opacity and seasonal date were systematically varied [2,3]. The energy balance model takes account of the following processes in determining the rates of CO_2 condensation and sublimation at each longitudinal and latitudinal grid point: solar radiation, infrared radiation from the atmosphere and surface, subsurface heat conduction, and atmospheric heat advection. Condensation rates are calculated both at the surface and in the atmosphere. In addition, the energy balance model also incorporates information from the GCM runs on seasonal redistribution of surface pressure across the globe, a process that has very little effect on CO_2 condensation and sublimation per se, but which can alias surface pressure measurements at local sites.

Numerical experiments with the energy balance model show that the following factors make important contributions to the seasonal pressure variations measured at local sites: albedo and emissivity of the seasonal CO_2 polar caps, topography of the polar regions, atmospheric heat advection, and seasonal redistribution of the surface pressure. The last factor contains contributions from seasonal variations in atmospheric dynamics and from scale height changes in the presence of topography. The model-derived values of cap emissivity may contain an influence from CO_2 ice clouds that are particularly prevalent in the north during its fall and winter seasons [4]. Atmospheric dust influences each of the above factors, albeit in different ways. For example, atmospheric heat transport to the poles rapidly increases as the dust opacity increases from 0 to 1, but then tends to approach an asymptotic value. We suggest that the similarity of the seasonal CO_2 cycle between years with and without global dust storms may reflect this type of saturation effect. Indeed, runs with the energy balance model performed using Viking-lander-measured opacities during years 1 and 2 [5] tend to substantiate this hypothesis.

We have used estimates of the surface temperature of the seasonal CO_2 caps [4] to define the infrared radiative losses from the seasonal polar caps. This information implicitly incorporates surface topography, a quantity that is poorly known in the polar regions. We have been able to closely reproduce the seasonal pressure variations measured at the Viking lander sites. Our best models are characterized by a lower cap emissivity in the north than in the south. We attribute this difference to the influence of CO_2 ice clouds [4]. According to our calculations the reduced amplitude of the north-cap-influenced pressure extrema, when compared to that of the south-cap-influenced extrema, are due to the following: lower cap emissivity in the north (due to a greater frequency of CO_2 ice clouds in the north), greater heat advection during northern winter when the dust opacity is elevated, and a larger amplitude to the seasonal pressure redistribution during northern winter when the dust opacity is higher. Opposing these factors is a lower CO_2 ice temperature in the south due to its higher elevation.

References: [1] Tillman J. E. (1988) *JGR, 93*, 9433–9451. [2] Pollack J. B. et al. (1993) *JGR, 98*, 3149–3181. [3] Pollack J. B. et al. (1990) *JGR, 95*, 1447–1473. [4] Forget F. and Pollack J. B. (1993) *LPI Tech. Rpt. 93-05*, in press. [5] Colburn D. S. et al. (1989) *Icarus, 79*, 159–189.

N94- 33228

S38 91 ABS. ONLY

THE WAVELENGTH DEPENDENCE OF MARTIAN ATMOSPHERIC DUST RADIATIVE PROPERTIES.

J. B. Pollack[1], M. E. Ockert-Bell[2], R. Arvidson[3], and M. Shepard[3], [1]NASA Ames Research Center, Moffett Field CA 94035-1000, USA, [2]San Jose State University, San Jose CA 95172-0130, USA, [3]Washington University, St. Louis MO 63130-4899, USA.

Motivation: One of the key radiative agents in the atmosphere of Mars is the suspended dust particles. We are carrying out a new analysis of two datasets of the martian atmosphere in order to better evaluate the radiative properties of the atmospheric dust particles. The properties of interest are the size distribution information, the optical constants, and other radiative properties, such as the single-scattering albedo and phase function. Of prime importance in this research is the wavelength dependence of these radiative properties throughout the visible and near-infrared wavelengths. Understanding the wavelength dependence of absorption and scattering characteristics will provide a good definition of the influence that the atmospheric dust has on heating of the atmosphere.

Data: The first dataset that we are analyzing is a set of Viking 1 and 2 Lander images. Our present work represents a significant improvement over our past analyses [1,2]. Color and IR images and a survey image have been calibrated and a correction for vignetting was added. The vignetting correction reconstructed the saturation near the top of the images and allowed us to use data closer to the Sun, which in turn gives a better definition of the diffraction peak and, thus, the size distribution of the particles. The second dataset is visible and near-infrared data from Bell and Mustard [3] and Mustard and Bell [4]. The dataset, taken in 1988 and 1989, covers a wide range of wavelengths (0.4–3.0 μm).

Analysis: The examination of the Viking Lander images involves modeling the reflectance data using radiative transfer calculations based on the doubling method [5]. A semi-empirical method is used to model the scattering by nonspherical particles [6]. Hapke [7,8] theory is used to model the photometric properties of the surface.

We used an iterative method to fit the parameters of interest to the observed data: small phase angles were used to find the size distribution information, phase angles of about 50° were used to determine the imaginary index, and the data at larger phase angles determined the shape of the particles. We calculate the intensity expected in a given range due to variation of one parameter and do a chi-squared fit to the variance to find the best fit of the parameter in question. The resulting best fit is used as a set parameter while another is varied, etc.

From the information obtained in the examination of the Viking Lander images, we have defined the particle size distribution using a log-normal distribution, and we have defined the wavelength dependence of the imaginary index of refraction and radiative properties for wavelengths between 0.5 and 0.9 μm.

For the investigation of the second dataset we operate under the assumption that the properties of the atmospheric dust closely mimic those of the "bright" soil on the surface. Since the optical depth of the atmospheric dust was low during the time period of the data acquisition, we can use Hapke theory [7,8] to extract the single-scattering albedo of the soil. By scaling the imaginary index of refraction of the soil to agree with the atmospheric dust in the visible, we derive the spectral dependence of the imaginary index in the entire visible and near-infrared domains.

The results of this inquiry will be presented. The particle single-scattering phase function from the Viking analysis and the wavelength dependence of the radiative properties within the visible and near-infrared wavelength regions will be given.

References: [1] Pollack J. B. et al. (1977) *JGR, 82,* 4479–4496. [2] Pollack J. B. et al. (1979) *JGR, 84,* 2929–2945. [3] Bell J. F. III and Mustard J. F. (1993) *LPS XXIV,* 81–82. [4] Mustard J. F. and Bell III J. F. (1993) *GRL,* submitted. [5] Hansen J. E. (1969) *Astrophys. J., 155,* 565. [6] Pollack J. B. and Cuzzi J. N. (1980) *JAS, 37,* 868–881. [7] Hapke B. (1981) *JGR, 86,* 3039–3054. [8] Hapke B. (1986) *Icarus, 67,* 264–280.

N94- 33229

S39 -91 ABS

EVIDENCE FOR ULTRAMAFIC LAVAS ON SYRTIS MAJOR.

D. P. Reyes and P. R. Christensen, Department of Geology, Arizona State University, Tempe AZ 85287-1404, USA.

Data from the Phobos 2 Imaging Spectrometer for Mars (ISM) compiled by [1] support the existence of komatiitic lavas on the Syrtis Major plateau. Using ISM data, Mustard et al. [1] determined that the composition of the low-albedo materials covering the Syrtis Major plateau originally consisted of augite-bearing basalt containing two cogenetic pyroxenes with no appreciable amount of olivine. Additionally, Syrtis Major ISM visible and near-infrared spectra were matched to the spectra of an Apollo 12 basalt and a Shergotite meteorite to show that the ISM spectra are consistent with a mafic basalt composition [1]. In this work, pyroxene compositions from ISM data determined by [1] compared with the pyroxene compositions of Apollo 12 pigeonite basalt, Shergotite meteorite, and pyroxenitic komatiite show that the Syrtis Major volcanic materials are consistent with pyroxenitic komatiite. Pyroxenitic komatiite is significant for the Earth because it contains a large amount of MgO, implying generation under unique circumstances compared to typical basaltic compositions [e.g., 2].

Background: Komatiites are subdivided by weight percent MgO into peridotitic (>20%), pyroxenitic (12–20%), and basaltic (8–12%) varieties [3]. Pyroxenitic and basaltic komatiites may be collectively referred to as mafic komatiites. Mafic komatiites are always found with peridotitic komatiites in the Archean and are also found alone in the few Proterozoic occurrences. Peridotitic komatiites are dominated by olivine, with interstitial clinopyroxene and glass. Mafic komatiites are dominated by pyroxene (augite ± pigeonite ± bronzite), with lesser plagioclase, and rare olivine. Olivine is only present in a few mafic komatiite flows were MgO content is >12% and even then olivine only accounts for <10% of the mode [4].

The upper portion of pyroxenitic komatiite flows are often composed of skeletal magnesium pigeonite with augite exteriors in a fine augite and plagioclase groundmass. Coexisting magnesium pigeonite and augite are unusual for most lavas on the Earth, but are an important characteristic of pyroxenitic komatiites [4]. According to Campbell and Arndt [5], rapid cooling in the upper parts of some komatiite flows may cause olivine to crystallize initially. However, the rate of olivine crystallization is not sufficient to prevent continued supercooling of the liquid to a point below the temperature of the stable pyroxene liquidus. This supercooling results in the crystallization of magnesian pigeonite in a liquid that would normally produce olivine under equilibrium conditions. As the liquid temperature drops further, augite crystallizes, followed by plagioclase.

Coexisting pigeonite and augite are also found in ~12 categories of lunar mare basalts and well-developed skeletal pigeonite mantled by augite is found in Apollo 15 and Apollo 12 pigeonite basalts [6]. All 12 of these basalt groups are magnesium rich, ranging in weight percent MgO from 7.03% to 19.97%, and averaging 10.7% [6]. Like komatiites, the coexisting pyroxenes in the Apollo 12 pigeonite basalts are thought to form by rapid metastable crystallization of a supercooled liquid [7]. Regardless of the specific mechanism that forms skeletal textures and coexisting pigeonite and augite, these features are characteristic of highly magnesian lavas like komatiites.

Discussion: Using ISM data, Mustard et al. [1] estimated the composition of Syrtis Major pyroxenes. According to Mustard et al., the pyroxene compositions represented by their ISM analysis falls in an area of "unusual" composition on the pyroxene quadrilateral, and therefore the data may represent an average composition of augite and pigeonite as intimate exsolution lamella. Telescopic reflectance measurements of several dark regions on Mars are indicative of coexisting pyroxenes, which correlates with the modal mineralogy of Shergotite meteorites, which may have originated from Mars [8]. Comparison with Shergotite meteorites and terrestrial komatiites suggests that exsolution lamella are not required by the results of [1]. If the ISM data represent an average of two pyroxene compositions, then discrete pyroxenes may be implied. Furthermore, if coexisting pyroxenes were detected by the ISM on Syrtis Major, then they may have formed by a mechanism like that previously described for the crystallization of pyroxenes in mafic komatiite and Apollo 12 pigeonite basalts.

Figure 1 shows a pyroxene quadrilateral with the Syrtis Major ISM pyroxene field of [1] superposed over the compositions of pyroxenes found in a pyroxenitic komatiite flow, the Shergotite meteorite, and an Apollo 12 pigeonite basalt. The majority of pyroxenitic komatiite pyroxene analyses do not fall within the ISM field because their source liquid contained relatively little Fe compared to potential martian lavas [e.g., 3,9]. Many individual pyroxene analyses from the Shergotite and the Apollo 12 pigeonite basalt do fall within the ISM field. More importantly, the averaged composition of coexisting pyroxenes in the plotted samples will also fall within the ISM field. These samples perform better than the komatiite because the higher Fe content in these rocks allows greater substitution of Fe in the pyroxene structure as Mg is consumed initially. A crystallization trend is defined that places these pyroxene analyses within and below the ISM field, as seen in Fig. 1. This analysis supports the possibility of komatiite-type lava on the Syrtis Major plateau because these coexisting pyroxenes are indicative of magnesian komatiite-type lava.

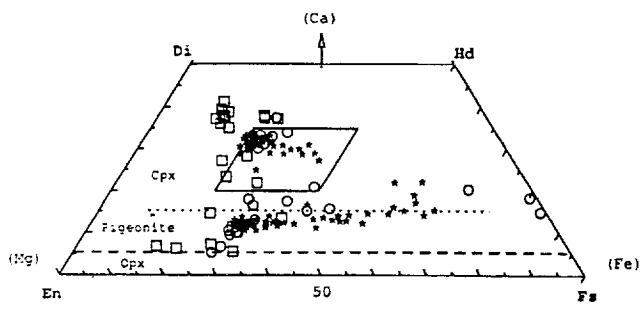

Fig. 1. Pyroxene compositions from Syrtis Major ISM and analogs. ISM field (rhomboid) from [1]; pyroxenitic komatiite data (squares) provided by D. P. Reyes, [sample DPY-10, unpublished data, Reyes, 1993]; and Apollo 12 pigeonite basalt (circles) and Shergotite meteorite (stars) data from [6].

An important caveat to the analysis presented here and to that of [1] is that Syrtis Major plateau is composed of a large sand sheet and dune field, with varying degrees of variable fine-grained dust coatings [1]. The question arises whether the materials observed represent locally derived or transported materials. Additionally, if local or distal in origin, certain phases in the Syrtis Major material may have been preferentially concentrated by eolian activity or chemical weathering. The relatively low spatial resolution of ISM (24 km) makes these questions difficult to answer.

A thermal emission spectrometer (TES) with a spectral resolution of 5–10 cm^{-1}, from 5 to 60 μm, and a spatial resolution of 3 km (e.g. the Mars Observer Thermal Emission Spectrometer [10]), would easily reveal the presence and nature of komatiitic lavas on Syrtis Major as indicated by the evidence discussed. In addition, TES-type data could be used to study weathering products and to trace sediment transport paths in an attempt to distinguish primary igneous materials from reworked sediments. Finally, a TES would reveal if Syrtis Major lava composition evolves from peridotitic to basaltic compositions over time as seen in terrestrial komatiites [3].

References: [1] Mustard J. F. et al., (1993) *JGR, 98,* 3387–3400. [2] Takahashi E. (1991) *JGR, 95,* 15941–15954. [3] Arndt N. T. et al. (1977) *J. Pet., 18,* 319–369. [4] Cameron W. E. and Nisbet E. G. (1982) In *Komatiites* (Arndt N. T. and Nisbet E. G., eds.), George Allen and Unwin, Boston, 29–50. [5] Campbell I. H. and Arndt N. T. (1982) *Geol. Mag., 119,* 605–610. [6] *BVSP, Basaltic Volcanism Study Project* (1981) Pergamon, New York, 1286 pp. [7] Klein C. et al. (1971) *Proc. LSC 2nd,* 265–284. [8] Straub D. W. et al. (1991) *JGR, 96,* 18819–18830. [9] McGetchin T. R. and Smyth J. R. (1978) *Icarus, 34,* 512–536. [10] Christensen P. R. et al. (1992) *JGR, 97,* 7719–7734.

N94-33230

5/10/91 ABS. ONLY

MARTIAN DELTAS: MORPHOLOGY AND DISTRIBUTION. J. W. Rice Jr.[1] and D. H. Scott[2], [1]Department of Geography, Arizona State University, Tempe AZ 85283, USA, [2]Astrogeology Branch, U.S. Geological Survey, 2255 N. Gemini Drive, Flagstaff AZ 86001, USA.

The identification of deltas on Mars has been an enigma over the years for planetary geologists. However, recent detailed mapping (1:500,000 scale) has revealed numerous examples of martian deltas. We will document and describe the location and morphology of these deltas.

Deltas are alluvial regions composed of sediment deposited in relatively still water (lakes, bays, seas) at river mouths. Deposition on deltas occurs when river velocity is reduced upon entering standing bodies of water. Factors that contribute to delta morphology are river regime, coastal processes, structural stability, and climate [1].

The largest delta systems on Mars are located near the mouths of Maja, Maumee, Vedra, Ma'adim, Kasei, and Brazos Valles. There are also several smaller-scale deltas emplaced near channel mouths situated in Ismenius Lacus, Memnonia, and Arabia.

Delta morphology will be used to reconstruct type, quantity, and sediment load size transported by the debouching channel systems

[2,3]. For example, arcuate deltas are deposited by bed load or mixed load systems that bring large quantities of coarse material to the coastline as opposed to the elongate (birdfoot) deltas composed of large quantities of fine sediment deposited by a combination of suspended load and mixed load rivers. Methods initially developed for terrestrial systems will be used to gain information on the relationships between martian delta morphology, river regime, and coastal processes.

References: [1] Morgan J. P. (1970) *SEPM, 15*, 31–47. [2] Axelsson V. (1967) *Geogr. Ann., 49*, 2–127. [3] Galloway W. E. (1975) *Houston Geol. Soc.*, 87–98.

N94-33231

54-91 ABS.ONLY

3

Q'

CARBONATE FORMATION ON MARS: LATEST EXPERIMENTS. S. K. Stephens[1], D. J. Stevenson[1], G. R. Rossman[1], and L. F. Keyser[2], [1]Division of Geological and Planetary Sciences, 170-25, California Institute of Technology, Pasadena CA 91125, USA, [2]Earth and Space Sciences Division, 183-901, Jet Propulsion Laboratory, California Institute of Technology, Pasadena CA 91109, USA.

Introduction: Laboratory simulations of martian CO_2 storage address a fundamental question about martian climate history: Could carbonate formation have reduced CO_2 pressure from a hypothetical >1 bar to the present 7 mbar in ≤3–4 b.y.? We address this problem with experiments and analysis [1,2] designed to verify and improve previous [3,4] kinetic measurements, reaction mechanisms, and product characterizations. Our theoretical modeling [5,6] has sought to improve existing models of martian CO_2 history [7–10], which generally assume an early CO_2 greenhouse atmosphere (questioned by Kasting [11]).

Experimental Results: A sensitive manometer monitored the pressure drop (PD) of CO_2 due to uptake by powdered silicate for periods of 3 to 100+ days. Initially we focused on monomineralic, crystalline samples, but more recently we ran basaltic glass (see Table 1). Grinding was done in a tungsten-carbide shatterbox. Di1 was not treated further, and all other monomineralic samples were heated at 120°C for ~1 day after sitting in weak acetic acid for 1+ days. Bas was simply heated. Runs were performed at warm (25°C) and cold (–25°C) temperatures, about 1 bar CO_2 pressure, and specific surface areas of ~1 m^2/g (~1 μm particles). Experiments included "vapor" (H_2O premixed with CO_2, for ~1–10 monolayer coverage), "damp" (H_2O pipetted onto powder before soaking in), and "wet" ($m_{H_2O} \sim m_{sample}$) runs.

BET specific surface areas were determined for Di1 and Bas, and quantitative results are given for experiments using these starting compositions (Table 2). Pressure drops (ΔP) for Di1 and Bas show rapid short-term (~1 day) CO_2 uptake and considerably slower long-term ΔP (Figs. 1 and 2). We know the changes are not due to H_2O adsorption since there is always sufficient water to maintain $P_{vap}(H_2O)$. However, we assume the short-term signal reflects CO_2 adsorption (consistent with previous measurements [7,12] and confirmed by desorption experiments). Curves for Di2, O11, and O12 are qualitatively similar to those for Di1, whereas Qtz and Plag show near-zero short-term ΔP and very slow long-term signal—indistinguishable from a leak (<10^{11} $mol/m^2/s$).

Discussion: Thermodynamic calculations [13] suggest that reactions should form carbonates from diopside and olivine, and possibly plagioclase, at martian P and T. PD results can be classified into three groups: diopsides and olivines, quartz and plagioclase, and basalt. Bas takes up more CO_2 than monomineralic, crystalline diopside, and olivine, despite the fact that it is probably >50% feldspar and quartz (i.e., relatively unreactive), suggesting a role for glass (vs. crystalline mineral).

No long-term ΔP was expected for Qtz (no cations), although adsorption was anticipated, while with Plag we expected a possible long-term signal, and again the absence of an adsorption effect was puzzling. One explanation involves the progressive polymerization of silicate tetrahedra: olivine (isolated tetrahedra) and pyroxene (chains) vs. feldspar and quartz (three-dimensional frameworks). The structure of olivine and diopside may make it easier for cations to physically adsorb (and/or chemically bond with) anions.

Also puzzling is the result of an X-ray photoelectron spectroscopy (XPS) analysis performed on Di2 exposed to similar $P(CO_2)$ and H_2O vapor conditions as the PD experiment with Di1 (vapor)

TABLE 1. Minerals and rocks used for experimental samples.

Sample	Approximate Composition	Sample Description	Locale
Diopside 1 [Di1]	$CaMgSi_2O_6$	Bulk, broken crystals, ~5% impurities	Dog Lake, Quebec
Diopside 2 [Di2]	$CaMgSi_2O_6$	Green, euhedral crystals, <2% impurities	Rajastan, India
Olivine 1 [Ol1]	$Mg_{.98}Fe_{.02}SiO_4$ [Forsterite 98%]	Bulk, broken crystals, ~5% impurities	Gabbs, Nevada
Olivine 2 [Ol2]	$Mg_{.88}Fe_{.12}SiO_4$	Translucent green pebbles (crystals), <2% impurities	San Carlos, Arizona
Quartz [Qtz]	SiO_2	Clear, euhedral crystal, <1% impurities	Mt. Ida, Arkansas
Plagioclase [Plag]	Ab_3An_7 [Ab = $NaAlSi_3O_8$, An = $CaAl_2Si_2O_8$]	Clear, euhedral crystal <1% impurities	Ponderosa Mine, Oregon
Basalt [Bas]	Tholeiite [50 wt%, SiO_2, 13% Al_2O_3, 12% FeO, 9% MgO, 11% CaO]	~98 wt% black glass, ~0.3 wt% dissolved H_2O ~1 wt% crystals, 1991 lava flow, quenched in air	Kilauea, Hawaii

TABLE 2. Conditions and results of PD experiemts for Dil and Bas.

Experiment	A_s* (m^2/g)	$P(CO_2)$† (bars)	T (°C)	H_2O Content‡ (Monolayers)	CO_2 Uptake After 1 day§ ("Monolayers")	Rate of CO_2 Uptake¶ Day 3 (10^{11} Molecules/m^2/s)	Day 7	>20 Days
Dil (crystalline)								
Cold**, vapor	3	0.96	-25	1	0.2	20	15	<3
Warm, damp	3	0.96	25	200	1.7	50	25	<6
Warm, wet	3	0.96	25	1000	3.6	60	—	—
Bas (glass)								
Warm, vapor††	0.6	0.96	25	20	1.5	50	20	—
Warm, ~damp	0.6	0.96	25	300	3.0	70	—	—
Warm, damp	0.6	0.96	25	1000	5.5	120	—	—

* BET specific surface area, measured using Ar and Kr adsorption.
† CO_2 pressure at start of run, not corrected for pressure drop over a period of days.
‡ Surface depth of water film for given A_s and ~10 Å² per H_2O molecule, in equivalent monolayers.
§ Surface depth of gas, assuming ~20 Å² per CO_2 molecule, all deposited on sample.
¶ Equivalent to rates of inferred carbonate formation.
** Data shown for cold (-25°C) portions of run only; warm (25°C) intervals were also monitored.
†† H_2O content may be up to twice the number shown due to ~0.3 wt% dissolved H_2O in basalt glass.

shown in Table 2. Although conducted at +25°C, the XPS experiment yielded no added carbonate on a freshly cleaved crystal surface, implying no significant bound reaction product. This might be due to a different surface texture or degree of fracturing compared to a powder.

From the dependence of CO_2 uptake on temperature and water content (Table 2, Figs. 1 and 2), we verified that "warm and wet" PD conditions store considerably more CO_2 than "cold and dry." For scenarios involving liquid water, CO_2 uptake is consistent with the formation of a monolayer of carbonate in ~10–100 days. The asymptotic decrease in the rate of uptake could represent the continuation of chemistry beyond the surface reaction that takes place as a monolayer of carbonate is formed [6], although it is interesting that initial CO_2 uptake is always of the order of 1 monolayer. Long-term uptake rates are comparable to those obtained by Booth [4], 10^{11}–10^{12} mol/m^2/s. However, Booth inferred carbonate formation by evolving CO_2 at the end of runs, assumed no limitation due to diffusion through a product layer (indeed, « 1 monolayer was inferred to have formed), and concluded that reactions depended on ionic reactions in a thin, approximately monolayer H_2O film at the high-T end of a cycle in temperature. Our results then are not directly comparable: we have considerably more water, higher temperatures, and no cycling, and we infer (from monitored PD experiments) nonreversible formation of about 1 monolayer of carbonate.

An extrapolation from long-term CO_2 uptake rates (Table 2) shows that an upper limit of 1–5 mbar/yr (at least for experimental P, T, and H_2O content, and for timescales on the order of months) can be taken up by a Bas regolith 100 m in thickness and covering

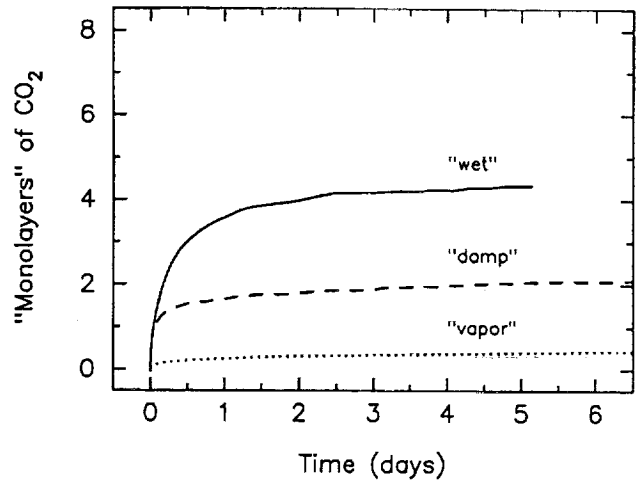

Fig. 1. PD results for Dil (crystalline). A_s = 3 m^2/g (see Table 2). Minor fluctuations in PD are due to small T changes.

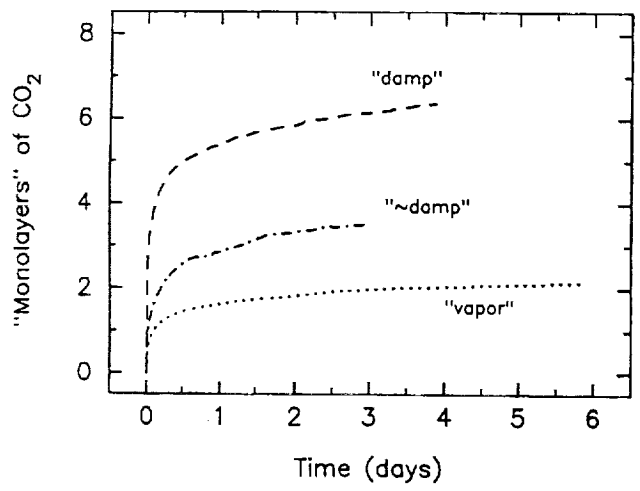

Fig. 2. PD results for Bas (glass). A_s = 0.6 m^2/g (see Table 2).

the surface of Mars. Modeling of nonaqueous, diffusion-limited growth of carbonate rinds [6] has established that, if long-term kinetics are anywhere near the laboratory rates implied by Booth and now by us, then the growth rate will decrease rapidly after a few 100 m.y. and we may require times approaching 3–4 b.y. to store 1 bar of CO_2 on Mars.

References: [1] Stephens S. K. et al. (1992) *LPI Tech. Rpt. 92-04*, 34–36. [2] Stephens S. K. et al. (1992) *Bull. A.A.S., 24*, 980. [3] Booth M. C. and Kieffer H. H. (1978) *JGR, 83*, 1809–1815. [4] Booth M. C. (1980) Ph.D. thesis, UCLA. [5] Stephens S. K. and Stevenson D. J. (1990) *LPS XXI*, 1198–1199. [6] Stephens S. K. and Stevenson D. J. (1992) *LPI Tech. Rpt. 92-02*, 136–137. [7] Fanale F. P. et al. (1982) *Icarus, 50*, 381–407. [8] Kahn R. (1985) *Icarus, 62*, 175–190. [9] Pollack J. B. et al. (1987) *Icarus, 71*, 203–224. [10] Haberle R. M. et al. (1993) *LPI Tech. Rpt. 93-03*, 13–14. [11] Kasting J. F. (1991) *Icarus, 94*, 1–13. [12] Zent A. P. et al. (1987) *Icarus, 71*, 241–249. [13] Gooding J. L. (1978) *Icarus, 33*, 483–513.

N94- 33232

542-91 ABS. ONLY

GEOLOGIC CONTROLS OF EROSION AND SEDIMENTATION ON MARS. K. L. Tanaka[1], J. M. Dohm[1], and M. H. Carr[2], [1]U.S. Geological Survey, Flagstaff AZ 86001, USA, [2]U.S. Geological Survey, Menlo Park CA 94305, USA.

Because Mars has had a history of diverse erosional and depositional styles, an array of erosional landforms and sedimentary deposits can be seen on Viking orbiter images. Here we review how geologic processes involving rock, water, and structure have controlled erosion and sedimentation on Mars, and how further studies will help refine our understanding of these processes.

Impacts: The early geologic record is dominated by large impacts, including dozens of circular basins that exceed 200 km in diameter [1,2]. Large impact events have strongly influenced erosional and sedimentary processes throughout Mars' geologic history by (1) comminuting crustal rocks into very poorly sorted debris [3]; (2) forming large topographic basins whose rims have been eroded and whose interiors have accumulated sediment (and, in some cases, temporary lakes) [4,5]; and (3) seismically disrupting [6] and driving hydrothermal circulation [7] in aquifers. Large volumes of sediment are contained in Argyre and Hellas Basins and the northern plains, which include several large impact basins and one proposed mega-impact, the 7700-km-diameter Borealis Basin [1,8].

Tectonism: For Earth, sedimentologists have said that "the major control of all sedimentation is tectonics" [9]. For Mars, tectonism has also been a major sedimentological control in that it has (1) produced topographic relief, (2) provided fractures that have served as zones of enhanced surface erosion, as well as subsurface conduits for the flow of water, and (3) produced seismicity. Possible tectonic lowering of the northern lowlands at the end of the Noachian Period may have caused the extensive erosion observed there and along the highland/lowland boundary [10,11]. This erosion formed vast areas of knobby terrain in the lowlands and fretted terrain and channels along the lowland boundary. In addition, the increased surficial activity appears to have been associated with a climate change that resulted in waning highland erosion [11,12]. Also, contemporaneous deformation of the Thaumasia highlands by folding and faulting led to local channel formation [e.g., 13].

The growth of Tharsis and Valles Marineris, which may have peaked in Late Hesperian time, resulted in high local to regional relief, as well as possible changes in axial orientation of the planet [14] and high obliquities [15]. In addition, this tectonism led to catastrophic flooding of the Chryse region [16] and of Mangala Valles [17] and possibly to the formation of small channels along the edge of the Thaumasia plateau [18]. This flooding also may have led to temporary climate change [19] that caused glaciation in the southern high latitudes [20].

Volcanism: Mars is renowned for its huge volcanic shields and extensive lava fields. Volcanism (and intrusion) apparently occurred throughout geologic time [21,22]. Their influences on erosion include (1) formation of topographic highs, (2) local production of easily erodible pyroclastic material [23], (3) local rises in crustal temperature, leading to increased hydrothermal circulation, and (4) local disruption of near-surface rocks. In the Tharsis region, many of these effects were associated with tectonism.

Crustal Ground Water and Ground Ice: The presence of large volumes of water and ice in the martian crust has been the major factor in producing the large-scale erosion evidenced by various landforms. At present, interstitial or massive ice may be common in the upper kilometer or so of the crust where freezing temperatures exist, particularly at high latitudes [24]. Steep slopes in ice-rich material may lead to the formation of debris aprons and rock glaciers. Perched subpermafrost aquifers (that may have provided pore water for sapping and catastrophic discharges) and ice-laden permafrost zones could have been charged from the water table by thermal liquid or vapor transport and by seismic pumping [25].

Eolian Activity: The transport by wind of dust and sand-sized particles on the martian surface is shown by extensive dune fields in the the north polar region and within local topographic traps [26] and by polar layered deposits and mantle material [27]. Moreover, winds can erode friable materials, producing the yardangs and deflation pits that are common in extensive equatorial deposits in the Medusae Fossae region. Ephemeral wind streaks all over Mars attest to the ongoing eolian transport of fine particles.

Future Work: Through geologic mapping of Mars at local (1:500,000) and regional (1:2,000,000 and 1:5,000,000) scales and by topical studies, workers have continued to assess the geologic settings and processes that have caused erosion and sedimentation on Mars. Detailed maps have been made of the Tharsis volcanotectonic region, the Elysium volcanics and channels, the Chryse channels and basin, the Hellas and Argyre basins, the Valles Marineris, Lunae Planum, Mangala Valles, and other regions. These maps provide the basis for more rigorous semiquantitative analyses of Mars' sedimentological history. To achieve this, we plan to augment the mapping studies with further research and compilation. Our objectives include (1) statistical studies of martian channels, including their morphology (lengths, type, drainage pattern, junction angles, etc.) and their distribution by age, elevation, slope, and geologic setting, and (2) determination of the intensities of erosional events along the highland/lowland boundary and their relation to infilling of the northern plains.

We have recently completed a digitized, vector-format, graphical database of channels on Mars as observed on the 1:2,000,000-scale photomosaic series. We plan to implement GIS software and merge other Mars databases (e.g., geology and topography) to accomplish our objectives. This approach will permit evaluation of

channel genesis as a function of channel type and morphology, slope, elevation, age, latitude, type of material dissected, and proximity to specific geologic features. In turn, the influence on channel origin by possible global or local anomalous climates may be assessed.

Although some work has been done to assess the timing of erosion and crater obliteration along the highland/lowland boundary [e.g., 28,29], we still know little about the volume of material eroded. We intend to measure depths of dissection by using photoclinometry, which will enable us to estimate these volumes of eroded material (and, consequently, volumes deposited in the northern plains).

References: [1] Schultz R. A. and Frey H. (1990) *JGR, 95,* 14175–14189. [2] Tanaka K. L. et al. (1992) In *Mars, 11,* 345–382, Univ. of Arizona. [3] MacKinnon D. J. and Tanaka K. L. (1989) *JGR, 94,* 17359–17370. [4] Schultz P. H. et al. (1982) *JGR, 78,* 9803–9820. [5] Scott D. H. et al. (1992) *Proc. LPS, Vol. 22,* 53–62. [6] Leyva I. A. and Clifford S. M. (1993) *LPS XXIV,* 875–876. [7] Brakenridge G. R. et al. (1985) *Geology, 13,* 859–862. [8] Wilhelms D. E. and Squyres S. W. (1984) *Nature, 309,* 138–140. [9] Blatt H. et al. (1972) *Origin of Sedimentary Rocks, 591,* Prentice-Hall, NJ. [10] McGill G. E. and Dimitriou A. M. (1990) *JGR, 95,* 12595–12605. [11] Tanaka K. L. (1991) *LPS XXII,* 1377–1378. [12] Craddock R. A. and Maxwell T. A. (1993) *JGR, 98,* 3453–3468. [13] Tanaka K. L. and Schultz R. A. (1991) *LPS XXII,* 1379–1380. [14] Schultz P. H. and Lutz A. B. (1988) *Icarus, 73,* 91–141. [15] Ward W. R. et al. (1979) *JGR, 84,* 243–259. [16] Carr M. H. (1979) *JGR, 84,* 2995–3007. [17] Tanaka K. L. and Chapman M. G. (1990) *JGR, 95,* 14315–14323. [18] Dohm J. M. and Tanaka K. L., work in progress. [19] Baker V. R. et al. (1991) *Nature, 352,* 589–594. [20] Kargel J. S. and Strom R. G. (1992) *Geology, 20,* 3–7. [21] Greeley R. (1987) *Science, 236,* 1653–1654. [22] Tanaka K. L. et al. (1988) *Proc. LPSC 18th,* 665–678. [23] Gulick V. C. and Baker V. R. (1990) *JGR, 95,* 14325–14344. [24] Fanale F. P. et al. (1986) *Icarus, 67,* 1–18. [25] Clifford S. M. (1993) *JGR, 98,* 10973–11016. [26] Ward W. R. et al. (1985) *JGR, 90,* 2038–2056. [27] Tanaka K. L. and Scott D. H. (1987) *U.S.G.S. Map I-1807-C.* [28] Frey H. V. et al. (1988) *Proc. LPSC 18th,* 679–699. [29] Maxwell T. A. and McGill G. E. (1988) *Proc. LPSC 18th.* 701–711.

N94- 33233

S43-91 ABS.

POLAR SEDIMENT ACCUMULATION: ROLE OF SURFACE WINDS AT THE TWO POLES. P. C. Thomas and P. J. Gierasch, CRSR, Cornell University, Ithaca NY, USA.

The accumulation of the large deposits of volatile and nonvolatile sediments at both martian poles has occurred through periods of likely climate change. Most data on wind directions near the martian poles and seasonal activity relate to a very short period of time, at one point in climate cycles. It is still uncertain what the net budgets to the poles are and how this budget (if known) would fit into longer climate/sediment cycles. Pending further data we examined the full suite of Viking high-resolution, high-latitude images for wind markers of all sizes and types. These probably represent timescales of formation from days to several tens of thousands of years. The goal is to estimate the effectiveness, and possible drivers, of wind systems that bring materials near the surface to the regions of polar sediments, and also remove materials from the polar areas.

The simple polar vortex model of French and Gierasch [1] accounts for only a part of the observed features; most particularly it lacks the poleward flow seen near 75–80 latitude in both polar regions, but especially the north. Observations of crescentic dunes, framing dunes, and some wind streaks show confinement of the north polar erg by off-pole winds near the margins of the layered deposits and prograde, on-pole winds slightly farther south. The on-pole winds have formed features as transitory as wind streaks and as long lived as large framing dune complexes. Exceptions to the pattern of confining, on-pole wind directions occur in some longitudes and might be due to topographic control. The present topographic data are inadequate to model these effects. In the south, intracrater dune fields are imaged well enough to show field orientations, and thus very-long-term winds, but the bedforms are largely transverse with 180° ambiguities in wind directions. Streaks show some on-pole flow, but in a retrograde sense.

It is desirable to discriminate between feedback effects, such as the dunes' low albedos, that might confine the winds to a narrow belt, and causes that are independent of the dune presence, which would allow poleward transport of the sand and some dust at the surface, for inclusion in the polar deposits. Surface transport of the saltating materials to the polar regions would remove the dilemma of saltating materials being present in deposits thought to be made up of suspension load and condensed volatiles.

References: [1] French R. G. and Gierasch P. J. (1979) *JGR, 84,* 4634–4642.

N94- 33234

S44-91 ABS. ON

THE MARTIAN SOURCES OF THE SNC METEORITES (TWO, NOT ONE), AND WHAT CAN AND CAN'T BE LEARNED FROM THE SNC METEORITES. A. H. Treiman, Code C-23, Lockheed Engineering and Sciences Co., 2400 NASA Road 1, Houston TX 77258, USA, now at Lunar and Planetary Institute, 3600 Bay Area Boulevard, Houston TX 77058-1113, USA.

The SNC meteorites almost certainly from the martian crust, have been inferred to come from a single impact crater site, but no known crater fits all criteria. Formation at two separate sites (S from one, NC from the other) is more consistent with the sum of petrologic, geochronologic, and cosmochronologic data, and eases crater selection criteria. If the source craters for the SNC meteorites can be located, Mars science will advance considerably. However, many significant questions cannot be answered by the SNC meteorites, and await a returned sample.

Introduction: The SNC meteorites are rocks of basaltic parentage, inferred to be samples of the martian crust, and have been important in providing "ground truth" to other observations of Mars throughout the MSATT and predecessor programs. Although the SNCs have provided essential information on mantle and magmatic processes, the hydrosphere, and the composition of the atmosphere, their utility is limited because their source site(s) on Mars are not known. The most comprehensive effort at determining a source impact crater for the SNC meteorites [1] was not entirely successful, as no martian crater met all the criteria for an SNC source. However, it seems likely that the SNC meteorites came from two separate sources on the martian surface, and a number of craters fit this relaxed criterion.

If efforts toward determining the martian sources of the SNCs are successful, we will reap a bountiful harvest of knowledge about Mars. However, the SNC meteorites cannot tell about the whole planet of Mars, and many significant questions will remain, answerable only by analysis of returned samples.

Source(s) for SNC Meteorites: Most studies have inferred that the SNC meteorites originated near a single source crater on Mars [1–4, but see 5,6]. The source crater has been inferred to be on or near Tharsis, home to the youngest basalt flows on Mars [1–4], because the SNCs all formed from basaltic lavas and are all quite young in planetary terms (Table 1). Nine potential source craters in Tharsis were located by [1], but none satisfied all known (or presumed) constraints.

Two Source Craters: S ≠ NC. Rather than invoking a single source crater, it is more plausible that the SNC meteorites originated from two separate sites. Support for this hypothesis follows from the profound differences between the shergottites (S) and the nakhlites and Chassigny (NC), the extent of which has not been appreciated.

Some of these differences are given in Table 1, from which it is clear that S and NC have been distinct at every stage of their development, from mantle through eruption through alteration through impact ejection. The most parsimonious conclusion from these data is that NC and S had essentially nothing to do with each other. They most likely formed at different sites on Mars, and were ejected from Mars as small meteoroids at the ages indicated by their cosmic ray exposures. (The cosmic ray exposure age of the shergottite EETA79001 is 0.5 m.y. [5], which probably dates a disruptive collision in space [15]). Problems related to the two-crater hypothesis [4] are discussed below.

Problems with Single-Crater Origins: The current paradigm for SNC origins, that they were ejected from Mars in a single impact event [1–5], seems unconvincing in detail. The size of the ejection crater is unconstrained by geology or petrology. A large crater might overlap two distinct terranes (for S and NC); a small crater might have impacted a thin veneer of younger basalt (S) over older (NC).

Ejection at ~180 m.y. [1–4] could be consistent with the SNC cosmic ray exposure ages only in the following scenario: (1) At least two boulders (>5 m diameter [5]) were ejected, one each for S and NC; (2) Two of these boulders were disrupted in space to form meter-sized and smaller fragments at 11 m.y. and 2.8 m.y., the precise (within error) cosmic ray exposure ages of all NC and all S respectively to form meter-sized and smaller fragments; (3) Following disruption in space, fragments that had been exposed to cosmic rays for ~180 m.y. were segregated from those that were totally shielded; and (4) Following both disruptions, all of the fragments that had been exposed to cosmic rays for ~180 m.y. were prevented from entering Earth-crossing orbits. Events (1) and (2) are plausible, but (3) and (4) strain credulity.

Ejection at a younger age, 11 m.y. to satisfy the cosmic ray exposure ages of NC (discussed in [4,5]), would require equally difficult scenarios. If the SNCs had been ejected as a single boulder, its core must have been all S and its rind all NC to satisfy cosmic ray exposure ages. This watermelon model of an SNC meteoroid seems fanciful. On the other hand, the NC could have been ejected as small meteoroids and S ejected as a meteoroid so large its core was shielded from cosmic rays. In this case, events like (3) and (4) from the paragraph above must have occurred, and credulity is again strained.

Implications of Two-Crater Model: If the SNC meteorites originated in two separate craters on the martian surface (as implied by petrology, geochronology, and cosmochronology), some other inferences about Mars must be revised.

First, some of the objections to the nine potential source craters of [1] are removed. It is no longer required that a single crater have access to all SNC lithologies, so craters in monolithologic, simple units are permitted. Among the choices of [1], S could have come from their craters 1, 3, 7, or 9 and NC could have came from craters 2 or 4–9.

Second, one of two current understandings of Mars must be incorrect: Either the mechanics of ejecting rock from Mars, or absolute ages inferred from crater-counts. If the ages are nearly correct, ejection of rock Mars to solar orbit must be possible with craters of 35 km (Table 1 of [1]), smaller than the 50 km suggested by current understanding of crater formation and rock ejection [4]. So either the mechanics are inaccurate to a factor of 1.5 or the ages inferred for the young martian surfaces are too old.

Third, the absence of meteorites from the older martian terranes must now be explained. In single-crater models, the lack of meteoroids from the older terranes, >95% of the Mars surface [1], can be ascribed to chance. But the odds of the only two meteorite-forming impacts on Mars hitting the young terrane are 0.0025. It is most likely that the older terranes have experienced impacts that could have yielded meteoroids. Perhaps the physical properties of the older terranes prevent ejection of meteorites, or perhaps meteorites from the older terranes do fall on Earth and are not recognized (e.g., granite, sandstone, or limestone?).

What If We Locate the SNC Source Craters?: If the source craters for the SNC meteorites can be located, following the method of [1], our understanding of Mars will be advanced significantly. First, it will be possible to assign absolute dates to martian crater-count chronologies, at least at the young end. This will remove some considerable uncertainties from models of the history of Mars (e.g., cooling, volatiles, etc.). Second, knowing the geologic settings of the SNCs will permit understanding of their aqueous alteration histories in terms of real martian geology, and greatly advance knowledge of the reservoirs of water on Mars. Third, we will be able to calibrate remote sensing data (both in hand and in the future) against known lithologies. These advances are only a few among many possibilities.

TABLE 1. Selected properties of SNC meteorites.

	S	NC
Source Nd/Sm, Rb/Sr, etc.	Enriched (>CI) [7]	Depleted (<CI) [8,9]
Magma incompatible elements	Depleted (>CI) [10]	Enriched (<CI) [8,9]
Crystallization age	~180 m.y. [11]	~1250 m.y. [8,9]
Preterrestrial aqueous alteration (where present; all include salts)	Aluminosilicate [14]	Smectite-iron oxide [12,13]
Shock pressure (maskelynite vs. plagioclase)	»29 GPa	<29 GPa
Cosmic ray exposure age	2.8 ± 0.3, 0.5 m.y. [5]	11 ± 1 m.y. [5]

But the SNCs cannot answer all the important questions about Mars. No matter how much is learned from the SNCs, they cannot replace a carefully considered successful Mars sample return mission. The SNCs are limited because they represent only one type of sample formed during a small part of Mars' history on a small part of Mars. For instance, continued study of the SNCs cannot determine: the mineralogy and origin of the martian dust; the abundances of many reactive gas species in the martian atmosphere; the natures and compositions of the martian highlands; the compositions of paterae volcanics; the natures and compositions of layered deposits; and whether living organisms ever existed on Mars. To solve these questions will require continued spacecraft investigations of Mars, including orbiters, landers, and especially sample returns.

Acknowledgments: Discussions with J. Jones and M. Lindstrom have helped clarify my ideas. I am grateful to D. Black and the LPI for facilitating the continuation of my research.

References: [1] Mouginis-Mark P. J. et al. (1992) *JGR, 97*, 10213–10336. [2] Wood C. A and Ashwal L. D. (1981) *Proc. LPSC XII*, 1359–1375. [3] Nyquist L. E. (1983) *Proc. LPSC XIII*, A785–A798. [4] Vickery A. M. and Melosh H. J. (1987) *Science, 237*, 738–743. [5] Bogard D. D. et al. (1984) *GCA, 48*, 1723–1740. [6] Ott U. and Begemann F. (1985) *Nature, 317*, 509–512. [7] Shih C.-Y. et al. (1982) *GCA, 46*, 2323–2344. [8] Nakamura N. et al. (1982) *GCA, 46*, 1555–1573. [9] Nakamura N. et al. (1982) *Meteoritics, 17*, 257–258. [10] Smith M. R. et al. (1984) *Proc. LPSC 15th*, in *JGR, 89*, B612–B630. [11] Jones J. H. (1986) *GCA, 50*, 969–977. [12] Treiman A. H. and Gooding J. L. (1991) *Meteoritics, 26*, 402. [13] Treiman A. H. et al. (1993) *Meteoritics, 28*, 86–97. [14] Gooding J. L. and Muenow D. W. (1986) *GCA, 50*, 1049–1059. [15] Treiman A. H. (1993) *Meteoritics, 28*, 451.

TEMPORAL CHANGES IN THE GEOGRAPHIC DISTRIBUTION, ELEVATION, AND POTENTIAL ORIGIN OF THE MARTIAN OUTFLOW CHANNELS. S. Tribe[1] and S. M. Clifford[2], [1]University of British Columbia, Canada, [2]Lunar and Planetary Institute, Houston TX 77058, USA.

Introduction: Observational evidence of outflow channel activity on Mars suggests that water was abundant in the planet's early crust. However, with the decline in the planet's internal heat flow, a freezing front developed within the regolith that propagated downward with time and acted as a thermodynamic sink for crustal H_2O. One result of this thermal evolution is that, if the initial inventory of water on Mars was small, the cryosphere may have grown to the point where all the available water was taken up as ground ice. Alternatively, if the inventory of H_2O exceeds the current pore volume of the cryosphere, then Mars has always possessed extensive bodies of subpermafrost groundwater. We have investigated the relative age, geographic distribution, elevation, and geologic setting of the outflow channels in an effort to (1) identify possible modes of origin and evolutionary trends in their formation, (2) gain evidence regarding the duration and spatial distribution of groundwater in the crust, and (3) better constrain estimates of the planetary inventory of H_2O.

The channels studied in this analysis were compiled from a variety of sources and include virtually all major channels identified in the literature whose bedforms exhibit significant evidence of fluvial erosion. Following a review of previously published work, these channels were investigated by a detailed examination of selected Viking photomosaics and high-resolution images. Where possible, channel ages were determined by reconciling previously published crater counts with those associated with the revised stratigraphic referents of Tanaka [1]. Where inconsistencies or conflicts in these ages were noted, the discrepancies were usually resolved by examining superpositional relationships with other units whose relative ages are better constrained. In the discussion that follows, all cited elevations refer to that of the channel source region or, in those instances where no identifiable source region is visible, the highest elevation at which the channel is first visible. All elevations are based on the U.S.G.S. Digital Terrain Model [2].

Observations and Discussion: Although there is considerable uncertainty regarding when the first outflow channels actually formed, three of the oldest—Ma'adim Vallis (–27°,183°), Al-Qahira Vallis (–19°,199°), and Mawrth Vallis (19°,13°)—are probably Late Noachian to Early Hesperian in age [1,3,4]. A fourth and much larger channel, located near Argyre (–65°,55° to –57°,46°), is also thought to date from this period [5]. A characteristic common to all four channels is their lack of a localized and readily identifiable source region, an observation that may reflect a subsequent period of intense localized erosion or possible burial by lavas and sediments. Whatever the explanation, the highest elevations at which three of the channels appear lie between 2 and 3 km, while the highest elevation of the fourth—Mawrth Valllis—occurs near 0 km. No statistically significant geographic clustering of these four channels is observed. Although Ma'adim Vallis and Al-Qahira Vallis are located within ~800 km of each other, the area of channel activity defined by this association is geographically distinct from the areas defined by the locations of the other two channels. This spatial separation, combined with the absence of any unique geologic characteristic common to the local environment of all four channels, suggests that the earliest martian outflow channels had a polygenetic origin.

As noted by previous investigators, outflow channel activity reached a conspicuous peak during the Late Hesperian. The majority of this activity was concentrated in and around the Chryse area; however, other regions of potential activity included Deuteronilus Mensae (42°,338°), Mangala Vallis (–19°,149°), as well as a number of smaller channels to the south of the Chryse system—including Nirgal Vallis (–28°,45°) and Uzboi Vallis (–29°,36°).

The abrupt emergence of the Chryse channels from regions of chaotic terrain is usually attributed to the widespread disruption and subsidence of the crust due to the catastrophic discharge of groundwater [e.g., 6]. Areas of chaos range from ~1000 km^2 for the source of Shalbatana Vallis (0°,46°), to over 25,000 km^2 for the chaos at the eastern end of Valles Marineris in Capri Chasma (–15°,52°). These areas are comparable to those affected by prolonged, high-volume groundwater extraction on Earth (e.g., extensive pumping in the San Joachim valley of California has resulted in up to 9 m of subsidence over an area of 13,500 km^2 [7]).

The spatial and temporal association of the Chryse outflow channels with the development of Valles Marineris and Tharsis has frequently been cited as evidence of a possible genetic relationship [6,8]. In this context, several mechanisms for initiating outflow channel activity appear viable. For example, prior to the development of Valles Marineris and Tharsis, Mars may well have possessed an extensive aquifer system consisting of subpermafrost groundwater confined beneath a thick (>1-km) layer of frozen

ground. With the updoming of Tharsis, the resulting gradient in hydraulic head may have driven the flow of groundwater to lower elevations where the local increase in hydraulic pressure was sufficient to disrupt the confining layer and permit the catastrophic discharge of groundwater to the surface [6]. With the continued growth of Tharsis, the development of destabilizing hydraulic pressures should have occurred at progressively greater distances from the central uplift, resulting in potentially testable correlations between channel elevation [which varies from a high of 7 km for Kasei Vallis (0°,80°) to a low of 0 km for Ares Vallis (–2°,18°)], distance, and age. Alternatively, the growth of tensional fractures associated with the updoming of Tharsis and rifting of Valles Marineris may have broken the confining layer of frozen ground and permitted the discharge of groundwater to the surface as the fractures propagated to the lower elevations toward the east [8]. Recent calculations also suggest that channel activity may have been seismicly triggered [9,10]. By this mechanism, shock waves generated by impacts, earthquakes, or explosive volcanic eruptions may have generated transient pore pressures sufficient to disrupt the confining layer of ground ice, permitting groundwater to flow onto the surface driven by whatever artesian pressure existed within the confined aquifer prior to the seismic event. It should be noted that these scenarios are not mutually exclusive, nor do they exhaust the number of possible mechanisms for generating the Chryse or other Late Hesperian channels.

Unlike the majority of channels that were active during the Late Hesperian, many Early and Middle Amazonian channels appear related (both spatially and temporally) to regions of likely geothermal activity. For example, in the region east of Hellas, Dao, Reull, and Harmahkis Valles are all located within several hundred kilometers of the Early Hesperian volcano Hadriaca Patera (–31°,268°) and appear closely associated with lava flows from the Late Hesperian-Early Amazonian volcano Tyrhena Patera (–22°,254°) [11]. Another major concentration of channels occurs to the west and northwest of Elysium Mons (25°,213°) and Hecates Tholus (32°, 210°), volcanos that were also thought to have been active during this period. Both the geologic setting and chronology of these channels suggests that they may have been fed by water melted as a result of the increased heat flow associated with local volcanism. The accumulated water may then have been released to the surface either by the eventual thawing of the ground-ice layer or by its mechanical disruption through the build-up of a large hydraulic head. The average elevation of channel source regions during this period is ~1 km, or approximately 2 km lower than the apparent average elevation of Late Hesperian channels.

A number of small Middle- to Late-Amazonian-aged channels have been identified to the east and southeast of the Olympus Mons escarpment [12], a relationship that again suggests a potential geothermal origin. There is also evidence of fluvial activity within Ophir Chasma (–4°,73°), which may be water-rich debris flows [13,14]. The most significant outflow event to have occurred during this time happened near Cerberus Rupes (8°,195°), where a large broad swath of predominantly featureless, sparsely cratered terrain lies within a topographic basin that covers an area of ~10^6 km^2 to the south of the fracture. With the exception of a few moderately sized areas located in the eastern half of the basin, the morphologic evidence is more consistent with a major ponding feature, such as a lake or sea, than with the type of outflow channel found in the Chryse system. The ultimate source of water that embayed this region was apparently a subsurface reservoir that was either breached by the formation of Cerberus Rupes or which, at some later time, was able to take advantage of the structural pathway provided by the existence of the fracture to reach the surface [15].

Summary: Outflow channel activity has apparently spanned most of martian geologic history, from the Late Noachian to Late Amazonian. The outflow channels that date back to the Late Noachian and Early Hesperian are few in number and exhibit no strong association with any single geographic region. The Late Hesperian saw a widespread and significant increase in channel activity, much of which was concentrated in the Chryse system, a distribution that is probably linked to the concurrent development of Tharsis and Valles Marineris. During the Amazonian, the occurrence of outflow channels appears to have become more localized around regions of potential geothermal activity. One possible explanation for this geographic shift in outflow channel activity is that by the Early Amazonian the cryosphere had grown thick enough that it was no longer easily susceptible to disruption by artesian pressure alone. Alternatively, the cryosphere may have simply grown so large that no groundwater, outside that transiently produced by the melting of ground ice in active geothermal regions, survived beyond the Late Hesperian. If this last interpretation is true, theoretical calculations indicate that the amount of H_2O required to saturate the pore volume of the cryosphere at this time would still exceed the equivalent of a global ocean many hundreds of meters deep [16]. A more detailed analysis of these results is currently in preparation.

References: [1] Tanaka K. L. (1986) *Proc. LPS 16th*, in *JGR, 91*, E139–E158. [2] U.S.G.S. (1991) *Map I-2160*. [3] Greeley R. and Guest J. E. (1987) *U.S.G.S. Map I-1802-B*. [4] Rotto S. L. and Tanaka K. L. (1990) *LPS XXIII*, 1173–1174. [5] Scott D. H. and Tanaka K. L. (1987) *U.S.G.S. Map I-1802-A*. [6] Carr M. H. (1979) *JGR, 84*, 2995–3007. [7] Coates D. R. (1983) in *Mega-Geomorphology*, Oxford, 240. [8] Masursky et al. (1977) *JGR, 82*, 4016–4038. [9] Leyva I. A. and Clifford S. M. (1993) *LPS XXIV*, 875–876. [10] Tanaka K. L. and Clifford S. M. (1993) *LPI Tech. Rpt. 93-04*, 17–18. [11] Crown D. A. et al. (1992) *Icarus, 100*, 1–25. [12] Mouginis-Mark P. J. (1990) *Icarus, 84*, 362–373. [13] Witbeck N. E. et al. (1991) *U.S.G.S. Map I-2010*. [14] Lucchitta B. K. (1987) *Icarus, 72*, 411–429. [15] Tanaka K. L. and Scott D. H. (1986) *LPS XVII*, 865–866. [16] Clifford S. M. (1993) *JGR, 98*, 10973–11016.

N94- 33236

546 91 ABS. ONLY

OBLIQUITY VARIATION IN A MARS CLIMATE EVOLUTION MODEL.

D. Tyler[1,2] and R. M. Haberle[2], [1]Department of Meteorology, San Jose State University, San Jose CA 95192, USA, [2]Ames Research Center, Moffett Field CA 94035-1000, USA.

The existence of layered terrain in both polar regions of Mars is strong evidence supporting a cyclic variation in climate. It has been suggested [1] that periods of net deposition have alternated with periods of net erosion in creating the layered structure that is seen today. The cause for this cyclic climatic behavior is variation in the annually averaged latitudinal distribution of solar insolation in response to obliquity cycles [2]. For Mars, obliquity variation leads to major climatological excursions due to the condensation and sublimation of the major atmospheric constituent, CO_2. The atmosphere will collapse into polar caps, or existing caps will rapidly sublimate into the atmosphere, dependent upon the polar surface

heat balance and the direction of the change in obliquity. It has been argued [2] that variations in the obliquity of Mars cause substantial departures from the current climatological values of the surface pressure and the amount of CO_2 stored in both the planetary regolith and polar caps.

Haberle et al. [3] have constructed a heat balance model based on the work of Gierasch and Toon [4] that simulates the evolution of CO_2 on Mars from the end of late heavy bombardment to the current time. The model partitions CO_2 between its various reservoirs based upon predictions for polar, equatorial, and global-mean surface temperatures. The exchangeable reservoirs are atmosphere, planetary regolith, and polar caps. The model also loses CO_2 irretrievably to a carbonate rock reservoir via aqueous chemical weathering according to the method of Pollack et al. [5]. The solar insolation is affected in time, however, only by varying solar luminosity; the relative distribution between equatorial and polar regions is invariant. Obliquity variation was avoided within the model by assuming that, throughout the 7.6-m.y. timestep, the current obliquity, $\Theta = 25.2$, sufficiently represents an average obliquity. It may be important, however, to explicitly study the climatological effects of obliquity variation since the size of the CO_2 reservoirs can be significantly changed, drastically affecting the temperature structure through feedbacks from the greenhouse effect and the dynamic transfer of equatorial heat into polar regions.

In this new work we have modified the Haberle et al. model [3] to incorporate variable obliquity by allowing the polar and equatorial insolation to become functions of obliquity, which we assume to vary sinusoidally in time. As obliquity varies in the model, there can be discontinuities in the time evolution of the model equilibrium values for surface pressure, regolith, and polar cap storage. The time constant, τ_r, for the regolith to find equilibrium with the climate is estimated [6], depending on the depth, thermal conductivity, and porosity of the regolith, between 10^4 and 10^6 yr. Thus, using 2000-yr timesteps to move smoothly through the 0.125-m.y. obliquity cycles, we have an atmosphere/regolith system that cannot be assumed in equilibrium. We have dealt with this problem by limiting the rate at which CO_2 can move between the atmosphere and regolith, mimicking the diffusive nature and effects of the temperature and pressure waves, by setting the time rate of change of regolith storage proportional to the difference between equilibrium storage and current storage.

Model integration begins with the exchangeable reservoirs in equilibrium at mean obliquity. Starting at 3.5 G.y. ago with 1.0 bar of total available CO_2, $\tau_r = 10^4$ yr and $10° \le \Theta \le 50°$, the model initializes without polar caps. When obliquity decreases in a cycle, the annual polar insolation decreases causing the polar surface temperature to fall. This trend continues until $\Theta = 23°$ and the polar surface temperature reaches the frost point of the 180-mbar atmosphere, causing atmospheric collapse [3]. Such a collapse is estimated [6] to take 10^2 yr, well within our model timestep; thus, model pressure drops discontinuously to 0.5 mbar and reaches a minimum of 1.2 μbar when $\Theta = 10°$. The regolith responds, governed by τ_r, freeing CO_2, which adds to the polar caps since atmospheric pressure is now buffered by the frost point relationship. When obliquity increases, model pressure and polar surface temperature increase until thermodynamic equilibrium can only be maintained at the polar surface after complete sublimation of the polar caps at $\Theta = 42°$. Sublimation leaves a 500-mbar atmosphere, vs. 180 mbar at mean obliquity, causing 10 K and 20 K increases in respective global and polar surface temperatures. Increased weathering is significant but short lived as the regolith finds equilibrium by quickly reducing atmospheric pressure. The obliquity peaks as the regolith nears equilibrium and the cycle repeats as obliquity begins to fall.

We find that including variable obliquity can cause our model to predict CO_2 losses to carbonate formation of less than half that lost when obliquity is held constant at the mean. This is the case with the scenario described above, but preliminary experiments with different values of τ_r have indicated that there is a complicated relationship between this parameter and the amount of CO_2 lost to carbonates through an obliquity cycle. This relationship and the effect of a variable polar cap albedo are being studied.

References: [1] Pollack J. B. (1979) *Icarus, 37,* 479–553. [2] Fanale F. P. et al. (1982) *Icarus, 50,* 381–407. [3] Haberle R. M. et al. (1993) *LPI Tech. Rpt., 93-03,* 13–14. [4] Gierasch P. J. and Toon O. B. (1973) *JAS, 30,* 1502–1508. [5] Pollack J. B. et al. (1987) *Icarus, 71,* 203–224. [6] Kieffer H. H. and Zent A. P. (1992) *Mars* (H. H. Kieffer et al., eds.), 1180–1218.

J47-91 ABS. ONLY **N94-33238**

DIELECTRIC PROPERTIES OF MARS' SURFACE: PROPOSED MEASUREMENT ON A MARS LANDER.

S. Ulamec and R. Grard, Space Science Department of ESA, P.O. Box 299, 2200 AG Noordwijk, The Netherlands.

Recent studies of missions to Mars (MESUR by NASA and Marsnet by ESA) have suggested the development of semihard landers, also of considerably different designs. One type was to be extremely basic, consisting mainly of a meteorological package, but with the possibility of other small, low-mass, low-power instruments. In particular, this type of lander was also considered for the exploration of the polar regions.

Two methods to investigate the surface material at the landing site are discussed. Both measure the dielectric constant ε of the ground material. This information can then be used to elucidate the surface composition and structure, and especially in the case of a landing on the polar ice, the determination of the permittivity would be of high scientific value.

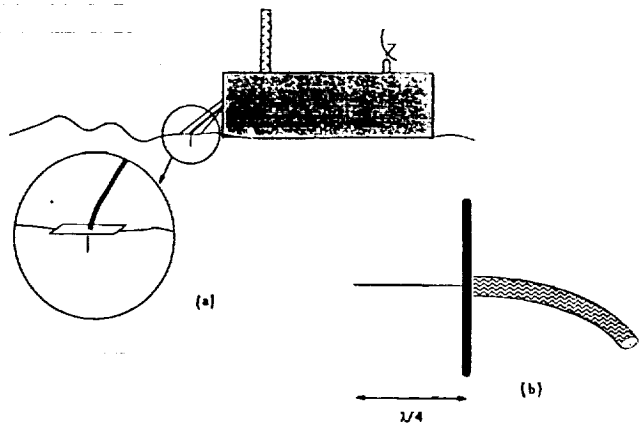

Fig. 1. (a) Possible arrangement of sensor on a Mars lander; (b) side view of suggested λ/4 antenna.

As has been shown in terrestrial snow, experimentally [1] and theoretically [2], the dielectric constant is not just a very good indicator of the density of snow, but also gives information on the texture of the particles. The ratio between water- and CO_2-ice can be determined. On the other hand, on soil or rocky ground the porosity and, to some extent, the composition of the material can be investigated. Since the landers are supposed to operate for an extended period of time, diurnial and annual changes in the ground (e.g., by CO_2 or water frost) can be studied. The discussed quadrupole experiment will also measure into some depth (usually in the range of the dimension of the quadrupole) and detect buried boulders or cavities.

One instrument uses very small high-frequency antennas, similar to the ones used during the KOSI (comet simulation) experiments, performed in the large space simulator in Cologne, Germany [3]. These antennas would have a resonance frequency somewhere between 1 and 12 GHz. So far, $\lambda/4$ groundplane structures have been tested, but other arrangements, e.g., $\lambda/2$ dipole-antennas, could be used as well. The traditional microwave bridge method could be used, but instead of using a waveguide containing the sample material, the antennas should be used as sensors. These sensors (with dimensions of a few centimeters) have to be in contact with the ground as shown in Fig. 1. By determining the actual resonance frequency ν_{res} (which is a function of the dimension of the sensor and the dielectric constant of the surrounding medium), the surface material is analyzed.

The advantage of this kind of instrument is its extreme low weight and low power demand. The sensor could be placed underneath the lander, e.g., on the bottom side of a landing leg. The electronics consist mainly of a sweep oscillator and a simplified swept amplitude analyzer, which finds ν_{res} of the antennas. Using a groundplane antenna, there is little or no influence by the lander body on the measurement. On the other hand, the antenna has to be embedded in the ground material. This is no major problem in case of soil or snow-ice, but problematic in case of rocks, since the sensor has to be embedded in material of a grain size, small compared to its own dimensions.

The second instrument is based on a principle that was first discussed by Wenner in 1915 [4] and Schlumberger 1920 [5]. The method was used originally to make Earth-resistivity maps of special areas and is nowadays basically used as a tool in archeology. Four electrodes form a quasistatic (the commonly used frequency is around 15 kHz) quadrupole. When an alternating current I is injected into two of the electrodes, a voltage V is induced between the other two. Thus, one obtains the mutual impedance of the quadrupole ($Z = V/I$), which is a function of ε of the ground. Traditionally, the four electrodes are stuck into the ground, but it has been shown that the measurement is also possible if the electrodes are just above the surface [6,7]. Also, the traditional linear configuration can be modified into a square configuration [6], as shown in Fig. 2.

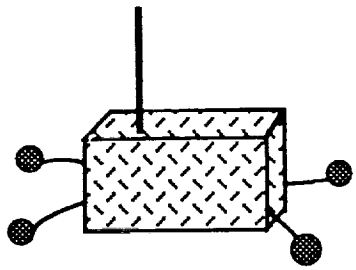

Fig. 2. Arrangement of quasistatic quadrupole.

References: [1] Tiuri M. et al. (1984) *IEEE J. of Oceanic Eng., Vol. OE-9 (5).* [2] Priou A. (1992) *Dielectric Properties of Heterogeneous Materials*, Elsevier. [3] Ulamec S. et al. (1993) *LPS XXIV*, 1451–1452. [4] Wenner F. (1915) *Bull., 12 Sci. Paper 259*, U.S. Bureau of Standards, 469–478. [5] Schlumberger C. (1920) *Etude de la Prospection Electrique du Sous-Sol*, Gauthier-Villars, Paris. [6] Grard R. (1991) *Meas. Sci. Technol., 1*, 295–301. [7] Grard R. and Tabbagh A. (1991) *JGR, 96*, 4117–4123.

THE INFLUENCE OF THERMAL INERTIA ON MARS' SEASONAL PRESSURE VARIATION AND THE EFFECT OF THE "WEATHER" COMPONENT. S. E. Wood and D. A. Paige, University of California, Los Angeles CA 90024, USA.

Using a Leighton-Murray type [1] diurnal and seasonal Mars thermal model, we found that it is possible to reproduce the seasonal variation in daily-average pressures (~680–890 Pa) measured by Viking Lander 1 (VL1), during years without global dust storms, with a standard deviation of less than 5 Pa [2]. In this simple model, surface CO_2 frost condensation and sublimation rates at each latitude are determined by the net effects of radiation, latent heat, and heat conduction in subsurface soil layers. An inherent assumption of our model is that the seasonal pressure variation is due entirely to the exchange of mass between the atmosphere and polar caps. However, the results of recent Mars GCM modeling [3,4] have made it clear that there is a significant dynamical contribution to the seasonal pressure variation. This "weather" component is primarily due to large-scale changes in atmospheric circulation, and its magnitude depends somewhat on the dust content of the atmosphere. The overall form of the theoretical weather component at the location of VL1, as calculated by the AMES GCM [3], remains the same over the typical range of Mars dust opacities (Fig. 1c). Assuming that $\tau = 0.3$ is representative of years without global dust storms, we subtracted the corresponding theoretical weather component at VL1 from the years 2 and 3 data to obtain the seasonal pressure variation due only to changes in the mass of the atmosphere. We found that fitting this new pressure curve allowed us to also fit the observed seasonal polar cap boundaries during their growth [5] and retreat [6,7] much better than before, and for more "reasonable" values of thermal inertia, frost albedo, and frost emissivity. However, the significance of this result depends on the ability of Mars GCMs to calculate the actual dynamical component at VL1, which is in turn limited by uncertainties in the available data on dust opacities. Furthermore, despite the importance of the weather component, it will be shown that the "thermal inertia component" could also be responsible for a large part of the seasonal pressure variations at VL1 given our current lack of knowledge regarding thermal inertias on Mars below diurnal skin depths.

As all studies of the seasonal CO_2 cycle [1–3,8] have demonstrated, the radiative properties of the CO_2 frost on Mars are key parameters, and obtaining good measurements of their actual values would be extremely beneficial to our ability to model and under-

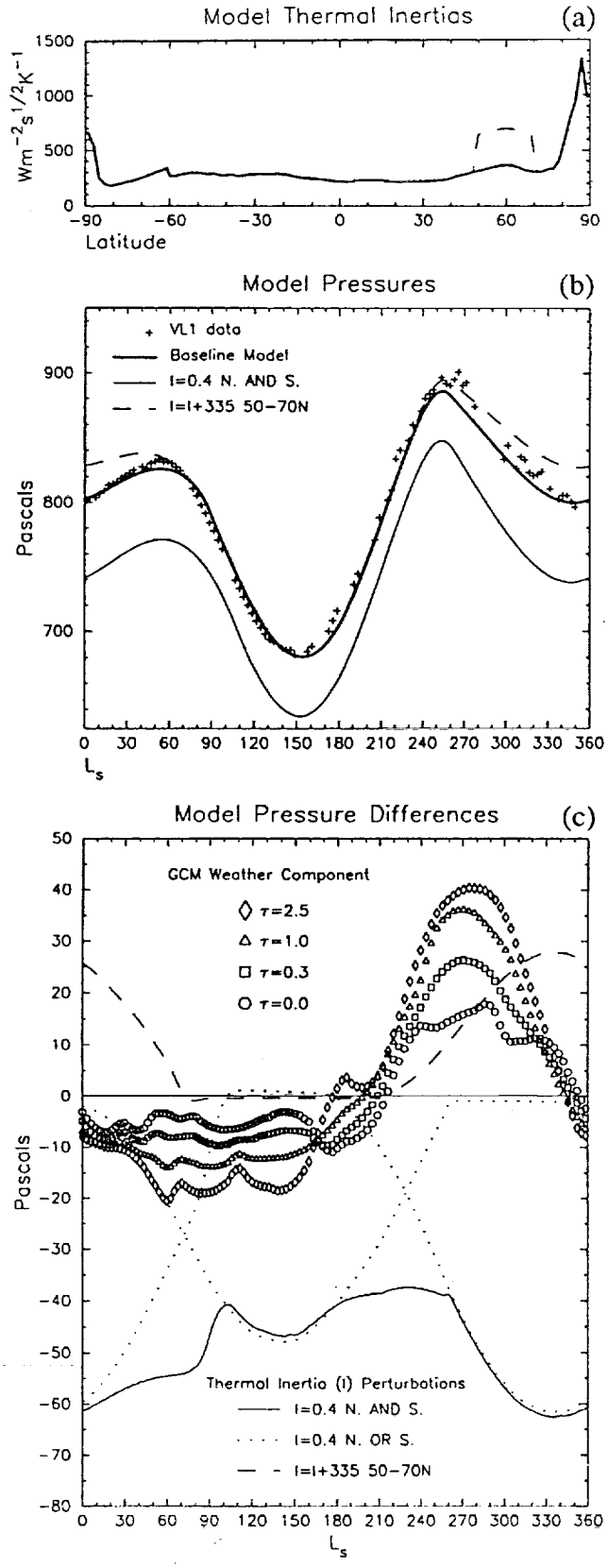

Fig. 1.

stand the martian climate. In our previous work we found that the seasonal pressure curve is very sensitive to which values are chosen for frost albedo and emissivity, and that interannual variations of more than 0.02 in the albedo or emissivity of either polar cap would be inconsistent with the observed interannual variations in the Viking daily-average pressure data [9]. The seasonal pressure variation is also very sensitive to which values for the subsurface thermal inertias are chosen. In fact, our best-fit values for the albedo and emissivity of the seasonal CO_2 polar caps covered a wide range and depended linearly on the assumed value of subsurface thermal inertia [1]. Maps of the near-surface thermal inertias in the polar regions have been made using Viking IRTM observations of diurnal temperature variations [10,11], but it is the subsurface thermal inertias at seasonal skin depths that have the greatest influence on the CO_2 cycle, and these are still largely unknown. In order to illustrate the potential effects of this uncertainty, we started with the same assumption made in the GCM simulations [3] mentioned above; that the thermal inertias of all subsurface layers equal the IRTM-derived diurnal values, although for our one-dimensional model (horizontally) we used the zonal averages (Fig. 1a). We then found the corresponding best-fit frost albedo and emissivity values; $A = 0.76$ and $\varepsilon = 0.57$ in the northern hemisphere and $A = 0.56$, $\varepsilon = 0.74$ in the south. Using this as a baseline model, and keeping the soil albedo and frost parameters constant, the relative effects of changing thermal inertias on the model-calculated pressure curve are shown. As an extreme case, if the thermal inertias are all set to less than 1 W m^{-2} s$^{1/2}$ K^{-1}, effectively reducing the subsurface heat flux to zero, the difference in the pressure curve is −40 to −65 Pa (Fig. 1b,c). To get an effect of the same magnitude as the dynamical component, we increased only the thermal inertias assumed for latitudes 50°–70°N by 335 W m^{-2} s$^{1/2}$ K^{-1} from their baseline values. This amount is much less than the latitudinal variation in derived diurnal inertias, but the resulting model-calculated pressures are up to 30 Pa higher during northern winter (Fig. 1b,c).

The seasonal pressure variations at the two Viking Lander sites provide an important and valuable constraint for any model of the atmosphere and polar caps of Mars because of the prolonged coverage, accuracy, and interannual repeatability of this data. However, the fact that many different models, from simple thermal models [2] to energy-balance climate models [8] to global atmospheric circulation models [3,4], have each been able to "fit" the Viking pressure data demonstrates that meeting that constraint cannot, by itself, be used to prove that any one particular process plays an important role. Furthermore, because many processes involved in the polar energy balance can mimic the effects of other processes, within a given model there may be many combinations of parameter values that yield good fits to the Viking pressure data, so the value of any single parameter cannot be uniquely determined on that basis alone. Modeling is still useful, however, for studying the sensitivity of the martian CO_2 cycle to the inclusion or neglect of potentially important processes, temporal variations, and assumptions about basic parameter values.

References: [1] Leighton R. R. and Murray B. C. (1966) *Science, 153*, 136–144. [2] Wood S. E. and Paige D. A. (1992) *Icarus, 99*, 1–14. [3] Pollack J. B. et al. (1993) *JGR, 98*, 3149–3181. [4] Talagrand O. et al. (1991) *Bull. A.A.S., 28*, 115. [5] Capuano J. (1993) Master's thesis, Univ. of Toledo. [6] James P. B. et al. (1979) *JGR, 84*, 2889–2922. [7] James P. B. (1979) *JGR, 84*, 8332–8334. [8] James P. B. and North G. R. (1982) *JGR, 87*, 10271–10283.

[9] Paige D. A. and Wood S. E. (1992) *Icarus, 99*, 15–27. [10] Paige D. A. and Keegan K. D. (1992) *JGR*, submitted. [11] Paige D. A. et al. (1993) *JGR*, submitted.

CARBONATES, SURFATES, PHOSPHATES, NITRATES, AND ORGANIC MATERIALS: THEIR ASSOCIATION IN A MARTIAN METEORITE. I. P.Wright[1], M. M. Grady[2], and C. T. Pillinger[1], [1]Department of Earth Sciences, Open University, Walton Hall, Milton Keynes MK7 6AA, UK, [2]Natural History Museum, Cromwell Road, London SW7 5BD, UK.

The debate concerning the evolution of CO_2 on Mars continues. It would appear that in order to explain the valley networks and other relict fluvial landforms it is necessary to accept that liquid water was once present at the surface of Mars. This in turn requires, at some point in the planet's history, a higher surface temperature than exists today, a proposition explained traditionally by an early dense CO_2 atmosphere [e.g., 1]. However, there are a number of problems with this notion: for instance, CO_2 alone is not an efficient greenhouse gas because of its tendency to form clouds [2]. Moreover, if there was an early dense CO_2 atmosphere, it is necessary to explain where the elemental constituents now reside. There are two possibilities for the latter, namely loss to outer space of atmospheric CO_2 or the formation of vast carbonate deposits. While some models of atmospheric loss predict that up to 0.4 bar of CO_2 could be removed from the martian surface [3], this is still not enough to account for the original atmospheric inventory, usually considered to have been in the range of 1–5 bar. Thus, most models of the evolution of the martian surface require removal of CO_2 from the atmosphere and into carbonate deposits. However, as yet, the evidence for the existence of carbonates on Mars is fairly scant [e.g., 4]. This is an issue that would have been resolved by results obtained from Mars Observer.

While the existence of carbonates on Mars remains unsubstantiated, their presence in meteorites from Mars is undisputed. Furthermore, their origin as low-temperature secondary minerals, introduced at some point after the rock fabric of the meteorite had crystallized and cooled, has been demonstrated by isotopic measurements [5,6] and petrographic descriptions [7]. That the carbonate minerals are not simply weathering products produced on Earth has been demonstrated in one case by ^{14}C measurements, which show that there has not been an input of modern terrestrial C to the sample [8]. However, measurements from another sample show the presence of the ^{14}C isotope, interpreted as resulting from terrestrial contamination [9]. These results are somewhat unexpected since the $^{12}C/^{13}C$ and $^{16}O/^{18}O$ ratios of the carbonate minerals from the two different samples are similar [5,10]. At this point the exact significance of the ^{14}C data is unclear, but it would seem that in any particular sample there may be a few components containing ^{14}C that have been added from the terrestrial environment in addition to preterrestrial (i.e., martian) carbonates, characterized by the absence of ^{14}C. The presence of terrestrial contaminants in any meteorite sample is to be expected [5,11]; what is important is the use of analytical protocols that can effectively identify the components of interest. It is with challenges of this nature in mind that work continues with the study of weathering components in martian meteorites.

A particularly interesting sample is EET A79001, a meteorite collected from Antarctica. While rocks that experience Antarctic conditions may suffer from the effects of terrestrial inorganic weathering processes (e.g., the build-up on the outer surfaces of magnesium carbonate and bicarbonates, and hydrated magnesium and calcium sulfates), they are relatively free of organic contamination. Thus, it is interesting to note the association, deep within the meteorite, of carbonate minerals and organic compounds [12]. The carbonates are Mg-bearing and also contain P, i.e., there could be magnesium phosphates present [7]. Calcium sulfate, possibly gypsum, is also present [7], and there is also some tenuous evidence for the presence of nitrates [5,13]. On the basis of N isotope measurements it is clear that the nitrates could not have formed by a mechanism that utilized martian atmospheric N as a source material [5,13].

Because of the potential ramifications for martian surface evolution of the coexisting salts and organic compounds in EET A79001, it was perhaps inevitable that a further study of Antarctic weathering processes was necessary in order to constrain the possible extent of such effects. In this regard it is worth noting that EET A79001 has a weathering category "A" (i.e., only minor effects) and a fracturing category "A" (i.e., minor cracks). Since the meteorite is a single stone of mass 7.9 kg, measuring about 20 cm across, it is clear that samples from the center of the specimen ought to be predominantly free of the effects of terrestrial weathering. In contrast, a recently discovered martian meteorite from Antarctica, LEW 88516 (weathering A/B; fracturing A), weighs only 13.2 g and is less than 2 cm in size. Since the terrestrial ages of both Antarctic meteorites are similar, i.e., <50,000 yr, [14,15] it may be anticipated that the effects of weathering in LEW 88516 would be more severe than in EET A79001. However, LEW 88516 was found to contain the lowest C content of any of the nine known martian meteorites [16], even when material was taken specifically from the surface layers for analysis. This tends to support the notion that terrestrial weathering processes are not necessarily responsible for the components observed in EET A79001. A further consideration here arises from O isotope measurements of water released by heating, which, at face value, seem to demonstrate that EET A79001 has been affected to some degree by terrestrial weathering [17]. However, since it is now considered that the O isotope data should be treated with caution [8], their true significance, for the time being, remains poorly established.

So how do we explain the association of carbonates, sulfates, phosphates, nitrates, and organic materials in EET A79001? It has to be accepted that some of the inorganic minerals could have formed by terrestrial weathering processes. However, it is known for certain that martian meteorites, including EET A79001, contain preterrestrial weathering products [e.g., 7]. Furthermore, the associated organic compounds are present in higher abundances (i.e., by about 2 orders of magnitude) than can reasonably be expected for any contamination episode or handling procedures [12]. It would appear, therefore, that the coexistence of inorganic weathering products and organic materials in EET A79001 was established on Mars. In order to explain this phenomenon, perhaps attention should be turned to recent work that advocates an early CH_4/CO_2 greenhouse on Mars [18], since this might ultimately lead to the formation of nonvolatile surface reservoirs of reduced and oxidized forms of C. An additional consideration, which could be pursued through chemical evolution modeling studies, infrared measurements of the

martian surface, or further analyses of martian meteorites, is that there exist on Mars large deposits of oxalate minerals, such as $CaC_2O_4.H_2O$, $CaC_2O_4.2H_2O$, $MgC_2O_4.2H_2O$, etc. On Earth these minerals fall at the very interface of inorganic and organic chemistry, being formed predominantly by biological processes. That they can form by purely inorganic reactions is demonstrated, however, by their presence in primitive carbonaceous chondrites [19]. If oxalates are present on Mars, this might explain the removal of CO_2 from the atmosphere without the formation of observable carbonate deposits.

References: [1] Pollack J. B. et al. (1987) *Icarus, 71*, 203–224. [2] Kasting J. F. (1991) *Icarus, 94*, 1–13. [3] Luhmann J. G. et al. (1992) *Workshop on the Evolution of the Martian Atmosphere*, LPI Contrib., 787, 19–20. [4] Pollack et al. (1990) *JGR, 95*, 14595–14627. [5] Wright I. P. (1988) *GCA, 52*, 917–924. [6] Clayton R. N. and Mayeda T. K. (1988) *GCA, 52*, 925–927. [7] Gooding J. L. (1988) *GCA, 52*, 909–915. [8] Karlsson H. R. et al. (1993) *LPS XXIV*, 757–758. [9] Jull A. J. T. et al. (1992) *LPS XXIII*, 641–642. [10] Carr et al. (1985) *Nature, 314*, 248–250. [11] Swart P. K. et al. (1983) *Meteoritics, 18*, 137–154. [12] Wright I. P. (1989) *Nature, 340*, 220–222. [13] Grady M. M. et al. (1993) *LPS XXIV*, 553–554. [14] Jull A. J. T. and Donahue D. J. (1988) *GCA, 52*, 1309–1311. [15] Nishiizumi K. et al. (1992) *Meteoritics, 27*, 270. [16] Wright I. P. et al. (1993) *LPS XXIV*, 1541–1542. [17] Karlsson H. R. et al. (1992) *Science, 255*, 1409–1411. [18] Brown L. L. and Kasting J. F. (1993) *LPI Tech. Rpt. 93-03, Part 1*, 3. [19] Fuchs L. H. (1973) *Smithsonian Contrib. Earth Sci., 10*, 39.

550-91 1185. 8. **N94-33240**

SIMULTANEOUS LABORATORY MEASUREMENTS OF CO_2 AND H_2O ADSORPTION ON PALAGONITE: IMPLICATIONS FOR THE MARTIAN CLIMATE AND VOLATILE RESERVOIR. A. P. Zent and R. Quinn, SETI Institute and NASA Ames Research Center, Moffett Field CA 94035, USA.

We are measuring the simultaneous adsorption of H_2O and CO_2 on palagonite materials in order to improve the formulation of climate models for Mars. We report on the initial co-adsorption data. Models of the martian climate and volatile inventory indicate that the regolith serves as one of the primary reservoirs of outgassed volatiles and that it exchanges H_2O and CO_2 with the atmosphere in response to changes in insolation associated with astronomical cycles. Physical adsorbate must exist on the surfaces of the cold particulates that constitute the regolith, and the size of that reservoir can be assessed through laboratory measurements of adsorption on terrestrial analogs. Many studies of the independent adsorption of H_2O and CO_2 on Mars analogs have been made and appear in the literature [1–5]. Empirical expressions that relate the adsorptive coverage of each gas to the temperature of the soil and partial pressure have been derived based on the laboratory data. Numerical models incorporate these adsorption isotherms into climatic models, which predict how the adsorptive coverage of the regolith, and hence the pressure of each gas in the atmosphere will vary as the planet moves through its orbit [e.g., 6]. These models suggest that the regolith holds several tens to hundreds of millibars of CO_2 and that during periods of high obliquity warming of the high-latitude regolith will result in desorption of the CO_2, and a consequent increase in atmospheric pressure. At lower obliquities, the caps cool, and the equator warms, forcing the desorption of several tens of millibars of CO_2, which is trapped into quasipermanent CO_2 caps.

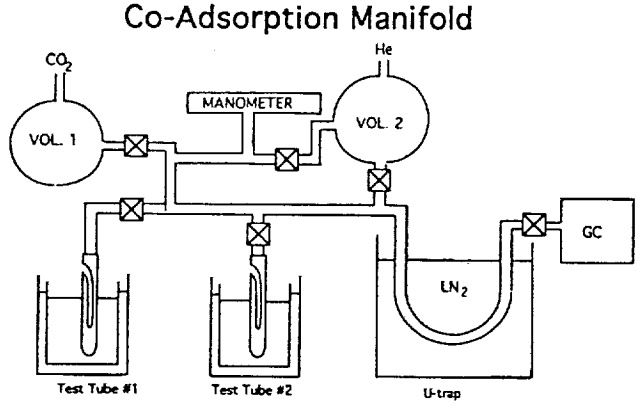

Fig. 1.

There are a number of uncertainties in these models. Extrapolating the martian orbit more than several 10^4 yr in either direction is difficult because of the chaotic nature of the martian orbit [7]. The extent of the regolith is unclear particularly with respect to the specific surface area of regolith materials that is in diffusive contact with the atmosphere. Finally, the adsorptive behavior of H_2O and CO_2 has always been assumed to be independent. Yet there are data that suggest that near room temperature, there is adsorptive competition between H_2O and CO_2 [8], and H_2O actively displaces CO_2 from the adsorbed state. If that is the case on Mars, then current models of the CO_2 inventory overestimate its size, and climate models must account for new estimates of the inventory size and the effects of H_2O on CO_2 exchange. We have therefore undertaken laboratory measurement of the adsorptive competition between H_2O and CO_2 at conditions appropriate to the martian regolith in order to eliminate this uncertainty in the climate models.

The experimental apparatus is shown schematically in Fig. 1. The manifold and sample are baked out overnight and we then fill volume 2 to a known pressure with He and expand into the sample to estimate the dead volume in the system. The sample is cryogenically cooled to a preselected temperature, T_1. Doubly distilled water in test tube #2 is cryogenically cooled to temperature T_2. We maintain $T_2 > T_1$ in order to keep the relative humidity in the soil chamber well below unity. T_1 and T_2 are constantly monitored. To acquire a data point, we fill volume 1 with a known pressure of CO_2 and

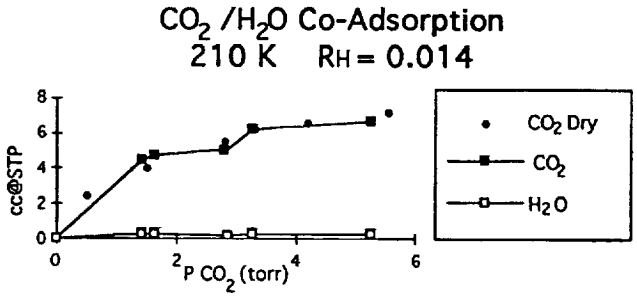

Fig. 2.

expand it into the sample chamber along with the H_2O vapor buffered at T_2. Equilibration to within the precision of our data analysis typically requires on the order of 6 hr. We have made several estimates of this timescale by varying the equilibration period and comparing analyses of several points. After equilibration, we isolate the soil sample and heat it to approximately 50°C while opening the head space to an LN_2 trap. After 5 hr, the U trap is isolated, removed from the manifold, and attached to a gas chromatograph. The U trap is heated to desorb gas on the interior walls and injections are made. Occasionally, a second injection is done and compared to the first, in order to disprove the possibility that substantial amounts of H_2O are adsorbed onto the warm walls of the U trap. We do not find evidence of significant H_2O adsorption in the warm trap. The data are discarded if any N_2 peaks appear in the chromatogram, indicating a leak in the manifold. While the U trap is attached to the GC, the sample is baked out under vacuum at 50°C for 16 hr. Since each data point is independently acquired, the spread about a smooth isotherm is a measure of the random error in the technique. The dry CO_2 isotherm is acquired by simply measuring the pressure drop of CO_2 over the soil and is an independent technique.

All data acquired to date are at 210 K, and low relative humidity ($R_H = 0.014$). We have found, contrary to our expectations, that CO_2 is not substantially displaced by adsorbed H_2O (see Fig. 2) relative to its adsorptive coverage from a dry atmosphere. We are currently performing adsorption curves at T= 210 K and $R_H \approx 50\%$ (relative to ice) in order to assess the capability of H_2O to displace adsorbed CO_2. We are continuing data acquisition, and will move to higher temperature isotherms.

Interpretation of the new data, insofar as conclusions can be drawn from such a limited set, is uncomplicated, since these data support the assumptions of independent adsorptive behavior that have already been published in the literature. We believe that at higher temperatures, H_2O will compete more effectively for adsorption sites than it does at low temperatures, requiring some modification of the climate models. At low temperatures and relative humidity, however, such as in the winter hemisphere or during periods of low obliquity when most H_2O may be cold trapped at quasipermanent CO_2 caps, there is no indication in the data that substantial modification of the current models is required.

References: [1] Fanale F. P. and Cannon W. A. (1971) *Nature, 230*, 502–504. [2] Fanale F. P. and Cannon W. A. (1974) *JGR, 79*, 3397–3402. [3] Mooney et al. (1952) *J. Amer. Chem. Soc., 74*, 1367–1371. [4] Fanale et al. (1982) *Icarus, 50*, 381–407. [5] Zent et al. (1987) *Icarus, 71*, 241–249. [6] Kieffer H. H. and Zent A. P. (1992) in *Mars*, Ch. 33, Univ. of Arizona. [7] Rubicam D. (1993) *JGR, 98*, 10827–10832. [8] Carter J. W. and Husain H. (1974) *Chem. Eng. Sci., 29*, 263–273.